論文 / 著書情報
Article / Book Information

題目(和文)	絶対古地磁気強度測定法の信頼性の検討とソサエティ諸島の古地磁気：過去400万年間の地磁気双極子モーメントの推定
Title(English)	Reliability of paleointensity determination methods and the paleomagnetism of the Society islands : implications for the last 4 Ma geomagnetic dipole moment
著者(和文)	山本裕二
Author(English)	
出典(和文)	学位:博士(理学), 学位授与機関:東京工業大学, 報告番号:甲第4984号, 授与年月日:2002年3月26日, 学位の種別:課程博士, 審査員:
Citation(English)	Degree:Doctor (Science), Conferring organization: Tokyo Institute of Technology, Report number:甲第4984号, Conferred date:2002/3/26, Degree Type:Course doctor, Examiner:
学位種別(和文)	博士論文
Type(English)	Doctoral Thesis

Doctoral Dissertation

Reliability of paleointensity determination methods and the paleomagnetism of the Society Islands: Implications for the last 4 Ma geomagnetic dipole moment

Yuhji Yamamoto

Department of Earth and Planetary Sciences
Graduate School of Science and Engineering
Tokyo Institute of Technology

February 2002

Abstract

The paleointensity of the geomagnetic field is able to characterize the ancient geodynamo as well as the polarity reversal. It has been believed that the time-averaged virtual dipole moment (VDM) and virtual axial dipole moment (VADM) for the last few million years are almost the same as the present geomagnetic dipole moment ($\sim 8 \times 10^{22} \mathrm{Am}^2$) on the basis of the absolute paleointensities reported so far. This estimation is, however, questionable because not a negligible number of the erroneous paleointensities are occasionally yielded from the historic lavas.

This suggestion directly demands a re-examination of the reliability of the absolute paleointensity determinations. Hence we performed comprehensive investigation of the paleointensity measurements and various rock magnetic analyses on the Hawaiian 1960 lava, which gave anomalous paleointensities in the several previous studies. The 19 cores from the lava are classified into three groups with degrees of the deuteric oxidation. The Coe's version of the Thellier method gave a mean paleointensity of $49.0 \pm 9.6 \mu$T (N=17), which is significantly larger than the expected value of 36.2μT. Those paleointensities showed a dependence on the oxidation indices, which could be explained by thermochemical remanent magnetization (TCRM) acquisition during the natural cooling stage of the lava. Although it is generally difficult to distinguish TCRM from thermoremanent magnetization (TRM), the double heating technique of the Shaw method combined with low temperature demagnetization (LTD-DHT Shaw method) allows us to detect the influence of TCRM on natural remanent magnetization (NRM). This method gave a better average of $39.4 \pm 7.9 \mu$T (N=9). Most of the inappropriate results were screened by a combination of the double heating test, the ARM correction and the LTD treatment, though the success rate was much lower. If two outliers are further excluded, the average is improved to be $35.7 \pm 3.3 \mu$T (N=7), which agrees well with the expected.

Therefore, we have applied the LTD-DHT Shaw method to volcanic rocks from the Society Islands, French Polynesia, in order to extract the reliable geomagnetic dipole moments. According to our K-Ar dating on the selected samples from 52 sites, they range from 0.5 to 4.6 Ma. The age variation against the localities is consistent with the absolute motion of the Pacific plate. If we correct the paleomagnetic data for the motion, 82 normal, 48 reversed and 10 intermediate directions were observed with a threshold VGP latitude of 50°. The magnetostratigraphy constructed from these polarities and K-Ar ages agrees well with the geomagnetic polarity time

scale. The LTD-DHT Shaw method provided 164 successful paleointensities for the last 4 Ma. They gave 28 reliable site-mean paleointensities with a mean VDM of $3.68\pm2.32\times10^{22}Am^2$ and a mean VADM of $3.76\pm2.24\times10^{22}Am^2$. This is about 30-50% lower than the previous estimation and this inconsistency is suggested to be caused by some bias in the previously reported paleointensities by the Thellier method. Since the newly determined average of the last 4 Ma VDM is nearly half of the present dipole moment, the present-day field is very intensive and thus it may not be representative of the geomagnetic field.

Contents

Chapter 1

General introduction

The geomagnetic field is one of the most important characteristics of the Earth. Since it is originated from the Earth's core, restoration of its variation is essential to understand our planet. By the paleomagnetic studies, we can extract such records from volcanics and sediments. They mainly capture the dipolar signal which usually dominates the Earth's magnetic field. It is our common understanding that the time-averaged field can be well approximated by a geocentric axial dipole.

The most remarkable variation of the dipolar field is the polarity reversal. Its history has been investigated by many paleomagnetists and condensed into the geomagnetic polarity time scales (e.g. Cande and Kent, 1995). Another distinctive variation is its change in intensity. The geocentric axial dipole generates the same field direction on the Earth's surface, regardless of its intensity. Therefore the paleointensity study is definitely required for revealing the geomagnetic characteristics. As natural remanent magnetization (NRM) of volcanic rocks and ceramics is basically originated from thermoremanent magnetization (TRM), comparison of NRM with TRM given in a laboratory field can yield an absolute paleointensity assuming the linearity law of TRM. We usually use the Thellier method (Thellier and Thellier, 1959) and the Shaw method (Shaw, 1974) for the paleointensity determinations.

In the Thellier-type experiment, a series of stepwise double heating are generally applied. The comparison between thermally demagnetized NRM and partially given TRM ideally shows a good linearity in the NRM-TRM diagram (Arai diagram) as a function of blocking temperatures. This is based on the additivity law of partial TRM (pTRM). The most commonly adopted version of the Thellier method is that of Coe's (Coe, 1967). In

this version, the pTRM test is conducted to examine the thermal alteration of the sample due to the laboratory heating. If the pTRM after the heating is the same as that before, no thermal alterations are regarded to occur during the heating. On the other hand, the Shaw method employs the stepwise alternating field demagnetization. NRM is compared with TRM given in laboratory heating above the Curie temperature as a function of coercive forces. Thermal alteration during the laboratory heating is checked by changes in the coercivity spectra of anhysteretic remanent magnetization (ARM) before and after the heating. This is based on the similarity of the linearity and additivity laws between ARM and TRM.

One of the serious problems in both methods is a low success rate due to the sample alteration in laboratory heating. Several correction methods have been proposed to improve the success rate. For the Thellier method, McClelland and Briden (1996) and Valet et al. (1996) proposed the similar correction methods assuming that the alteration during heating at T_j affects only to the pTRMs with unblocking temperatures lower than T_{j-1} at the previous heating step. For the Shaw method, Kono (1978) proposed that TRM acquisition was correctable using the slope of linear portion in the ARM diagram before and after heating. Rolph and Shaw (1985) generalized this correction technique to the nonlinear relationship in the ARM diagram. Tsunakawa and Shaw (1994) pointed out that the validity of the ARM correction should be examined by the double heating test.

By these methods, a number of the absolute paleointensities have been measured and accumulated in the last decades. They provide us with the information of the ancient dipole moment. Since the intensity of the geomagnetic field usually varies with time, the time-averaged value of the ancient dipole moments is one of the keys to evaluate geomagnetic activities. Especially for the last few million years, it is very important to know the recent geomagnetic behavior. For example, McFadden and McElhinny (1982) estimated the time-averaged virtual dipole moment (VDM) as $8.67\pm3.63\times10^{22}\mathrm{Am}^2$ for the last 5 Ma based on 166 volcanic data. This is almost the same as the present dipole moment ($\sim8\times10^{22}\mathrm{Am}^2$), and this conclusion was not largely changed in the later analysis by Kono and Tanaka (1995). They analyzed the updated database (Tanaka and Kono, 1994) and obtained a mean VDM of $7.84\pm3.80\times10^{22}\mathrm{Am}^2$ for the last 10 Ma.

This database, however, involves the paleointensity data with irrespective of the qualities. Since most paleomagnetists consider that the Coe's version of the Thellier method is the only reliable technique to provide robust paleointensity estimates (e.g. Selkin and Tauxe, 2000), Juarez and Tauxe (2000) claimed the quality of the database. They carefully examined the Montpellier 1998 database (Perrin et al., 1998), which was updated from Tanaka and Kono (1994), applying more stringent selection criteria and rejecting data other than those by the Coe's version of the Thellier method. Adding their new paleointensities from submarine basaltic glasses, they determined the time-averaged virtual axial dipole moment (VADM) for 0.3-5 Ma period to be $5.49\pm2.36\times10^{22}$Am^2. This is not far from the several calibrated relative paleointensity records (e.g. $3.9\pm1.9\times10^{22}$Am^2 for the last 4 Ma (Valet and Meynadier, 1993) and $6.0\pm1.5\times10^{22}$Am^2 for the last 800 ka (Guyodo and Valet, 1999a)), though these calibrations seem to be insufficient (e.g. Guyodo and Valet, 1999b).

On the contrary to the robustness of the Coe's version of the Thellier method, recent studies have revealed that this method occasionally yields the erroneous absolute paleointensities. For instance, Tanaka and Kono (1991) obtained 48% higher paleointensity from one out of five specimens from the Hawaiian 1960 lava. Tanaka et al. (1995) observed 15-26% overestimated field intensities from 3 out of 5 samples of the Oshima 1951 lava. In their study, 1 out of 3 results from the Oshima 1986 lava also gave 25% higher value than the expected. Miki (1999) reported that 1 out of 8 samples from the 1946 Sakurajima lava showed 25% higher filed intensity. Accordingly, it is then questioned that the VADM estimation by Juarez and Tauxe (2000) may also take such erroneous data.

In this thesis, we will retrieve the reliable geomagnetic dipole moments for the last 4 Ma. First, the reliability of the paleointensity determinations is examined by applying the Coe's version of the Thellier method to the Hawaiian 1960 lava (Chapter 2). This is one of the typical hotspot basalts frequently used for the absolute paleointensity studies. The validity of the recently proposed paleointensity determination method (LTD-DHT Shaw method; Tsunakawa et al., 1997; Tsunakawa and Yamamoto, 1999) is also tested since it seems to work as the alternative one. Secondly, the paleodirectional and geochronological studies are performed on the volcanic rocks from the Society Islands, French Polynesia (Chapter 3). This is because the precise paleointensity studies require authentic paleodirectional and geochronological records. Finally, by the LTD-DHT Shaw method, the

reliable absolute paleointensities are measured from the Society samples for the last 4 Ma (Chapter 4). Based on the obtained results, the geomagnetic dipole fields are discussed.

Chapter 2

Paleointensity study of the Hawaiian 1960 lava: Implications for possible causes of erroneously high intensities

2.1 Introduction

The complete restoration of the ancient geomagnetic field requires the absolute paleointensities together with the field directions. As natural remanent magnetization (NRM) of volcanic rocks is basically originated from thermoremanent magnetization (TRM), comparison of NRM with TRM given in a laboratory field can yield an absolute paleointensity assuming the linearity law of TRM. There are two major methods to determine the paleointensity; the Thellier method (Thellier and Thellier, 1959) and the Shaw method (Shaw, 1974).

The Thellier method and its modified version by Coe (1967) have been considered as the most reliable paleointensity determination. However, there are some problems on obtaining accurate paleointensities. One is a non-ideal behavior of multi-domain (MD) components. Levi (1977) reported that the Thellier method with MD magnetites resulted in non-linear (concave-up) trends on Arai diagrams and their lower blocking temperature portions led to apparently high paleointensities. This MD effect was confirmed by Xu and Dunlop (1995) since the degree of convexity increased with grain size in their studies.

There is another serious problem, namely, TCRM problem. TCRM (thermochemical remanent magnetization) is acquired by grain growth of new magnetic minerals below their Curie temperatures and can be a part of NRM during initial cooling of volcanic rocks. Kellogg et al. (1970) studied the TCRM effect on the paleointensity determination, applying the Thellier method to the basaltic samples from the northern New Mexico. They suggested that the paleointensity experiments could give reasonable values even if TCRM shared considerable part of the NRM. However, Tanaka and Kono (1991) obtained an anomalous paleointensity from the Hawaiian 1960 lava in the big island of Hawaii by the Coe's version of the Thellier method. This result gave 48% stronger value than the expected, despite that it satisfied all the strict criteria. Several authors (Mankinen and Champion, 1993; Tsunakawa and Shaw, 1994) have mentioned that TCRM might be a source of the erroneous result of the Hawaiian 1960 lava. Since the TCRM problem is critical for the paleointensity determination, we will examine its possibility by the Thellier method.

We will also apply the Shaw method for the comparative study. The Shaw method has been criticized mainly because of the poor theoretical background. The most severe critique against the Shaw method is its laboratory heating above the Curie temperature, which usually changes TRM acquisition capacity of samples. The ARM correction in the modified Shaw method (Kono, 1978; Rolph and Shaw, 1985) have not been well studied theoretically besides a few studies (e.g. Tanaka, 1999), and sometimes lead to an erroneous paleointensity. Kono (1987) showed that the ARM correction would give a different paleointensity up to 40% for some recent basalts by 300-minute laboratory heating. Vlag et al. (2000) pointed out that the ARM correction by Rolph and Shaw (1985) might not be valid for the laboratory transformation of Ti-rich titanomagnetite into a magnetite-ilmenite intergrowth because of insensitivity of ARM coercivity spectra to the transformation. Comprehensive reviews of the global paleointensity database published recently did not accept the results by the Shaw method (e.g. Juarez and Tauxe, 2000; Selkin and Tauxe, 2000; Tarduno et al., 2001).

Most of the previous Shaw-type measurements have been performed with a single laboratory heating. There have been, however, some studies on improvement of the Shaw method. Tsunakawa and Shaw (1994) proposed the double heating technique of the Shaw method (DHT Shaw method) which can test the validity of the ARM correction

for individual samples by heating them twice. They applied this technique to some lava flows with known paleofield and the samples passing the double-heating test, except for one, showed good agreement with the expected values within 10% difference. For the Hawaiian 1960 lava, they rejected two erroneously high intensities by this technique and successfully obtained an appropriate value of 34.5μT. Tanaka et al. (1997) also reported a validity of the double heating test in the Shaw method.

In this chapter, we have performed the systematic paleointensity determinations on the Hawaiian 1960 lava in order to examine causes of its anomalous behavior. This lava yielded both reasonable and anomalous paleointensities in the previous studies, though they are typical hotspot basalts usually used for the absolute paleointensity studies. The applied methods were the Coe's version of the Thellier method (Coe, 1967) and the double heating technique of the Shaw method combined with low temperature demagnetization (LTD-DHT Shaw method; Tsunakawa et al., 1997; Tsunakawa and Yamamoto, 1999). In the Thellier method, the LTD was also conducted for some specimens to evaluate the effect of multi-domain (MD) components. Microscopic observations and measurements of hysteretic parameters were further performed to clarify the relationship between the rock magnetic properties and the resultant paleointensities.

2.2 Samples

We collected paleomagnetic core samples from the Hawaiian 1960 lava flow by a portable engine drill in March of 1998. All the samples were orientated by both sun and magnetic compasses. The sampling site is a roadcut of the exposed lava with about 4m in thickness and about 15m in width (19°30.43N, 154°50.46W). As the core positions were separated into four sub-sites (Figure 2.1), their sample IDs were named as A-1 to A-5, B-1 to B-7, B-8 to B-10 and C-1 to C-5 with a reference of their rock magnetic properties described in the next section. Each core was cut into several sister specimens in order to apply the Thellier and the LTD-DHT Shaw methods. The expected field intensity is 36.2μT from the DGRF 1965 (Tanaka and Kono, 1991).

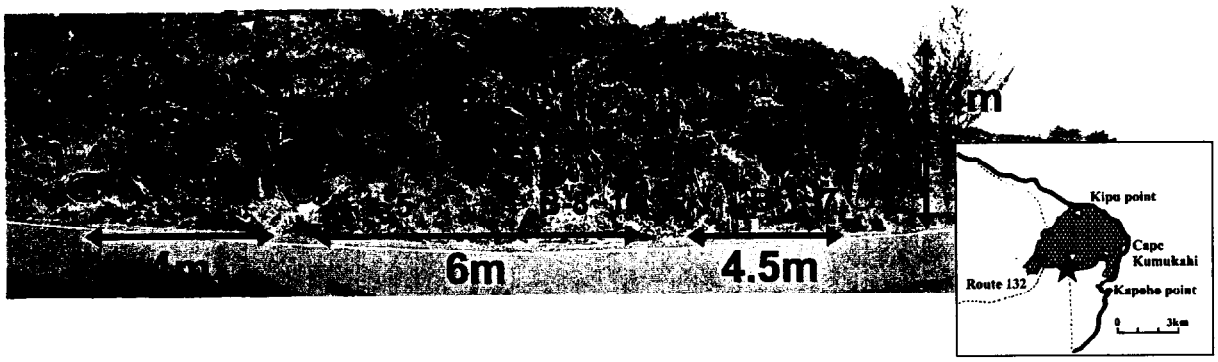

Figure 2.1: Sampling site of the Hawaiian 1960 lava.
In the lower right figure, the sampling location is shown by solid star. Daubed area and hatched region indicate the scoria cone and flow of the 1960 lava, respectively (After the Geologic map of the island of Hawaii compiled by Wolfe and Morris).

The paleointensity of this lava has been already measured in the previous studies. Tanaka and Kono (1991) obtained 48% higher field intensity from one out of five successful results, whereas other four specimens gave the concordant average of 37.0±3.9μT. Tsunakawa and Shaw (1994) reported an intensity of 34.5μT from one specimen by the DHT Shaw method while the other two specimens did not pass their selection criteria. Valet and Herrero-Bervera (2000) compared the coercivity spectra between NRM and TRM without the ARM test and gave an average of 41.1μT from 7 out of 10 specimens. Hill and Shaw (2000) applied the microwave method to the samples from two vertical sections of the lava. One section exhibited a good linear behavior with a mean paleointensity of 33.0±3.9μT. However, the other section showed an anomalous two-slope behavior, resulting in a mean value of 43.4±9.7μT when the first slopes were adopted. Compiling the paleointensities reported so far, they range from 27.0μT to 68.7μT.

2.3 Rock magnetic properties

Based on the ARM spectra obtained in the LTD-DHT Shaw method (see the section 2.4.2), the four sub-sites can be classified into three rock magnetic groups of A (sample ID of A-1~5), B (B-1~10) and C (C-1~4). Their averaged patterns of the LT memories and the LT demagnetized components are illustrated in Figures 2.2(A)-(C). As these LT memories are similar to those of NRMs and TRMs, they can represent the LTD characteristics of the remanences.

Thermomagnetic analyses were carried out for the representative samples of each rock magnetic group in helium gas flow by a vibrating sample magnetometer (MicroMag 3900 VSM, Princeton Measurement Corporation). All of the samples had the similar main phase corresponding to titanium-poor titanomagnetite with $x \sim 0.05$ (Figures 2.2(D)-(F)). We also measured hysteresis properties of saturation magnetization (M_s), remanent saturation magnetization (M_{rs}), coercivity (H_c) and remanent coercivity (H_{rc}) for five small chips from each core. The Day plot (Day et al., 1977) show clusters corresponding to the rock magnetic groups as in Figure 2.2(G). Though all the points are plotted in the pseudo-single domain (PSD) area, they can be interpreted as an admixture of SD and MD, referring the microscopic observations. If such an admixture is assumed, MD components decrease in the order of the groups C, B and A. This order is supported from the ratio of the LT demagnetized components to the LT memories for ARM (Figures 2.2(A)-(C)). MD components are, however, considered to be not so large in NRM because the total amount of NRM demagnetized by LTD was less than 13%.

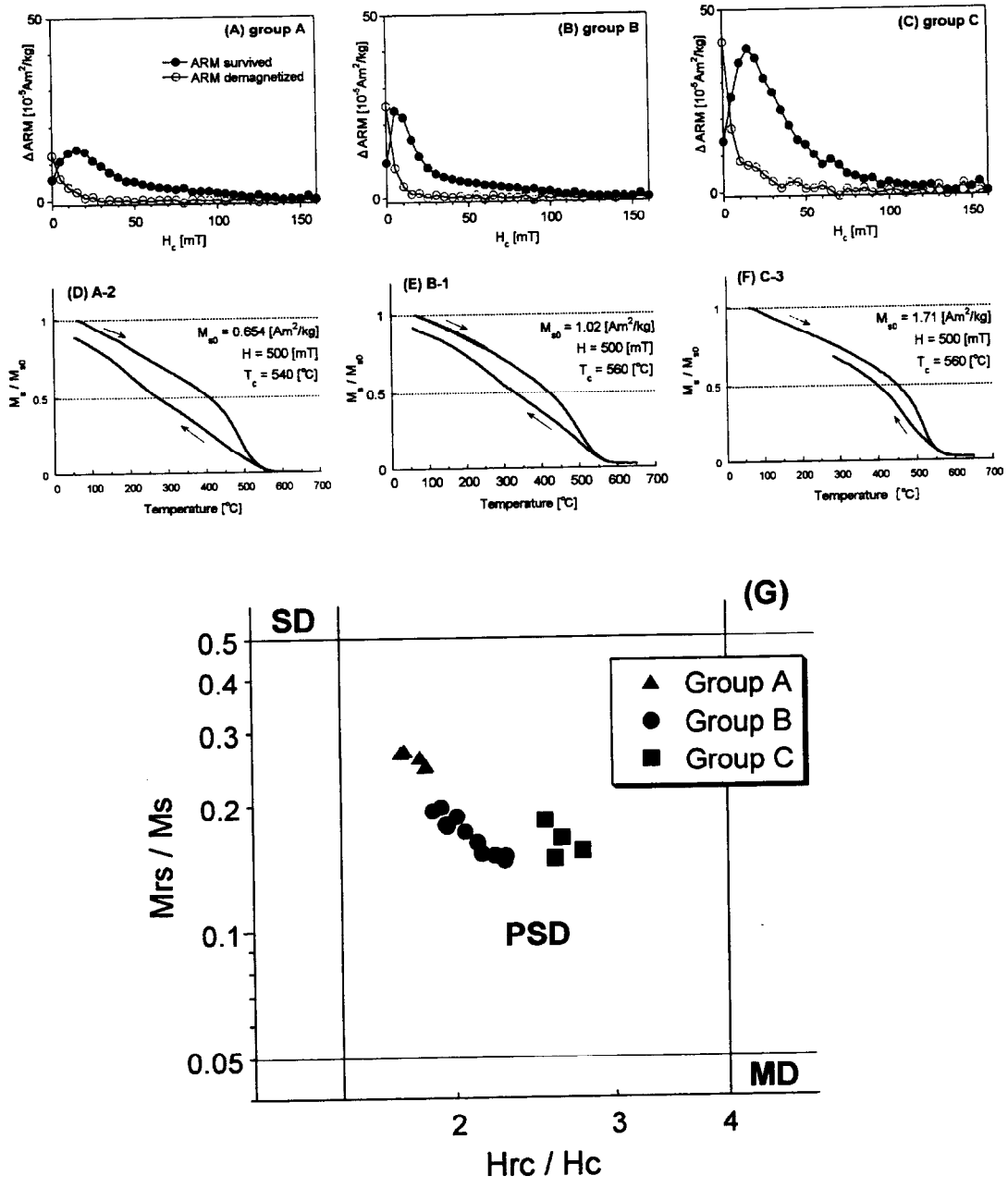

Figure 2.2: Results of the rock magnetic experiments.
(A)-(C) Patterns of the ARM coercivity spectra survived and demagnetized by LTD before laboratory heating. The vertical axis indicates a difference of ARM between adjacent coercivities while the horizontal axis indicates coercivity.
(D)-(F) The measured thermomagnetic curves for each group. The vertical axis indicates a normalized saturation magnetization in a DC field of 0.5T.
(G) Day plot for all the measured cores. The coordinates are logarithmic. The data points are resulted from the averages for five small chips of each core.

Several samples from each group were observed by a microscope with reflected light (Figure 2.3). According to Wilson and Watkins (1967), high temperature oxidation indices were defined as follows.

I. Homogeneous titanomagnetite.

II. Titanomagnetite containing a few ilmenite lamella.

III. Titanomagnetite with abundant ilmenite lamella.

IV. Titanomagnetite shows signs of incipient alteration to titanohematite.

V. Both ilmenite and titanomagnetite are oxidized to rutile, although some relic areas of titanomagnetite may exist.

VI. Maximum degree of oxidation characterized by the high temperature index mineral pseudobrookite.

The dominant phase was recognized to be Class II, III and VI for the groups A, B and C, respectively. Taking other minor phases into account, we identify these oxidation indices as I-III, II-IV and IV-VI. Especially there are many pseudobrookites in the group C. This classification was confirmed by the observations with an electron probe micro analyzer (EPMA) in Figure 2.4, and by the total intensities of ARM before the laboratory heating. The ARM intensities clearly increased in the order of the groups A, B and C. It is consistent with the observations by Watkins and Haggerty (1967) that there is a positive relationship between the magnetization intensity and the oxidation degree. Hence the deuteric oxidation might have progressed in the order of A, B and C. This can be explained by that the higher degree of deuteric oxidation produces more amounts of titanium-poor titanomagnetites.

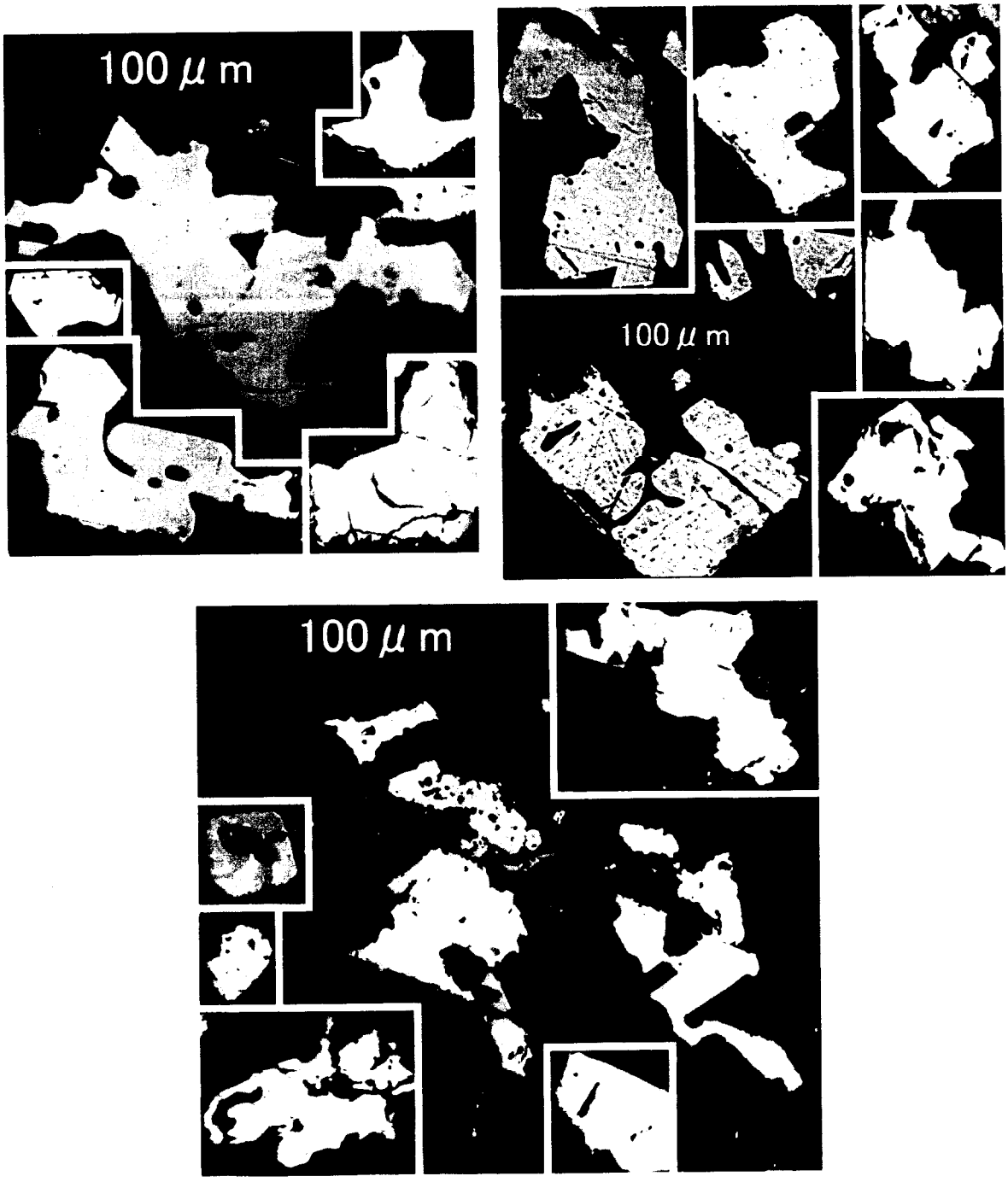

Figure 2.3: Reflected light microscopy of the opaque minerals for each rock magnetic group. (A) Oxidation index of I-III for group A, (B) II-IV for B and (C) IV-VI for C. The black bar indicates a scale of 100μm.

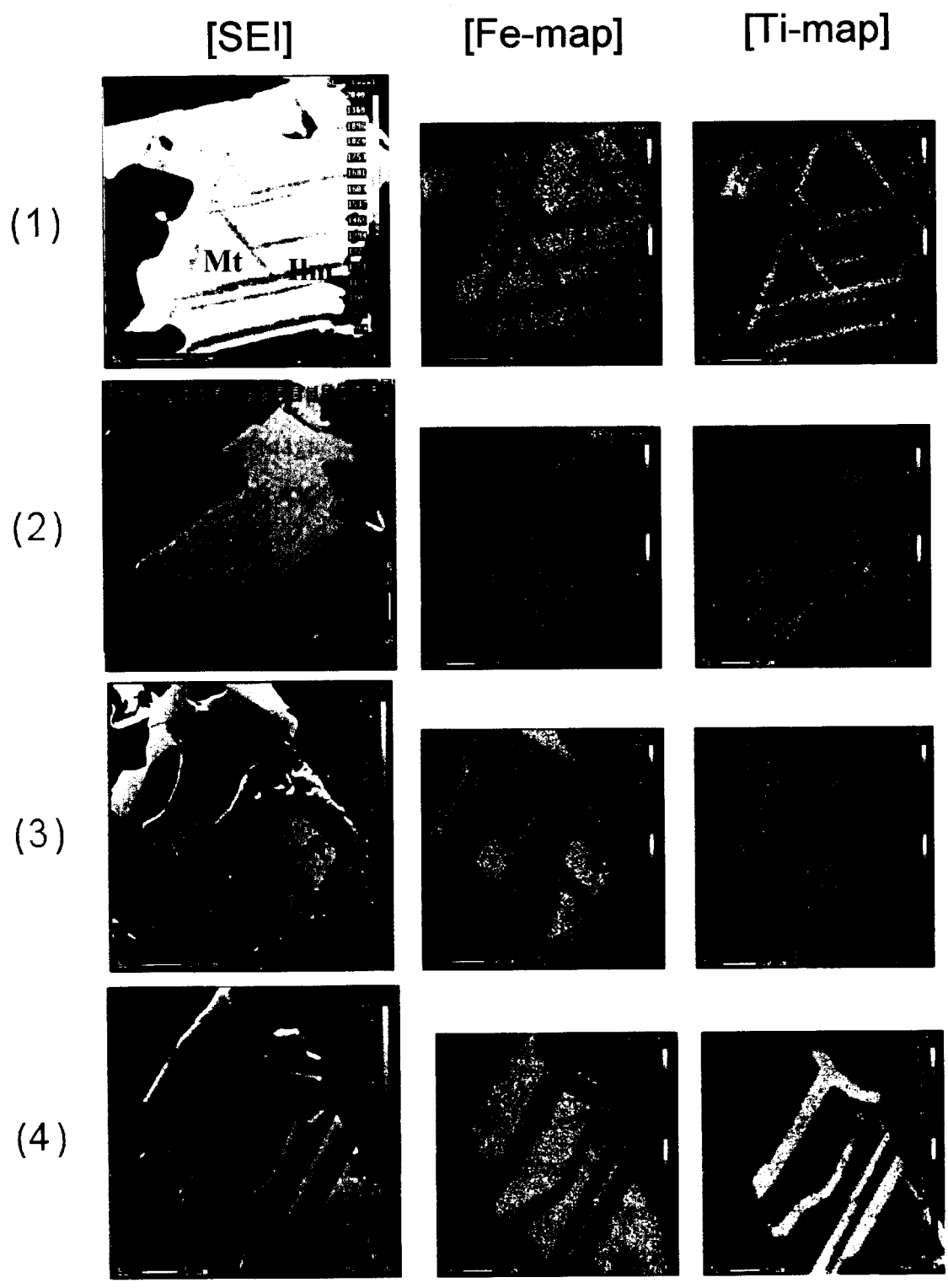

Figure 2.4: EPMA photographs of the representative magnetic minerals in (1) B-1, (2) A-2 and (3, 4) C-3. The oxidation index is identified to be (1) II, (2) III, (3) IV and (4) VI. The left, middle and right columns are secondary electron images (SEI), maps of Fe and Ti, respectively. Labels are as follows; Mt: titanomagnetite, Ilm: ilmenite, Hem: titanohematite, Rt: rutile.

2.4 Paleointensities

2.4.1 Coe's version of the Thellier method

The Coe's version of the Thellier method (Coe, 1967) was applied to 19 core specimens. The specimens were subjected to the stepwise heating at $20-50°C$ intervals up to 600°C in air with an electric furnace (Natsuhara-Giken TDS-1). As we held the top temperature as shortly as possible in order to avoid the sample alteration, the hold time was taken to be 6 minutes. The reproducibility of the top temperature was better than $\pm 1°C$. TRM was given in a $30\mu T$ DC field at each step, and all the remanent magnetizations were measured by a spinner magnetometer (Natsuhara-Giken SMD-88) with a resolution better than $\pm 10^{-8} Am^2$. The experimental results are judged by the following selection criteria.

1. Primary component of NRM is recognized in the orthogonal plot of thermal demagnetization.

2. Linear portion of the primary component in the Arai diagram is not less than 15% of the original NRM. This portion is defined by a number of the data points ($N \geq 5$), and is composed of the low-temperature segment rather than the high-temperature. Excessive systematic curvature should be avoided.

3. Considering the experimental uncertainties due to the precision of magnetization measurements, the reproducibility of heating temperatures and the precision of applied field magnitudes, pTRM is not significantly different from the corresponding TRM at a 2σ level in the pTRM test.

The results are discarded unless they satisfied the criteria. These criteria are almost the same as Coe's (Coe, 1978) but more stringent in terms of a number of the data points. Magnetic susceptibilities were also measured at each step with a susceptibility magnetometer (Bartington MS2) as another monitor of the sample alteration in the laboratory heating. Their changes, however, did not exceed $\pm 10\%$ of the original values in all the cases.

The experimental results are summarized in Table 2.1 with a correlation coefficient (r), a quality factor (q; Coe, 1978) and NRM fraction (f) of the linear portions. The calculated paleointensities range from 36.0μT to 69.0μT with a success rate of 17/19. The overall average of 49.0±9.6μT is about 35% higher than the expected. According to the rock magnetic classification, these results are described below for each group. Their representative diagrams are also shown in Figures 2.5(A)-(C).

Group A

4 out of 5 specimens passed the pTRM test up to 450-500°C. Linear portions consist of 29-50% of NRM. The average paleointensity of 41.9±4.2μT (N=4) is slightly higher than the expected.

Group B

9 out of 10 specimens passed the criteria and yielded the paleointensities higher than 47μT. The linear portions, consisting of 36-95% of NRMs, give an average intensity of 56.0±7.6μT (N=9) which is 55% higher than the expected. Since the relatively high blocking temperature portions did not pass the pTRM test for most specimens, some thermal alteration occurred during the laboratory heating at high temperatures.

Group C

All the specimens show good linearity extending to the high blocking temperature portions. Thus they have the best quality factors (q>44) among the groups. The linear portions are composed of more than 90% of their NRMs and an average paleointensity is calculated to be 40.6±3.2μT (N=4).

The average intensities of the groups A and C are concordant with the expected value in a 2σ level while that of the group B is significantly larger. In the group B, the standard deviation was 14% (1σ) of the mean, indicating a relatively good result of the internal consistency, that is, the multi-specimen test. If we do not know either the expected field intensity or the data from other sub-sites, the higher average of 56.0μT may be regarded as the representative. This suggests that it is very important to collect and measure samples with various rock magnetic properties.

One may consider that the erroneous paleointensities can be excluded by more stringent selection criteria, though no definite criteria have been established. If a relatively crucial condition of $q \geq 5$ is adopted, only one result of A-5-3 (44.4μT) is rejected (Table 2.1). The correlation coefficient is another candidate as a crucial criterion, for example, $r \geq 0.980$ in Tanaka et al. (1995). If we adopt the further stringent criteria of $q \geq 5$ and $r \geq 0.995$, they screen the results of A-1-3 (45.3μT) and A-5-3 (44.4μT) for the group A and B-1-3 (61.5μT), B-7-3 (63.3μT) and B-8-1 (51.9μT) for the group B. This drastically changes the overall success rate, decreasing to be 12/19, but the mean intensity of the group B is still a higher value of 54.6$\pm$8.4μT. If the condition of $r \geq 0.999$ is applied, only the paleointensities from the group C are survived and then give a reasonable average. These results indicate that the usual selection criteria do not work well to discriminate inappropriate data, at least, for the Hawaiian 1960 lava.

specimen	NRM_0	PTRM	T_1-T_2	N	r	q	f	slope	F (μT)
A-1-3	173	20-500	250-500	7	0.987	5.10	0.455	1.51±0.11	45.3**
A-2-3	172	20-500	165-500	8	0.997	11.4	0.477	1.39±0.05	41.7
A-3-3	229	20-500	20-500	8	0.995	9.90	0.498	1.20±0.05	36.0
A-4-3	227	-	-	-	-	-	-	-	-
A-5-3	211	20-450	20-450	6	0.991	3.45	0.288	1.48±0.10	44.4*
B-1-3	330	20-500	20-475	7	0.987	5.88	0.513	2.05±0.15	61.5**
B-2-1	332	20-500	250-500	7	0.998	14.3	0.474	1.63±0.04	48.9
B-3-3	342	20-500	300-500	6	0.997	10.1	0.476	1.97±0.07	59.1
B-4-3	312	20-580	250-475	6	0.996	6.41	0.359	2.30±0.10	69.0
B-5-1	323	20-500	20-500	8	0.998	16.6	0.516	1.82±0.05	54.6
B-6-3	321	20-570	165-570	10	0.997	27.5	0.947	1.60±0.05	48.0
B-7-3	402	20-540	250-520	8	0.988	8.08	0.609	2.11±0.13	63.3**
B-8-1	142	20-540	250-520	8	0.991	8.86	0.579	1.73±0.10	51.9**
B-9-3	146	20-500	250-500	7	0.998	13.4	0.465	1.59±0.05	47.7
B-10-1	163	20-350	-	-	-	-	-	-	-
C-1-3	352	20-600	20-600	13	0.999	76.3	0.988	1.33±0.01	39.9
C-2-3	583	20-600	20-600	13	0.999	47.0	0.966	1.49±0.02	44.7
C-3-3	521	20-600	20-600	13	1.00	98.0	0.981	1.36±0.01	40.8
C-4-1	249	20-580	20-580	12	0.999	44.1	0.921	1.23±0.02	36.9
A-4-4L	209	20-450	20-425	5	0.989	2.60	0.301	2.85±0.24	85.5*
B-9-4L	129	20-500	20-425	5	0.999	9.53	0.286	2.72±0.06	81.6
C-4-4L	367	20-600	250-560	10	0.999	45.9	0.873	1.25±0.02	37.5

Table 2.1: Experimental results by the Thellier method.
NRM_0, NRM intensity in $10^{-5}Am^2/kg$; PTRM, acceptable temperature intervals in the pTRM test; T_1-T_2 , N, temperature intervals and number of the data included in the linear segments; r, q, f, correlation coefficient, quality factor and NRM fraction of the linear NRM-TRM portion in the Arai diagram; slope, slope of the linear NRM-TRM fraction; F, calculated paleointensity. TRM was induced in a laboratory DC field of 30.0μT. A-4-4L, B-9-4L and C-4-4L are the results of the LTD version (see the text).
* Rejected if the additional selection criterion of $q \geq 5$ is applied.
** Rejected if the additional selection criteria of $q \geq 5$ and $r \geq 0.995$ are applied.

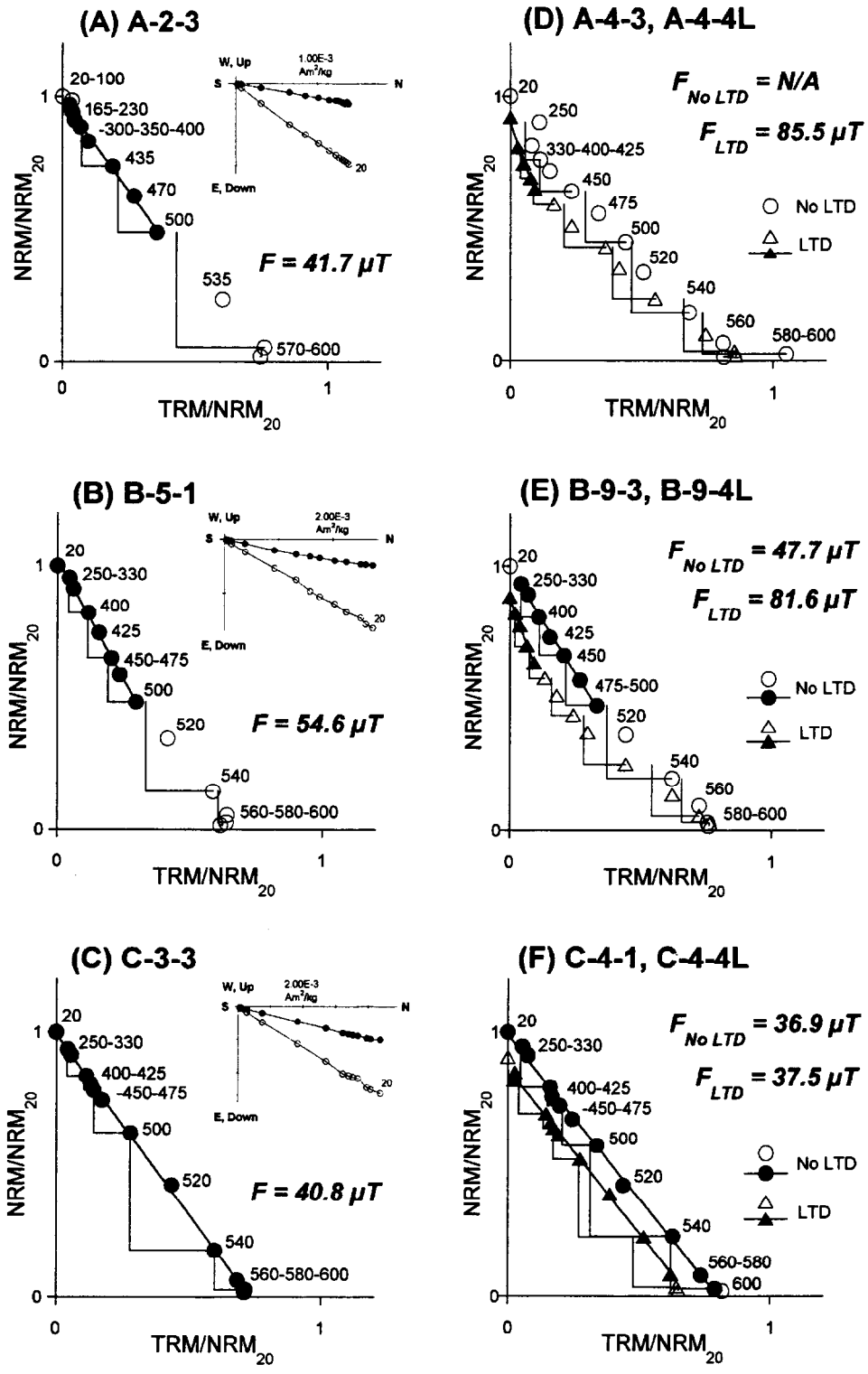

Figure 2.5: Results of the Thellier experiments.
(A)-(C) Representative results for each rock magnetic group. Linear portions consist of closed symbols.
(D)-(F) Experimental results by the Thellier method with and without the LTD treatment for each group. In these figures, the LT memories of NRM and TRM are plotted. The temperature steps are the same in both versions.

2.4.2 LTD-DHT Shaw method

We applied the LTD-DHT Shaw method (Tsunakawa et al., 1997; Tsunakawa and Yamamoto, 1999) to sister specimens from the 19 cores used in the Thellier method. Its procedures are shown in Figure 2.6. Since LTD is known to be an effective technique for extracting single-domain (SD) like remanences and demagnetizing MD-like components of titanium-poor titanomagnetite (e.g. Ozima et al., 1964; Heider et al, 1992), the LT memories of the measured samples are considered to be composed mainly of SD and PSD components. The LTD-DHT Shaw method has the following additional treatments compared with the previous DHT Shaw method (Tsunakawa and Shaw, 1994).

1. NRM, TRM1 and TRM2 are subjected to LTD and their LT memories are measured.

2. For ARM, the AF demagnetization is firstly conducted before the LTD treatment (ARM00, ARM10 and ARM20). Then the same ARM is given again and subsequently subjected to LTD and AF demagnetization (ARM0, ARM1 and ARM2).

3. As for the LTD treatment, the specimens are soaked into liquid nitrogen in a plastic bottle for 10 minutes. This bottle is placed in a magnetically shielded case where a residual field is less than 100nT. Taken from the bottle, the specimens are warmed up to the room temperature in the same case for about 60 minutes.

The AF demagnetization was carried out at 5 or 10mT intervals up to a peak field of 160mT, sometimes up to 180mT. All the specimens were heated twice at 610°C in the electric furnace for 10 minutes in the first heating (TRM1) and 20 minutes in the second heating (TRM2), applying a DC field of 30μT to give a whole TRM. In the experiment, most specimens were heated in air while two (A-5-2N and B-6-1N) in nitrogen gas flow. ARM was given in a 100μT DC field parallel to NRM or TRM, associated with an AC field of 160mT or 180mT. All the remanence measurements and the AF demagnetizations were performed by an automatic spinner magnetometer (Natsuhara-Giken DSPIN-2) (Kono et al., 1984; Kono et al., 1997) with a resolution better than $\pm 10^{-7}$Am^2. The total time for demagnetization and measurement of a specimen was about 1 hour.

All the magnitudes of remanences were calculated from vector subtraction between the measured AF step and the maximum AF step. The ARM correction was applied to

TRM1 and TRM2 in the following way (Rolph and Shaw, 1985).

$$\mathrm{TRM1}^* = \mathrm{TRM1} \cdot \frac{\mathrm{ARM0}}{\mathrm{ARM1}}$$

$$\mathrm{TRM2}^* = \mathrm{TRM2} \cdot \frac{\mathrm{ARM1}}{\mathrm{ARM2}}$$

where TRM1, TRM2, ARM0, ARM1 and ARM2 are the remanence magnitudes at each AF step. This correction was tested in the second heating experiment for the individual specimens. The experimental results are judged by the following selection criteria similar to the Thellier method.

1. Primary component of NRM is recognized in the orthogonal plot of AF demagnetization.

2. Linear portion in the NRM-TRM1* diagram, which should consist of the primary component of relatively higher coercivity, is not less than 15% of the original NRM ($f_N \geq 0.15$). The linear portion is defined by the correlation coefficient ($r_N \geq 0.995$) and the number of data points ($N \geq 5$).

3. Linear portion in the TRM1-TRM2* diagram is determined in the same way as in the above ($r_T \geq 0.995$, $N \geq 5$). This fraction is not less than 15% of the original TRM1 ($f_T \geq 0.15$).

4. A slope of the linear portion in the TRM1-TRM2* diagram ranges in 1.00±0.05, because the representative experimental error is estimated to be ±5% in the present study.

The experimental results are summarized in Table 2.2 and shown in Figure 2.7 for their representatives. The successful paleointensities range from 31.2μT to 52.8μT. In spite of the low success rate of 9/19, the average of 39.4±7.9μT is fairly improved when compared with the Thellier results. Major reasons of such a low success rate are that (1) the linear portions are not detected in the NRM-TRM1* diagrams ($r_N < 0.995$) and that (2) the slopes of the linear portion in the TRM1-TRM2* diagrams are out of 1.00±0.05. It is easily seen that the two paleointensities of B-4-2 (52.8μT) and C-2-2 (51.9μT) are much higher than the others (31.2~39.9μT). Thus the standard deviation is not small (20%). If these two are excluded as outliers, the standard deviation becomes significantly smaller (9%) with the corresponding average of 35.7±3.3μT (N=7). This average value is consistent with the expected one.

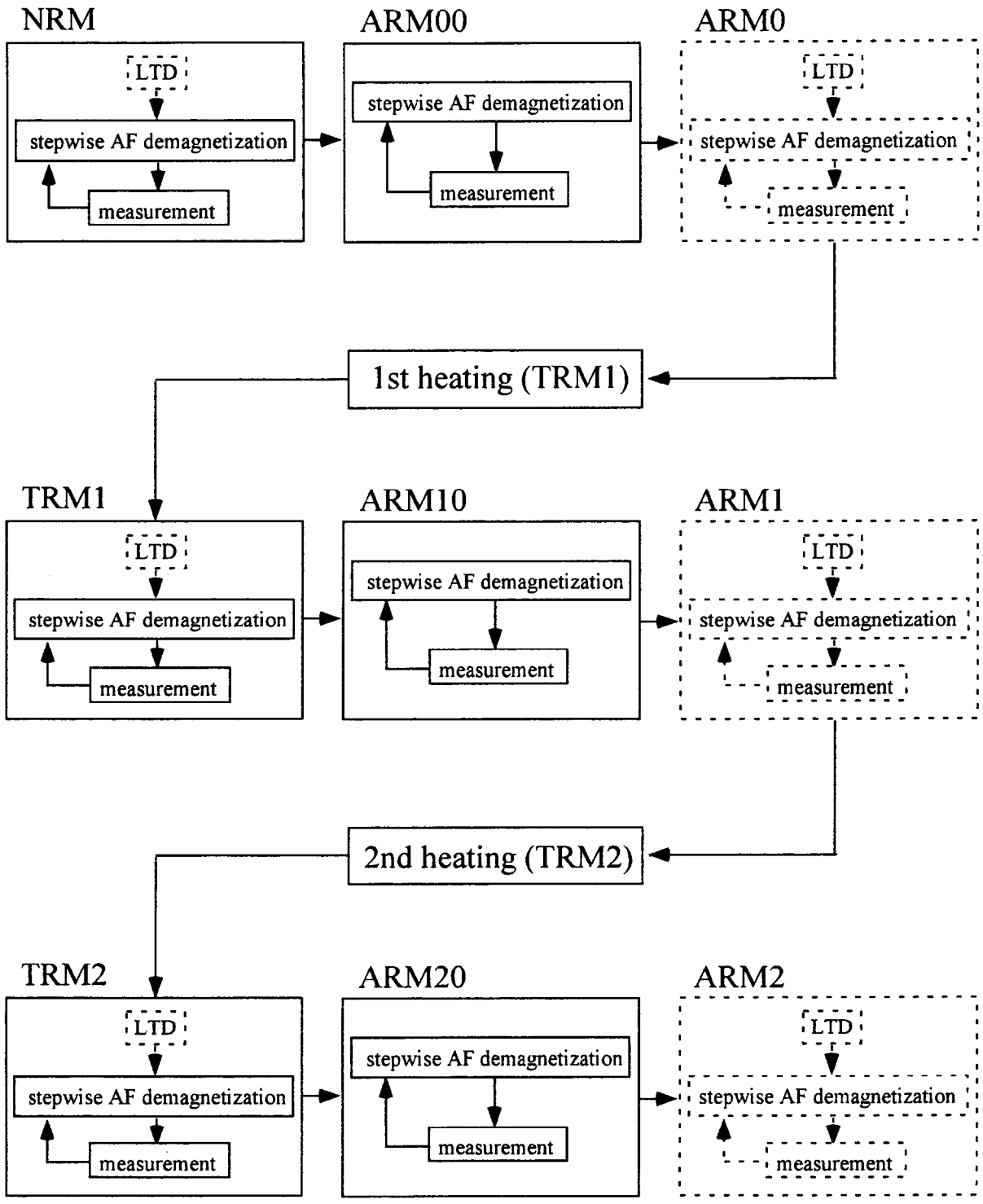

Figure 2.6: Experimental procedures of the LTD-DHT Shaw method (Tsunakawa et al., 1997; Tsunakawa and Yamamoto, 1999). This method employs some additional procedures as indicated by the dotted-line box when compared with the previous double heating technique (Tsunakawa and Shaw, 1994).

specimen	First heating					Second heating					F
	H_L	$slope_A$	$slope_N$	f_N	r_N	H_L	$slope_A$	$slope_T$	f_T	r_T	(μT)
A-1-2	0	0.827	0.845	1.00	0.996	0	0.847	*1.08*	1.00	1.00	-
A-2-1	0	1.07	1.12	1.00	0.996	0	0.901	1.05	1.00	0.999	33.6
A-3-2	35	1.24	1.58	0.536	*0.981*	0	0.956	1.03	1.00	0.999	-
A-4-2	55	1.27	1.10	0.338	0.995	0	0.822	1.01	1.00	0.999	33.0
A-5-2N	35	1.26	1.33	0.526	0.998	0	0.961	1.03	1.00	1.00	39.9
B-1-1	25	1.01	1.62	0.458	*0.992*	0	1.03	1.03	1.00	0.999	-
B-2-1	30	0.850	1.23	0.388	0.995	0	0.907	0.989	1.00	1.00	36.9
B-3-1	25	1.03	1.67	0.478	*0.991*	0	0.924	*1.11*	1.00	1.00	-
B-4-2	20	1.00	1.76	0.582	0.997	0	0.969	1.01	1.00	0.999	52.8
B-5-2	35	0.966	2.12	0.467	0.997	0	0.949	*1.09*	1.00	0.999	-
B-6-1N	45	1.09	1.72	0.382	0.997	45	0.898	*1.28*	0.281	0.998	-
B-7-1	30	0.985	2.15	0.491	*0.994*	0	0.931	1.05	1.00	0.999	-
B-8-3	35	0.815	1.15	0.351	0.995	0	0.891	*0.933*	1.00	0.999	-
B-9-1	35	1.01	1.83	0.363	*0.984*	0	0.953	1.02	1.00	0.999	-
B-10-2	20	0.733	1.04	0.566	0.995	0	0.832	0.958	1.00	1.00	31.2
C-1-2	5	0.847	1.18	0.962	0.999	40	1.12	0.954	0.294	0.998	35.4
C-2-2	5	0.844	1.73	0.971	0.999	10	1.04	0.968	0.825	1.00	51.9
C-3-2	10	0.889	1.32	0.860	0.999	30	1.13	1.01	0.420	0.998	39.6
C-4-2	5	0.774	1.13	0.958	0.997	50	1.06	*1.20*	0.210	0.994	-

Table 2.2: Experimental results by the LTD-DHT Shaw method.
H_L, the lowest coercivity force taken for the linear segments; $slope_A$, slopes of ARM spectra ($\geq H_L$) before and after the heating; $slope_N$, $slope_T$, slopes of the linear segments in the NRM-TRM1* and TRM1-TRM2* diagrams; r_N, r_T, correlation coefficients of the linear NRM-TRM1* and TRM1-TRM2* segments; f_N, f_T, NRM and TRM1 fractions of the linear NRM-TRM1* and TRM1-TRM2* segments; F, calculated paleointensity. TRM was induced in a laboratory DC field of 30.0μT. "N" denotes the specimens heated in nitrogen gas flow. Italic numbers are indicated to be out of the selection criteria.

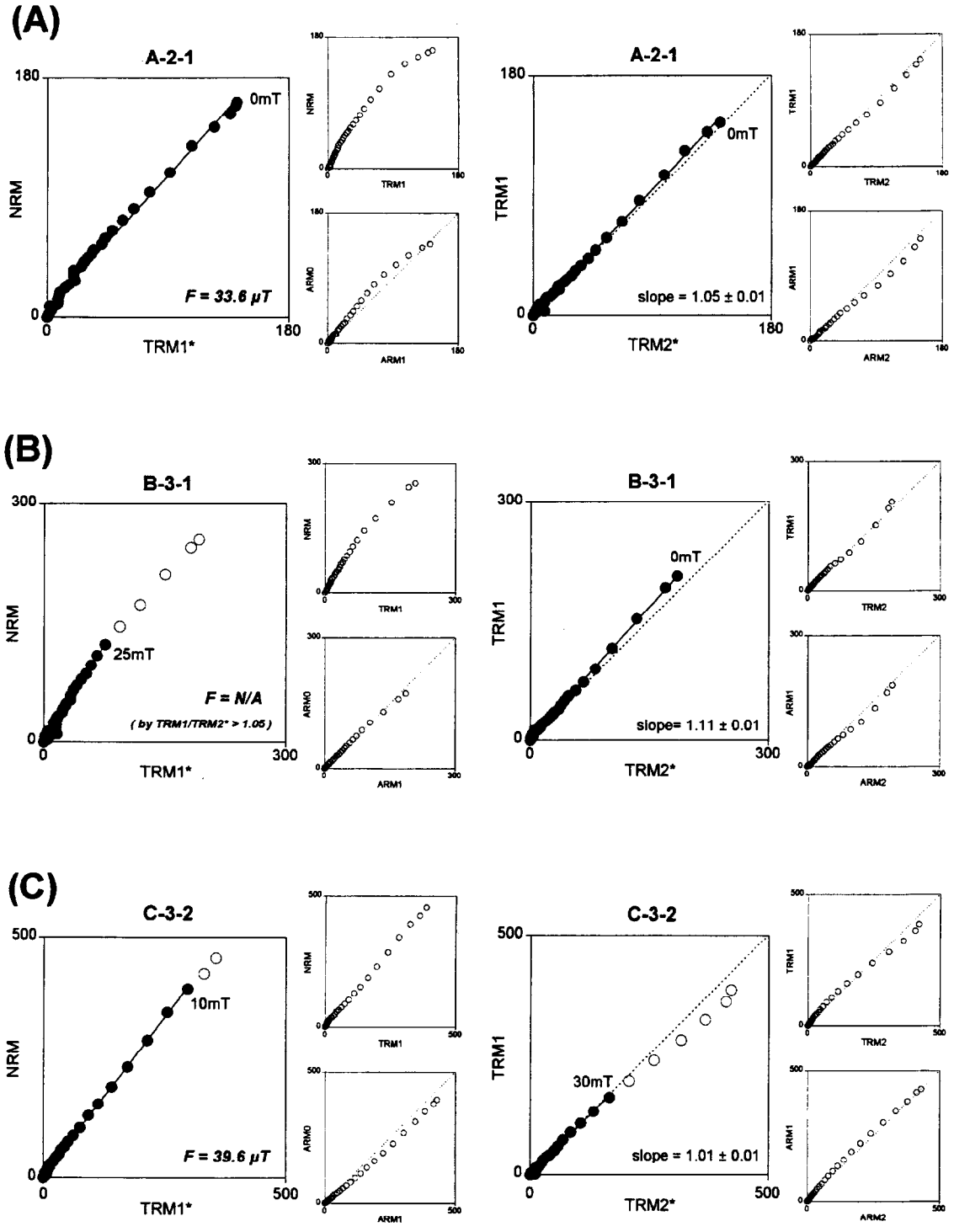

Figure 2.7: Representative results by the LTD-DHT Shaw method.
Each figure is shown for (A) the group A, (B) the group B and (C) the group C. Solid symbols indicate the linear portion. The result of B-3-1 is rejected because the slope in the TRM1-TRM2* diagram is larger than 1.05.

2.5 Discussion

2.5.1 Causes for the high paleointensities

In the present study, the erroneously high paleointensities were yielded especially from the specimens of the group B by the Thellier method. This is very surprising because these samples have ordinary rock magnetic properties. In this section, four possible reasons for the high paleointensities are examined; (1) terrain effect, (2) multi-domain (MD) components, (3) pseudo-single-domain (PSD) components and (4) thermochemical remanent magnetization (TCRM).

Terrain effect

Baag et al. (1995) measured the ambient geomagnetic field above the recent basalts on the island of Hawaii. According to their observations, the local magnetic field directions are substantially different from the IGRF by up to 20° except for those composed of shelly pahoehoe and a flat thin lava pond. This suggests that we should pay attention to the local terrain effect for a precise paleomagnetic study. In this study, however, the local magnetic anomaly is unlikely to be a main cause for the anomalous paleointensities because of the following reasons.

1. According to the aeromagnetic survey in 1978 (Hildenbrand et al., 1993), the anomaly of the total intensity does not exceed 1μT in Hawaii Island.

2. The magnetic north direction at our sampling site is consistent with that expected from the IGRF 1995 (D=10.1°), since the difference between the orientation data by both sun and magnetic compasses is $-1.9° \pm 2.2°$ (N=18). Assuming that the standard deviation of 2.2° is produced solely by randomly oriented magnetization vectors with constant length, its magnitude is calculated to be 1.4μT, not causing about 55% stronger paleointensities.

3. If the ambient magnetic field were disturbed by the local anomaly, intense NRMs would be acquired at the region with the strong field while weak ones at the low field. In this case the paleointensities should be resulted in proportional to these NRMs, but there is no correlation between the NRM intensities and the paleointensities (Table 2.1).

MD components

It is known that existence of MD components evokes a concave-up curve in an NRM-TRM plot resulting in an apparent high paleointensity (Levi, 1977; Xu and Dunlop, 1995). As the magnetic carriers of our samples are composed of Ti-poor titanomagnetites (x~0.05), the LTD treatment can effectively erase their MD components. We therefore applied the Thellier method combined with the LTD treatment to some sister specimens (A-4-4L, B-9-4L and C-4-4L). As shown in Figures 2.5(D)-(F) together with those by the normal Thellier method, the intensity decreased by LTD is 8-12% in NRM.

The LTD treatment exhibited kind of concave-up features for the groups A and B (Figures 2.5(D) and 2.5(E)). If the MD components seriously affected the present results, the linearity of the diagrams would be improved and gave appropriate paleointensities by the treatment. Their low blocking temperature portions, however, gave much higher paleointensities above 80μT. On the other hand, the good linearity of the group C in the NRM-TRM plot is preserved as in Figure 2.5(F). Resultant paleointensities with and without the treatment (36.9μT and 37.5μT) are almost the same. These results indicate that the MD effect is not a main reason. The Day plot in Figure 2.2(G) may support this conclusion since the largest contribution of MD components appears in the group C.

PSD components

Kosterov and Prévot (1998) studied non-ideal behaviors of the Thellier experiments characterized by a rapid decay of NRM without a relative acquirement of pTRM at moderately low temperatures. They suggested that this behavior was due to the transformation of the micromagnetic structure of PSD grains from a metastable configuration to a more stable one. An irreversible decrease in coercivity at relatively low temperature (up to 200-250°C) would cause such a phenomenon accompanying with an apparently anomalous paleointensity in the Thellier method. This PSD effect may cause the higher paleointensities in this study because all the samples are plotted in the PSD region of the Day-Plot (Figure 2.2(G)). However, the erroneously high paleointensities in the Thellier method are yielded especially from the group B and it is difficult to think that the transformation of PSD selectively works in this group. The two high paleointensities from B-4-2 and C-2-2 by the LTD-DHT Shaw method also do not seem to support the PSD effect since this method does not employ the stepwise laboratory heating. There-

fore the effect of PSD components cannot be the main reason for the high paleointensities.

TCRM

The most striking feature of the Thellier results was that the group C with the highest oxidation indices yielded an appropriate paleointensity whilst all the paleointensities from the group B with intermediate oxidation were systematically higher than the expected. It, therefore, suggests that the oxidation state is related with the erroneous paleointensities. As stated in the several previous studies (Mankinen and Champion, 1993; Tsunakawa and Shaw, 1994), there is a possibility that the Hawaiian 1960 lava acquired TCRM during its initial cooling stage.

In the present study, the specimens from the group C contain pseudobrookites. Since the pseudobrookite cannot form below 585°C (e.g. p.409, Dunlop and Özdemir, 1997), true TRMs are expected to consist of NRMs for the group C. This may be a reason why the group C gives an appropriate paleointensity. On the other hand, a number of small domains of titanium-poor titanomagnetite surrounded by ilmenite lamellas are observed in the group B. This suggests that continuous oxidation possibly occurred below the Curie temperature in the initial cooling stage of the lava. In this case, the titanium-poor titanomagnetites are newly produced and acquire TCRM during the initial cooling. McClelland (1996) modeled the grain-growth chemical remanent magnetization (CRM) of magnetite and hematite and suggested that CRM, equivalent to TCRM in this case, possibly gained a larger intensity than TRM in the lower blocking temperature range. Therefore, the TCRM acquisition during the initial cooling seems likely to cause the high paleointensities of the group B. This may also affect NRMs of the other groups more or less. However, since TCRM acquisition depends on the temperature and the time scale during the CRM growth, the theoretical analysis is difficult. The further discussion of TCRM will be given in the next section.

2.5.2 Detection of TCRM

It is important to distinguish TCRM from TRM to avoid incorrect paleointensities. Although its detection seems quite difficult, there are some possible ways. McClelland (1996) suggested that grain-growth CRM was detectable by non-linear Arai diagrams over certain temperature intervals because of the difference of the blocking temperature spectra between CRM and TRM in an identical set of magnetic grains. McClelland and Briden (1996) also pointed out that a linear Arai diagram for an original TRM would not be preserved if some amount of CRM is involved.

We found such a behavior in the experimental result of B-4-3 (Figure 2.8). This specimen passed the pTRM test almost throughout the heating temperatures and gave a high paleointensity of 69.0μT for 250-475°C range (Table 2.1). However, another linear segment can be seen for the high blocking temperatures of 475-580°C. It yields a paleointensity of 37.2μT (r=0.997, q=11.8 and f=0.553) in agreement with the expected intensity. This suggests that the lower blocking temperature portion is affected by TCRM while the higher one may be composed of TRM. The similar behavior of two segments was also observed by Hill and Shaw (2000). In their study, almost all the samples from one vertical section of the 1960 lava exhibited relatively higher two-slope Arai diagrams. Their first segments gave paleointensities between 36.0 and 68.7μT.

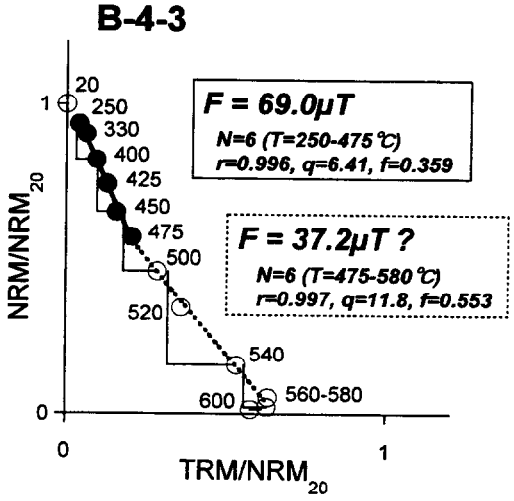

Figure 2.8: Experimental result of the spceimen B-4-3 by the Thellier method.
High blocking temperatures of 475-580°C can yield another linear segment which gives a paleointensity of 37.2μT (r=0.997, q=11.8 and f=0.553).

The Thellier method with the LTD seems to detect this kind of two-slopes behavior due to TCRM more clearly. In the results of groups A and B (Figures 2.5(D) and 2.5(E)), the low blocking temperature segments yielded very high paleointensities of 85.5μT (A-4-4L) and 81.6μT (B-9-4L). This is probably because that the grain-growths would more easily produce SD than MD and that these SD components detectable as LT memories carry TCRM, if the high temperature oxidation continued below the Curie temperature. For the pseudobrookite-bearing sample in the group C (C-4-4L, Figure 2.5(F)), the LTD treatment reveals that no significant TCRM is carried by the LT memory. Therefore the Thellier method combined with LTD is regarded as one of the tools for TCRM detection.

The LTD-DHT Shaw method also seems to be one of the useful tools for TCRM detection. In this method, a number of the anomalous results are rejected especially for the group B when compared with the Thellier experiments (Figure 2.9). The reasons for the rejection come from the double heating test, the ARM correction and the LTD treatment. Since a CRM/TRM ratio is not wholly constant throughout the grain size for the grain-growth CRM (McClelland, 1996), a TCRM/TRM ratio is considered to be variable with a grain size, that is, a coercivity. If NRM is shared by both TRM and TCRM while TRM1 is of a true TRM, the NRM-TRM1* diagram does not show a linearity. If TCRM is further gained in the laboratory heating, its effect is probably different between TRM1 in the first heating and TRM2 in the second. In this case, the TRM1-TRM2* diagram does not have a unit slope. The LTD treatment may more clearly expose these TCRM effects by removing MD components, similarly to the Thellier experiments. Although two anomalous results of B-4-2 and C-2-2 still survived after applying the selection criteria (Figure 2.9), they are more distinguishable than in the Thellier method. As a result, the multi-specimen test seems to work better for the TCRM-affected samples in the LTD-DHT Shaw method.

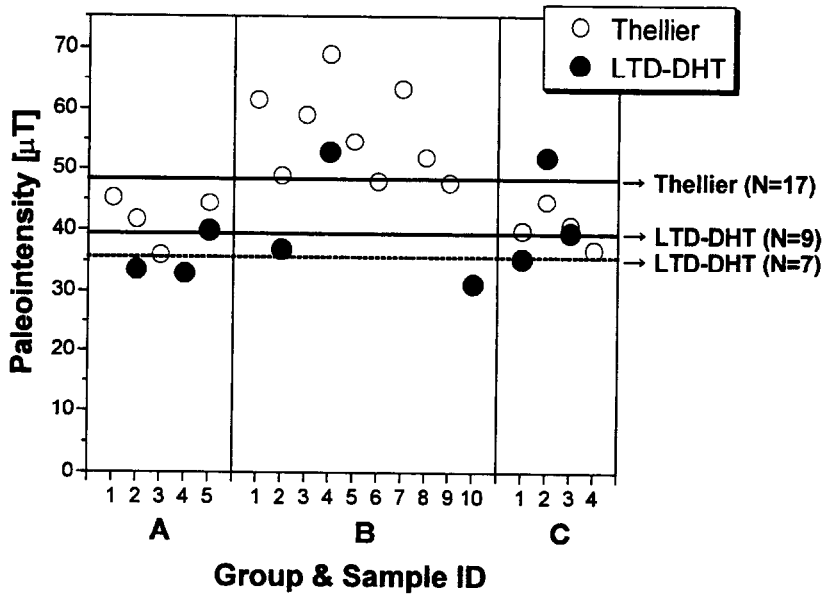

Figure 2.9: All the paleointensity results by the Thellier and LTD-DHT Shaw methods. Vertical and horizontal axes indicate the calculated paleointensity and the sample ID number, respectively. The results by the Thellier method are shown as open symbols while those by the LTD-DHT Shaw method are as closed ones. The averaged paleointensities are also shown by solid lines, and an alternative average of the LTD-DHT Shaw method is by a dashed line if two outliers of B-4-2 and C-2-2 are excluded. The expected field intensity is 36.2μT from DGRF 1965 (Tanaka and Kono, 1991).

2.6 Conclusions

We have systematically performed the paleointensity measurements on the Hawaiian 1960 lava. Based on the various rock magnetic analyses, 19 cores used in this study are classified into three groups of A, B and C. Deuteric oxidation progresses in this order. The Coe's version of the Thellier method (Coe, 1967) gave an average intensity of 49.0±9.6μT (N=17), about 35% higher than the expected field intensity (36.2μT). These high paleointensities are observed mostly from the group B, which shows the medium high temperature oxidation indices of II-IV, and then the multi-specimen test does not work well in the Thellier method. The LTD-DHT Shaw method (Tsunakawa et al., 1997; Tsunakawa and Yamamoto, 1999), on the other hand, resulted in a better mean of 39.4±7.9μT (N=9) since most results from the group B are rejected by the selection criteria. If two outliers were excluded, the average was improved to be 35.7±3.3μT (N=7) in good agreement with the expected value.

As several reasons of the high paleointensities are examined, the TCRM acquisition during the initial cooling is likely to cause the anomalous results. Although it is difficult to distinguish TCRM from TRM, we can detect its effect by the LTD treatment combined with the Thellier experiment. Another possible tool of the TCRM detection is the LTD-DHT Shaw method. The combination of the double heating test, the ARM correction and the LTD treatment effectively screens a number of the anomalous results, though the success rate in this method is much lower than in the Thellier method. A few erroneously high paleointensities are still observed in the LTD-DHT Shaw method, but they are easily judged to be outliers by the multi-specimen test. Therefore, the LTD-DHT Shaw method combined with the multi-specimen test will be one of the useful tools to obtain the accurate paleointensity from volcanic rocks. It is also concluded that the paleointensity determination of volcanic rocks should be made for samples with various oxidation states to discriminate erroneously high intensities due to TCRM.

Chapter 3

Geomagnetic paleosecular variation for the last 5 Ma in the Society Islands, French Polynesia

3.1 Introduction

Paleodirectional studies are quite important to know the paleosecular variation and time-averaged feature of the geomagnetic field. For the last few million years, several paleomagnetic studies have proposed the inclusive models in the last decade (e.g. Gubbins and Kelly, 1993; Johnson and Constable, 1995, 1997; Kelly and Gubbins, 1997; Kono *et al.*, 2000). The common conclusion from these models is that the time-averaged field (TAF) is dominated by the dipole field and associated with some amount of the non-dipole fields. Because of the existence of such non-dipole components, there is a latitudinal dependence in the angular standard deviation (ASD) of the virtual geomagnetic poles (VGPs) as pointed out by Cox (1970). McFadden *et al.* (1988, 1991) elucidated it by variations in the dipole and quadrupole families in terms of the dynamo theory, named Model G. Non-dipole fields also generate systematic inclination offsets from the geocentric axial dipole field, that is the inclination anomaly. McElhinny *et al.* (1996) suggested that the inclination anomaly for the last 5 Ma time-averaged field was attributed to the zonal quadrupole (g_2^0) and octupole (g_3^0).

Although all of these studies require a large number of the reliable paleodirectional data distributed over the whole globe, they are still very scarce in the southern hemisphere. For example, one of the most comprehensive database covering the past 5 Ma by Johnson and Constable (1996) have 1610 independent paleodirectional data from the northern hemisphere while only 590 from the southern hemisphere. Hotspot basalts in the southern hemisphere are good candidates to improve this situation. It is because they are expected to have stable remanences and because frequent eruptions can yield detailed paleomagnetic records.

French Polynesia is one of the regions composed of such hotspots. It consists of five main chains of oceanic islands, that is Marquesas, Tuamotu, Society, Pitcairn-Gambier and Cook-Austral Islands. For the Society Islands, Duncan (1975) paleomagnetically studied volcanic rocks from 5 islands of Tahiti, Moorea, Huahine, Raiatea and Borabora. He retrieved 35 normal, 18 reversed and 6 intermediate polarities, applying the threshold VGP latitude of 50°. However, these data are not sufficient for the modern paleosecular variation studies because their magnetic cleaning was done only with low field alternating field demagnetizations by 40mT. Roperch and Duncan (1990) reported the transient geomagnetic field record from the Huahine Island and Chauvin et al. (1990) observed 35 normal, 41 reversed and 47 intermediate directions from 123 sites in Tahiti Nui. The coverage time spans, however, were short since they were interested in the transitional and reversal behaviors of the geomagnetic field.

In this chapter we report new paleodirectional data from the Society Islands together with the K-Ar ages. The paleodirections are obtained from 154 sites in Tahiti, Moorea, Huahine, Raiatea, Tahaa, Borabora and Maupiti Islands by both thermal and alternating field demagnetizations. Based on these results, the magnetostratigraphy, paleosecular variation and time-averaged field in the Society Islands are discussed for the last 5 Ma.

3.2 Samples, experiments and direction analysis

The Society archipelago is composed of 10 volcanic islands and several seamounts. They are hotspot origin and show a chain-like configuration in a northwest-southeast direction delineating the Pacific plate motion. The present source of hotspot is located in the southeastern end of the archipelago where some active submarine volcanoes are observed. The volcanism, producing basalts, initiated about 5 Ma (Duncan and McDougall, 1976). The samples were collected from 101 sites of the lava sequences and from 53 sites of the dikes and the single lavas, mostly by the portable engine drill. The sample orientation was carried out by a magnetic compass and/or a sun compass. As in Figure 3.1, the sampling sites are distributed in Maupiti (24 sites), Borabora (21), Tahaa (20), Raiatea (24), Huahine (21), Moorea (33) and Tahiti (11).

K-Ar ages were determined for the selected samples from 52 sites at the Geological Survey of Japan. Before the measurements, the samples were crushed into 30-60 mesh grains and cleaned by an ultrasonic washer. Then the groundmasses were extracted from the cleaned grains by an isoseparator and 1-2g part of them was further ground in a triturator for the potassium measurement. Potassium content was measured by frame emission spectrometry (FIP-3D) following Matsumoto (1989), and the measurements were repeated twice with the standard samples at different times. Radiogenic ^{40}Ar amount was determined with VG Isotopes 603 mass spectrometer by the isotope dilution method (Shibata, 1968; Uto et al., 1995) or by VG Isotopes 1200C spectrometer for the peak comparison method (Matsumoto et al., 1989b).

As for the paleodirections, they are statistically calculated from the primary remanences measured by the thermal and alternating field (AF) demagnetizations. For each site, not less than three specimens were subjected to the stepwise thermal demagnetization up to 600°C in air at 20-50°C intervals. The AF demagnetization was also performed on other specimens at 5 or 10mT intervals up to 160mT peak field. All the remanences were measured by a spinner magnetometer (Natsuhara-Giken SMD-88) in thermal demagnetizations and by an automatic spinner magnetometer (Natsuhara-Giken DSPIN-2; Kono et al., 1984, Kono et al., 1997) in AF demagnetizations. All the paleodirections were determined by the principal component analysis (Kirschvink, 1980). For 101 paleodirections from the lava sequences, a serial correlation is tested for the adjacent flows in the later section (section 3.4.3).

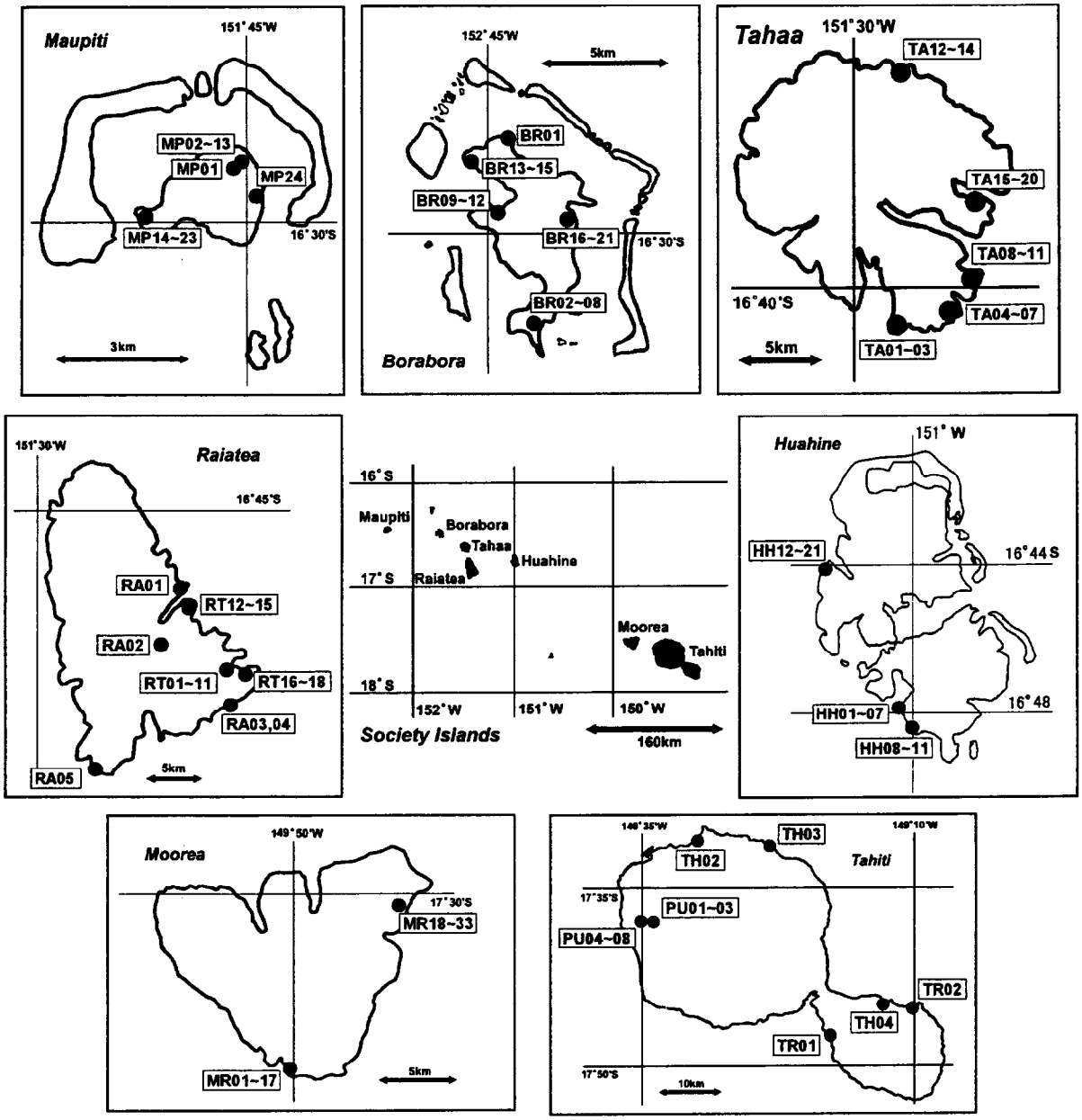

Figure 3.1: The map showing the sampling sites.
Samples were collected from 101 sites of the lava sequences and 53 sites of the dikes and the single lavas distributed at several localities in each island.

3.3 K-Ar ages and the Pacific plate absolute motion

The obtained K-Ar ages are summarized in Table 3.1. Our data cover almost the last 5 Ma except a period of 1.7-2.4 Ma. Most of them are consistent with the previously reported ages of 3.9-4.51 Ma for Maupiti, 3.10-3.45 Ma for BoraBora, 2.8-3.2 Ma for Tahaa, 2.44-2.75 Ma for Raiatea, 2.0-2.6 Ma for Huahine, 1.36-1.72 Ma for Moorea and 0.62-1.19 Ma for Tahiti (Duncan and McDougall, 1976; Chauvin et al., 1990; Blais et al., 1997; Guillou et al., 1998; Blais et al., 2000).

It should be noticeable that the absolute motion of the Pacific plate may evoke a few degree changes in the sampling site positions during million years. Hence the localities of the sampling sites should be corrected for the precise paleodirection analysis. According to HS2-NUVEL1 model (Gripp and Gordon, 1990), the Pacific-plate absolute motion has an Euler pole at (60.2°S, 90.0°E) and an angular speed of 0.98°/Ma. Applying this model, the original positions were estimated from a weighted mean age of each island (Maupiti, 4.54 Ma; Borabora, 3.51 Ma; Tahaa, 3.01 Ma; Raiatea, 2.63 Ma; Huahine, 2.80 Ma; Moorea, 1.55 Ma; Tahiti, 0.88 Ma). Note that age of HH09 is not considered for the calculation in Huahine (see the section 3.4.2). As a result, the estimated positions are gathered and then make a cluster as shown in Figure 3.2, supporting the validity of our age determinations. This correction is important for the paleodirectional analysis because an inclination of the geocentric axial dipole field changes from $-33.0°$ at 18°S to $-31.4°$ at 17°S. Therefore we corrected the sampling site localities for the plate motion and used their original positions in the VGP calculations.

Site ID	K_2O (wt. %)	$^{40}Ar_{rad}$ (10^{-6}mlSTP/g)	Air (%)	Age (Ma)	Polality
		Maupiti			
MP02H	1.76	0.257	18.3	4.52±0.05	N
MP12	1.63	0.240	40.8	4.55±0.05	N
MP13	2.07	0.309	31.4	4.61±0.05	N
MP19H	1.85	0.270	49.2	4.52±0.05	N
		Borabora			
BR02H	1.07	0.111	60.8	3.21±0.09	N
BR04	1.90	0.230	42.4	3.75±0.05	R
BR07	1.12	0.133	49.8	3.67±0.05	R
BR08H	1.93	0.210	49.2	3.37±0.05	N
BR10H	0.585	0.0757	61.1	4.01±0.31	N
BR15	1.30	0.144	55.0	3.43±0.06	R
BR16	2.01	0.214	36.2	3.30±0.06	N
BR18	1.21	0.137	54.8	3.51±0.05	N
		Tahaa			
TA01	1.79	0.181	43.9	3.14±0.06	-
TA03	1.64	0.151	76.0	2.85±0.06	I
TA04	1.34	0.132	43.8	3.04±0.04	I
TA07	1.11	0.115	62.9	3.24±0.05	I
TA08	1.78	0.180	62.2	3.14±0.06	R
TA11	0.472	0.0391	84.1	2.57±0.13	R
TA13H	0.971	0.0975	24.5	3.11±0.04	R
TA15	2.60	0.243	61.3	2.90±0.05	N
TA16	2.43	0.233	43.2	2.97±0.04	N
TA17H	2.97	0.286	48.9	2.99±0.04	N
		Raiatea			
RT03H	1.93	0.165	75.2	2.65±0.03	N
RT10H	1.63	0.146	44.1	2.77±0.04	I
RT12H	2.08	0.175	27.5	2.61±0.03	N
RT18H	1.63	0.141	23.8	2.67±0.03	N
RA01	1.14	0.0900	54.7	2.45±0.05	N
RA02a	1.86	0.157	59.7	2.62±0.04	-
RA02b	2.04	0.175	54.1	2.67±0.04	-
RA03	1.41	0.124	58.4	2.72±0.05	-
RA04	1.39	0.114	54.3	2.55±0.03	-
RA05	1.38	0.116	79.9	2.60±0.07	N
		Huahine			
HH01	1.85	0.162	46.1	2.72±0.03	N
HH05	1.95	0.169	48.4	2.68±0.04	N
HH06	2.17	0.181	39.1	2.58±0.05	N
HH08	1.37	0.141	37.0	3.19±0.13	N
HH09	1.23	0.160	44.8	4.01±0.05	N
HH11	2.31	0.231	43.2	3.09±0.04	N
HH12	1.40	0.114	56.2	2.52±0.04	N
HH20	1.56	0.143	50.7	2.83±0.09	N
		Moorea			
MR01	1.43	0.0730	69.7	1.58±0.04	R
MR06	1.31	0.0686	78.6	1.62±0.08	R
MR16	1.38	0.0672	77.9	1.51±0.04	R
MR23	1.23	0.0618	86.0	1.55±0.06	R
MR30	3.78	0.186	31.9	1.53±0.02	-
MR32	1.15	0.0559	75.2	1.50±0.04	R
		Tahiti			
PU01H	0.687	0.0248	88.3	1.12±0.02	R
PU04	1.67	0.0497	80.2	0.92±0.03	N
PU05	1.31	0.0434	72.6	1.03±0.02	N
PU06	1.04	0.0333	93.4	0.99±0.08	R
TH02	1.59	0.0371	81.0	0.72±0.11	N
TH04	0.657	0.0108	95.1	0.51±0.10	N

Table 3.1: K-Ar ages for the selected samples from the Society Islands.
K_2O, concentrations of K_2O; $^{40}Ar_{rad}$, amount of radiogenic ^{40}Ar; Air, fraction of atmospheric ^{40}Ar in total ^{40}Ar; Age, calculated K-Ar age with its standard deviation; Polarity, paleomagnetic polarity observed after the correction for the absolute plate motion (N, normal; R, reversed; I, intermediate). 'H' at the end of the site ID indicates that the sample was leached by HCl before the analysis.

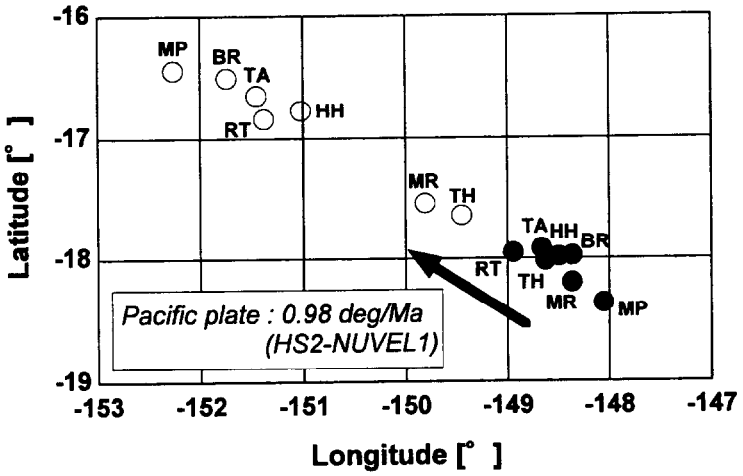

Figure 3.2: The present and original positions of the studied 7 islands in the Society. These are estimated from the absolute plate motion of the Pacific plate (Gripp and Gordon, 1990); MP for Maupiti, BR for Borabora, TA for Tahaa, RT for Raiatea, HH for Huahine, MR for Moorea and TH for Tahiti. Solid circles indicate the original positions after the correction for the absolute plate motion while open ones the present positions.

3.4 Paleodirections of the geomagnetic field

In this section we take a threshold VGP latitude of 50° in the definition of polarity so that VGP latitude of normal or reversed polarity is higher than 50°. If the VGP is located at a latitudinal band between 50°N and 50°S, it is interpreted as the intermediate polarity. As discussed later, the data set of this study is almost immune from the selection of threshold latitude around 50°.

3.4.1 Demagnetization characteristics

The thermal and AF demagnetizations were performed on 885 paleomagnetic cores from 154 sites. Their NRM intensities range from 1.29×10^{-4} to 1.50×10^{-2}Am^2/kg with a peak around 1×10^{-3}Am^2/kg.

Primary remanences were easily isolated from 140 sites with both thermal and AF demagnetizations (Figure 3.3(A)), yielding site mean paleodirections with $\alpha_{95} \leq 15°$. These samples have stable and relatively strong magnetizations ($\sim 10^{-3}$Am^2/kg) with high blocking temperatures and coercivities. Secondary components of them were efficiently removed by 350-450°C heating or by 10-20mT AF cleaning. Most of their MAD values in the principal component analysis were less than 5.0°. For 6 sites, primary components were extracted (Figure 3.3(B)) but the internal consistency was not good ($\alpha_{95} > 15°$). Therefore meaningful VGP positions were not determined for these sites. The magnetizations of other 6 sites were weak ($\sim 10^{-4}$Am^2/kg) and stable components were not observed (Figure 3.3(C)). As we did not collect enough cores from 2 sites of RA02b and RA03 in Raiatea, they gave only reference directions.

These measurement results are summarized in Table 3.2 for the dikes and single lavas, and in Tables 3.3 and 3.4 for the lava sequences. The VGP positions were calculated for 140 sites with $\alpha_{95} \leq 15°$. The correction of the sampling localities for the absolute motion of the Pacific plate was also applied in the calculations.

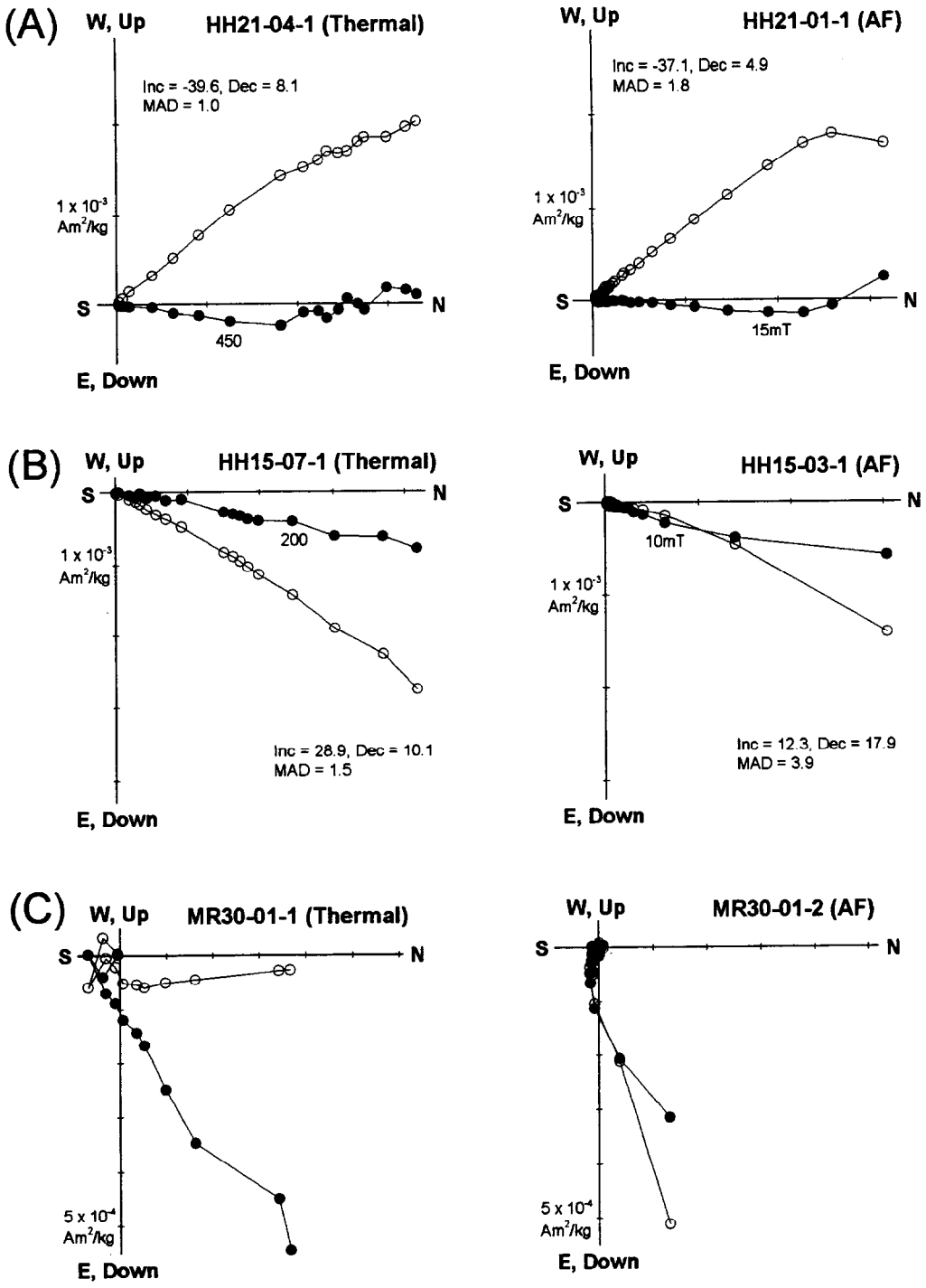

Figure 3.3: Representative orthogonal plots of stepwise thermal and AF demagnetizations.
(A) Primary remanences were isolated by both demagnetizations ($\alpha_{95} \leq 15°$).
(B) Primary components were detected but internal consistency was not good ($\alpha_{95} > 15°$).
(C) The magnetizations were very weak and unstable.

Site	Dec	Inc	n/N	α_{95}	Lat	Long	PLat	PLong	Lat'	Long'	PLat'	PLong'
						Maupiti						
MP01	-80.4	-79.7	5/5	4.3	-16.4	-152.3	18.7	48.6	-18.4	-148.0	20.1	53.1
MP14	25.4	-50.8	5/5	5.8	-16.5	-152.3	62.5	-24.5	-18.4	-148.1	64.5	-22.4
MP15	22.1	-54.9	5/5	4.7	-16.5	-152.3	62.7	-14.2	-18.4	-148.1	64.8	-11.3
MP16	17.3	-7.2	5/5	7.6	-16.5	-152.3	68.7	-97.4	-18.4	-148.1	68.4	-99.1
MP17	8.0	-29.3	3/6	20.2	-16.5	-152.3	-	-	-18.4	-148.1	-	-
MP18	4.7	-40.4	5/5	7.0	-16.5	-152.3	82.0	-5.3	-18.4	-148.1	84.2	-2.7
MP19	-3.0	-36.8	5/5	3.2	-16.5	-152.3	85.0	62.2	-18.4	-148.1	85.5	-267.6
MP20	-3.5	-49.6	5/5	6.3	-16.5	-152.3	75.6	39.9	-18.4	-148.1	77.2	50.3
MP21	-9.7	-18.0	5/5	4.2	-16.5	-152.3	78.1	-206.1	-18.4	-148.1	76.1	-198.6
MP22	-	-	0/7	-	-16.5	-152.3	-	-	-18.4	-148.1	-	-
MP23	0.1	-25.3	5/5	4.0	-16.5	-152.3	86.8	-151.3	-18.4	-148.1	84.8	-160.0
MP24	4.5	-38.6	5/5	9.2	-16.4	-152.2	83.2	-10.6	-18.4	-148.0	85.3	-10.8
						Borabora						
BR01	202.8	43.2	4/7	12.5	-16.5	-151.7	-67.1	-215.7	-17.9	-148.5	-68.5	-215.2
BR02	-8.8	-31.7	7/7	3.2	-16.5	-151.7	81.6	112.7	-18.0	-148.5	80.8	-234.7
BR03	-4.0	-28.9	5/5	5.3	-16.5	-151.7	86.0	-226.2	-18.0	-148.5	84.6	-210.3
BR08	-3.7	-53.4	7/7	2.4	-16.5	-151.7	72.3	38.4	-18.0	-148.5	73.6	45.0
BR09	2.8	-41.9	4/8	5.7	-16.5	-151.7	81.9	9.5	-18.0	-148.5	83.6	15.4
BR10	17.6	-13.1	6/6	3.0	-16.5	-151.7	70.2	-89.5	-18.0	-148.5	70.2	-91.2
BR11	20.5	-37.3	7/7	9.0	-16.5	-151.7	70.1	-45.9	-18.0	-148.5	71.3	-46.4
BR12	3.3	-21.1	6/8	6.0	-16.5	-151.7	83.6	-121.3	-18.0	-148.5	82.6	-129.8
BR13	212.6	23.3	4/7	5.1	-16.5	-151.8	-58.2	114.8	-18.0	-148.5	-58.9	-244.7
BR16	16.9	-39.0	7/7	4.9	-16.5	-151.7	73.1	-40.0	-18.0	-148.5	74.4	-40.8
BR17	27.4	-49.7	5/5	14.4	-16.5	-151.7	61.4	-27.5	-18.0	-148.5	62.9	-26.0
						Tahaa						
TA12	206.3	43.9	5/5	4.5	-16.6	-151.5	-63.9	-216.6	-17.9	-148.7	-65.1	-215.8
TA13	158.6	37.3	9/10	6.3	-16.6	-151.5	-69.3	-76.6	-17.9	-148.7	-68.9	-70.4
TA14	203.0	76.0	5/5	68.7	-16.6	-151.5	-	-	-17.9	-148.7	-	-
						Raiatea						
RT01	4.6	-39.3	7/7	3.2	-16.8	-151.4	83.1	-9.2	-18.0	-148.9	84.3	-8.8
RT02	7.6	-42.4	6/7	4.9	-16.8	-151.4	79.5	-12.7	-18.0	-148.9	80.8	-12.0
RT03	1.3	-26.4	6/7	4.6	-16.8	-151.4	86.8	-127.8	-18.0	-148.9	85.9	-140.3
RT08	8.9	-42.7	5/5	6.3	-16.8	-151.4	78.5	-16.3	-18.0	-148.9	79.8	-15.9
RT09	5.9	-48.8	5/5	2.7	-16.8	-151.4	76.1	7.0	-18.0	-148.9	77.3	10.1
RA01	6.0	-24.7	4/4	3.2	-16.8	-151.4	83.0	-94.1	-17.9	-149.0	82.8	-102.1
RA02a	-	-	0/3	-	-16.8	-151.4	-	-	-17.9	-149.0	-	-
RA02b	4.4	9.2	2/2	-	-16.8	-151.4	-	-	-17.9	-149.0	-	-
RA03	-3.5	-23.9	1/1	-	-16.9	-151.4	-	-	-18.0	-148.9	-	-
RA04	2.4	-19.1	1/3	-	-16.9	-151.4	-	-	-18.0	-148.9	-	-
RA05	-2.3	-36.2	4/4	14.7	-16.9	-151.5	86.1	62.6	-18.0	-149.0	86.5	84.0
						Huahine						
HH05	-1.2	-31.3	7/7	4.4	-16.8	-151.0	88.8	111.9	-18.0	-148.4	87.9	-209.4
HH06	0.9	-48.1	7/7	2.5	-16.8	-151.0	77.6	25.3	-18.0	-148.4	78.8	30.8
HH07	-1.5	-28.3	6/7	5.0	-16.8	-151.0	87.7	-190.0	-18.0	-148.4	86.4	-184.3
HH08	4.9	-26.4	6/6	2.4	-16.8	-151.0	84.4	-91.2	-18.0	-148.4	84.3	-102.6
HH12	16.6	-13.6	6/6	5.1	-16.7	-151.0	71.1	-90.4	-17.9	-148.4	71.0	-92.0
HH13	10.1	29.5	5/5	6.6	-16.7	-151.0	56.0	-133.5	-17.9	-148.4	55.1	-132.6
HH14	24.6	-21.5	5/5	10.6	-16.7	-151.0	65.5	-71.0	-17.9	-148.4	65.9	-71.4
HH15	26.2	20.7	5/5	30.6	-16.7	-151.0	-	-	-17.9	-148.4	-	-
						Tahiti						
PU04	20.3	-62.3	6/7	4.1	-17.6	-149.6	58.9	1.4	-18.0	-148.8	59.3	2.1
PU05	19.9	-33.4	7/7	6.1	-17.6	-149.6	71.1	-54.7	-18.0	-148.8	71.3	-55.0
PU06	185.8	32.1	10/10	5.1	-17.6	-149.6	-84.5	118.9	-18.0	-148.8	-84.7	-244.4
TR01	-1.0	-45.2	8/10	11.0	-17.8	-149.3	81.0	36.2	-18.2	-148.5	81.3	38.7
TR02	-8.0	-23.8	6/6	5.1	-17.7	-149.2	80.6	-205.4	-18.1	-148.4	80.3	-203.6
TH02	12.5	-29.4	4/4	4.7	-17.5	-149.5	77.9	-66.3	-17.9	-148.7	78.1	-67.4
TH03	4.7	-18.3	4/4	7.7	-17.5	-149.4	80.7	-119.6	-17.9	-148.6	80.5	-121.1
TH04	7.4	-18.6	4/4	3.7	-17.7	-149.2	79.1	-106.9	-18.1	-148.4	79.0	-108.3

Table 3.2: Paleodirections for the dikes and single lavas from the Society Islands.
Site, Site ID; n, N, number of the specimens used for the calculation and demagnetization; α_{95}, a 95% confidence circle; Lat, Long, latitude and longitude of the site; PLat, PLong, latitude and longitude of VGP. The prime (') denotes the values after the correction for the absolute plate motion.

Site	individual lava								vector group							
	Dec	Inc	n/N	α_{95}	PLat	PLong	PLat'	PLong'	Dec	Inc	n/N	α_{95}	PLat	PLong	PLat'	PLong'
Maupiti																
<sequence at 16.4°S, 152.3°W (18.4°S, 148.0°W for the corrected location)>																
MP13	-3.8	-20.2	5/5	5.3	82.9	-184.5	80.7	-180.0								
MP12	-4.6	-20.1	5/5	5.8	82.4	-189.4	80.3	-183.8								
MP11	2.4	-24.5	5/5	3.6	85.7	-118.5	84.4	-135.1								
MP10	0.3	-29.4	5/5	7.9	89.2	-129.9	87.2	-165.2								
MP09	-3.0	-29.4	5/5	2.9	87.1	-229.2	85.3	-205.3								
MP08	-5.5	-27.8	5/5	3.8	84.5	-225.8	82.7	-209.8								
MP07	-4.8	-25.3	5/5	7.7	84.4	-208.9	82.3	-197.6								
MP06	-2.0	-27.6	5/5	6.5	87.4	-198.8	85.2	-187.2								
MP05	-1.0	-25.6	5/5	2.3	86.9	-169.8	84.7	-171.0								
MP04	-4.7	-28.0	5/5	2.5	85.2	-223.9	83.4	-207.1								
MP03	0.0	-25.3	5/5	2.4	86.9	-153.0	84.8	-161.0								
MP02	3.3	-25.0	5/5	3.7	85.4	-107.9	84.4	-126.1	-1.9	-25.7	60/60	1.4	86.5	-185.5	84.3	-180.2
Borabora																
<sequence at 16.5°S, 151.7°W (18.0°S, 148.5°W for the corrected location)>																
BR07	183.1	24.6	7/7	4.2	-85.3	67.6	-84.5	54.0	183.1	24.6	7/7	4.2	-85.4	67.9	-84.5	53.9
BR04	199.6	29.6	7/7	4.2	-71.2	-241.1	-72.0	-242.6								
BR05	200.9	26.7	5/5	2.4	-69.7	114.2	-70.4	-247.1	200.2	28.4	12/12	2.5	-70.6	116.6	-71.3	-244.8
BR06	189.4	28.9	5/5	3.0	-80.9	112.5	-81.4	-254.9	189.4	28.9	5/5	3.0	-80.9	112.6	-81.5	-254.8
<sequence at 16.5°S, 151.8°W (18.0°S, 148.5°W for the corrected location)>																
BR15	200.8	42.2	7/7	2.8	-69.0	-216.1	-70.4	-215.9								
BR14	199.8	37.6	5/6	3.1	-70.7	-224.9	-71.9	-225.5	200.3	40.3	12/13	2.2	-69.8	-220.2	-71.1	-220.3
<sequence at 16.5°S, 151.7°W (18.0°S, 148.5°W for the corrected location)>																
BR21	11.5	-39.4	5/5	6.5	77.6	-31.6	79.1	-33.1								
BR20	6.4	-40.6	5/5	5.4	81.0	-12.8	82.7	-12.4								
BR19	7.8	-41.3	5/5	5.3	79.8	-15.9	81.4	-15.7								
BR18	15.0	-45.8	8/8	3.2	72.4	-21.5	74.0	-20.5	10.7	-42.4	23/23	2.4	77.1	-21.7	78.7	-21.7
Tahaa																
<sequence at 16.7°S, 151.5°W (18.0°S, 148.7°W for the corrected location)>																
TA03	131.6	13.1	5/5	13.5	-41.7	-55.4	-40.8	-51.8	131.6	13.1	5/5	13.5	-41.7	-55.4	-40.8	-51.8
TA02	124.1	5.8	4/9	61.5	-	-	-	-	124.1	5.8	4/9	61.5	-	-	-	-
TA01	165.0	-8.1	7/7	16.4	-	-	-	-	165.0	-8.1	7/7	16.4	-	-	-	-
<sequence at 16.7°S, 151.5°W (17.9°S, 148.7°W for the corrected location)>																
TA07	-67.4	70.3	5/5	5.3	-1.1	-184.0	-2.5	-181.4								
TA06	-44.0	75.6	5/5	11.0	3.4	-170.0	2.0	-167.5								
TA05	-43.6	78.5	7/7	4.2	-0.2	-166.6	-1.6	-164.0								
TA04	-14.4	68.5	4/5	11.8	20.4	-160.9	19.1	-158.5	-43.4	74.8	21/22	4.0	4.6	-170.7	3.2	-168.1
<sequence at 16.6°S, 151.4°W (17.9°S, 148.7°W for the corrected location)>																
TA11	173.4	22.6	7/7	12.4	-81.9	-25.1	-80.6	-18.9	173.4	22.6	7/7	12.4	-81.9	-25.1	-80.6	-18.9
TA10	186.4	21.4	5/5	6.9	-81.6	77.5	-81.2	70.7								
TA09	182.2	20.5	5/5	3.3	-83.6	47.9	-82.5	42.0								
TA08	179.1	17.8	7/7	7.5	-82.4	21.7	-81.1	20.6	182.1	19.7	17/17	3.6	-83.2	46.4	-82.1	41.1
<sequence at 16.7°S, 151.4°W (17.9°S, 148.7°W for the corrected location)>																
TA20	-16.8	-55.5	5/5	5.4	65.6	62.9	66.2	68.4								
TA19	-12.9	-54.3	5/5	9.2	68.5	58.4	69.2	64.3								
TA18	-26.5	-50.8	6/6	3.7	61.7	82.0	61.8	87.2	-19.5	-53.5	16/16	3.5	65.3	70.0	65.8	75.6
TA17	-16.8	-59.0	7/7	5.9	62.6	57.4	63.4	62.5								
TA16	-5.9	-60.9	5/7	7.7	64.2	38.7	65.3	43.3	-12.4	-59.9	12/14	4.4	63.6	50.0	64.5	55.0
TA15	-23.0	-49.2	7/7	2.0	65.1	81.8	65.2	87.5	-23.0	-49.2	7/7	2.0	65.1	81.8	65.2	87.5
Raiatea																
<sequence at 16.8°S, 151.4°W (18.0°S, 148.9°W for the corrected location)>																
RT04	-20.0	52.5	6/7	42.3	-	-	-	-	-20.0	52.5	6/7	42.3	-	-	-	-
RT05	2.7	51.7	6/7	3.0	40.7	-148.4	39.6	-146.7	2.7	51.7	6/7	3.0	40.7	-148.4	39.6	-146.7
RT06	-4.5	59.9	5/5	4.8	32.3	-155.4	31.1	-153.5	-4.5	59.9	5/5	4.8	32.3	-155.4	31.1	-153.5
RT07	-47.3	67.8	3/7	2.8	10.7	-179.6	9.4	-177.4	-47.3	67.8	3/7	2.8	10.7	-179.6	9.4	-177.4
RT10	-41.4	-28.3	7/7	9.3	50.2	115.2	49.6	-241.2								
RT11	-39.2	-24.7	5/5	8.8	52.0	-240.9	51.4	-237.3	-40.4	-26.8	12/12	5.9	51.0	116.8	50.4	-239.6
<sequence at 16.8°S, 151.4°W (17.9°S, 149.0°W for the corrected location)>																
RT15	4.3	-35.9	6/7	2.9	84.9	-23.5	86.0	-28.4								
RT14	1.3	-35.2	5/5	2.4	87.1	3.2	88.4	8.8								
RT13	5.0	-39.2	5/5	4.2	82.8	-12.2	84.1	-12.4								
RT12	7.3	-39.2	7/7	2.0	81.3	-22.3	82.4	-23.6	4.7	-37.5	23/24	1.5	83.9	-17.4	85.1	-19.4
<sequence at 16.8°S, 151.4°W (18.0°S, 148.9°W for the corrected location)>																
RT16	6.1	-34.7	5/5	8.5	83.7	-39.1	84.7	-45.4								
RT17	5.8	-36.4	5/6	13.3	83.5	-28.6	84.7	-32.7								
RT18	14.3	-24.7	6/7	4.9	75.6	-75.2	75.9	-77.9	9.3	-31.5	16/18	5.2	81.1	-58.7	81.7	-63.9

Table 3.3: Paleodirections for the lava sequences in Maupiti, Borabora, Tahaa and Raiatea. Results are listed in the sequential order from the older (bottom) to the younger (top).

Site	individual lava								vector group							
	Dec	Inc	n/N	α_{95}	PLat	PLong	PLat'	PLong'	Dec	Inc	n/N	α_{95}	PLat	PLong	PLat'	PLong'
							Huahine									
	<sequence at 16.8°S, 151.0°W (18.0°S, 148.4°W for the corrected location)>															
HH03	4.7	-17.3	5/5	2.7	80.8	-120.6	80.1	-125.0								
HH02	6.6	-20.8	8/8	1.8	81.2	-103.3	80.8	-109.2	5.9	-19.5	13/13	1.7	81.1	-110.1	80.6	-115.7
HH01	3.1	-22.8	7/7	1.8	84.2	-119.0	83.4	-127.2								
HH04	6.2	-21.2	5/5	2.0	81.6	-104.4	81.2	-110.7	4.4	-22.1	12/12	1.5	83.2	-111.6	82.6	-119.3
	<sequence at 16.8°S, 151.0°W (18.0°S, 148.4°W for the corrected location)>															
HH11	7.0	-26.8	6/6	4.4	82.7	-81.3	82.8	-89.6	7.0	-26.8	6/6	4.4	82.7	-81.3	82.8	-89.8
HH10	20.0	-34.3	6/6	4.7	70.8	-51.9	71.7	-52.7								
HH09	22.3	-31.1	7/7	3.4	68.7	-57.8	69.4	-58.5	21.3	-32.6	13/13	2.7	69.7	-55.3	70.5	-56.0
	<sequence at 16.7°S, 151.0°W (17.9°S, 148.4°W for the corrected location)>															
HH16	9.9	-34.6	7/7	2.1	80.3	-45.8	81.2	-49.6	9.9	-34.6	7/7	2.1	80.3	-45.8	81.2	-49.7
HH17	6.7	-40.8	5/5	2.9	80.9	-13.6	82.2	-13.3								
HH18	7.4	-38.1	5/5	4.4	81.6	-26.4	82.8	-28.6								
HH20	1.3	-40.8	7/7	1.7	83.3	18.7	84.5	25.9								
HH19	2.1	-39.1	5/5	2.3	84.2	9.0	85.6	14.5								
HH21	4.8	-37.5	5/5	1.9	83.8	-17.2	85.1	-19.3	4.3	-39.4	27/27	1.3	83.1	-6.0	84.5	-4.8
							Moorea									
	<sequence at 17.6°S, 149.8°W (18.2°S, 148.4°W for the corrected location)>															
MR01	170.4	31.0	7/7	2.5	-80.8	-56.0	-80.3	-51.0								
MR02	172.6	29.5	5/5	3.8	-82.6	-46.6	-82.1	-41.4	171.3	30.4	12/12	2.0	-81.6	-52.6	-81.1	-47.5
MR03	171.6	36.1	5/5	2.4	-81.7	-78.2	-81.5	-72.0								
MR04	172.3	37.9	5/5	0.9	-81.9	-88.3	-81.8	-81.7	172.0	37.0	10/10	1.2	-81.8	-83.1	-81.7	-76.7
MR05	173.7	32.5	5/5	2.4	-84.0	-61.6	-83.6	-54.4								
MR06	173.5	30.5	7/7	4.8	-83.7	-50.0	-83.2	-43.9	173.6	31.3	12/12	2.7	-83.9	-54.7	-83.4	-48.1
MR07	179.5	24.3	5/5	3.2	-85.1	25.0	-84.4	23.0	179.5	24.3	5/5	3.2	-85.1	25.0	-84.4	23.0
MR08	172.9	30.2	4/4	4.8	-83.1	-49.4	-82.6	-43.8								
MR09	163.6	34.1	5/5	4.6	-74.4	-66.4	-74.0	-62.7	167.8	32.4	9/9	4.0	-78.4	-61.8	-78.0	-57.4
MR10	170.7	26.1	5/5	3.6	-80.3	-37.9	-79.7	-34.1	170.7	26.1	5/5	3.6	-80.3	-37.9	-79.7	-34.1
MR11	172.8	32.5	5/5	2.1	-83.2	-61.5	-82.8	-54.9								
MR12	174.9	29.3	5/5	3.3	-84.7	-39.6	-84.1	-33.6								
MR13	172.5	25.5	5/5	3.9	-81.6	-31.1	-81.0	-27.4								
MR14	174.1	25.4	5/5	4.7	-82.9	-24.2	-82.2	-20.7	173.6	28.2	20/20	1.9	-83.3	-38.1	-82.7	-33.2
MR15	188.3	23.2	5/5	5.7	-80.3	86.9	-80.2	83.8	188.3	23.2	5/5	5.7	-80.3	86.9	-80.2	83.8
MR16	174.1	32.8	7/7	3.0	-84.4	-63.2	-84.0	-55.5								
MR17	179.9	30.2	5/5	7.8	-88.6	26.6	-87.9	18.4	176.6	31.7	12/12	3.5	-86.7	-53.1	-86.2	-42.8
	<sequence at 17.5°S, 149.8°W (18.1°S, 148.3°W for the corrected location)>															
MR18	-	-	0/7	-	-	-	-	-								
MR19	193.9	40.8	5/5	5.7	-75.7	-213.4	-76.3	-213.8	193.9	40.8	5/5	5.7	-75.7	-213.4	-76.3	-213.8
MR20	183.0	54.0	5/5	6.6	-72.8	-158.2	-73.5	-155.9	183.0	54.0	5/5	6.6	-72.8	-158.2	-73.5	-155.9
MR21	162.8	13.5	5/5	1.8	-70.2	-29.4	-69.5	-27.1	162.8	13.5	5/5	1.8	-70.2	-29.4	-69.5	-27.1
MR22	168.0	56.4	5/5	4.4	-67.9	-123.6	-68.3	-120.7								
MR23	181.8	61.4	7/7	6.0	-64.9	-153.0	-65.6	-150.9								
MR24	168.5	55.1	5/5	4.5	-69.2	-122.6	-69.6	-119.5								
MR25	171.8	57.9	5/6	3.3	-67.8	-132.7	-68.3	-129.9								
MR26	167.9	55.7	5/5	3.4	-68.4	-122.5	-68.8	-119.6	172.0	57.7	27/28	2.2	-68.0	-132.8	-68.5	-130.0
MR27	197.0	45.5	5/5	4.2	-71.7	-205.7	-72.4	-205.4	197.0	45.5	5/5	4.2	-71.7	-205.7	-72.4	-205.4
MR28	184.2	31.6	5/5	3.9	-86.0	115.4	-86.3	-253.7	184.2	31.6	5/5	3.9	-86.0	115.4	-86.3	-253.7
MR29	176.7	-0.2	5/5	3.8	-72.1	19.5	-71.4	20.0	176.7	-0.2	5/5	3.8	-72.1	19.5	-71.4	20.0
MR30	-	-	0/7	-	-	-	-	-								
MR31	177.7	51.9	5/5	3.4	-74.8	-142.3	-75.4	-139.2	177.7	51.9	5/5	3.4	-74.8	-142.3	-75.4	-139.2
MR32	185.7	68.0	7/7	3.6	-56.2	-156.2	-56.9	-154.4	185.7	68.0	7/7	3.6	-56.2	-156.2	-56.9	-154.4
MR33	162.6	60.7	5/5	5.2	-61.6	-121.8	-62.0	-119.3	162.6	60.7	5/5	5.2	-61.6	-121.8	-62.0	-119.3
							Tahiti									
	<sequence at 17.6°S, 149.6°W (18.0°S, 148.7°W for the corrected location)>															
PU03	162.1	35.6	3/6	8.1	-72.9	-69.4	-72.7	-67.3								
PU02	-	-	0/6	-	-	-	-	-								
PU01	160.8	33.1	7/7	4.6	-71.8	-63.9	-71.6	-62.0	161.2	33.9	10/13	3.5	-72.1	-65.4	-71.9	-63.5

Table 3.4: Paleodirections for the lava sequences in Huahine, Moorea and Tahiti.

3.4.2 Magnetostratigraphy

From the VGP latitudes (Tables 3.2, 3.3 and 3.4), 82 normal, 48 reversed and 10 intermediate paleofields have been determined. Although one intermediate VGP is changed to the normal one if the alternative threshold VGP of 45° is applied, it does not change the overall feature. Based on these results and K-Ar ages, the magnetostratigraphy is constructed and shown in Figure 3.4 together with the geomagnetic polarity time scale (GPTS) by Cande and Kent (1995). It is clearly seen that our results agree well with the GPTS at a 2σ level, though a few exceptions are found; 2 normal polarities (PU04 and HH09) and 4 intermediate ones (RT10, TA03, TA04 and TA07).

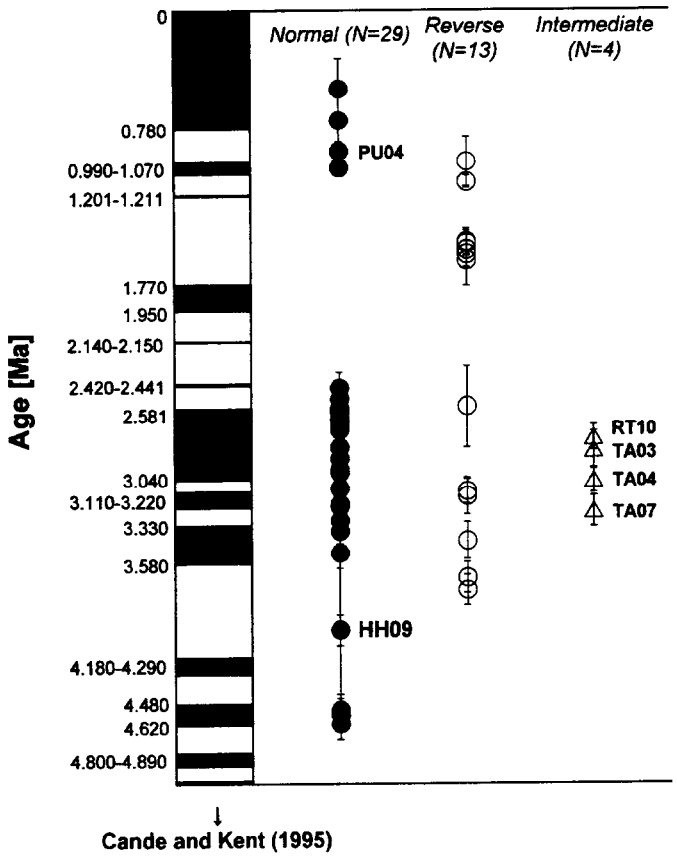

Figure 3.4: Magnetostratigraphy constructed from the present results.
The geomagnetic polarity time scale by Cande and Kent (1995) is shown together. Each point is plotted with its 2σ error of the age.

Singer et al. (1999) reported that the Jaramillo event started at 1.053±0.006 Ma and ended at 0.986±0.005 Ma from their $^{40}Ar/^{39}Ar$ dating for the lava flow in the Punaruu Valley, Tahiti. As our samples of PU04 are collected from the Punaruu Valley and its K-Ar age of 0.92±0.03 Ma is close to these ages, PU04 probably recorded the same event. As for the intermediate directions, it is possible that most of them experienced the polarity transitions when we consider their error limits of the age. TA04 (3.04±0.04 Ma) might record the transition from the Kaena reversed subchron (3.110-3.040 Ma) to the Gauss normal chron while TA07 (3.24±0.05 Ma) might record it from the Mammoth reversed subchron (3.330-3.110 Ma) to the Gauss normal chron. Another possibility is that an unknown geomagnetic excursion caused these intermediate paleofield. Roperch and Duncan (1990) reported that N-N excursion was observed from the volcanic rocks of the Huahine Island with K-Ar ages between 2.91 and 3.08 Ma. Since all of our intermediate sites show similar ages (2.77-3.24 Ma), these intermediate paleofield might possibly record the same transition as in Huahine. They compose two continuous VGP records in Figure 3.5; one is TA04, TA05, TA06 and TA07; the other is RT11, RT10 (2.77±0.04 Ma), RT07, RT06 and RT05. These 9 VGP positions are consistent with those by Roperch and Duncan (1990). It is also noticeable that they appear to make a cluster around a center of the Pacific Ocean, which is quite different from the preferred longitudinal bands of the transitional VGP path (Laj et al., 1991, 1992)

The normal direction observed from HH09 (4.01±0.05 Ma) is inconsistent with the GPTS. The GPTS by Cande and Kent (1995) is based partly on the astronomical age calibration which does not have the same physical background of the radiometric isotopic dating. However, the discrepancy seems too large to be ascribed from the calibration problem. As the age of HH09 is quite older than the other ages in the Huahine island (2.6-3.2 Ma), it may be due to excess Ar or some unknown short normal event. Therefore, the directional data from HH09 is temporarily incorporated into the analysis in the later discussion.

3.4.3 Paleosecular variation

As our data of the paleodirections cover almost the last 5 Ma, they are suited for the paleosecular variation (PSV) study. All the VGP positions calculated from these data are illustrated in Figure 3.5. Excluding the intermediates, they seem to be distributed around the geographic north pole and thus no significant far-sided effect (e.g. McElhinny et al., 1996) is seen.

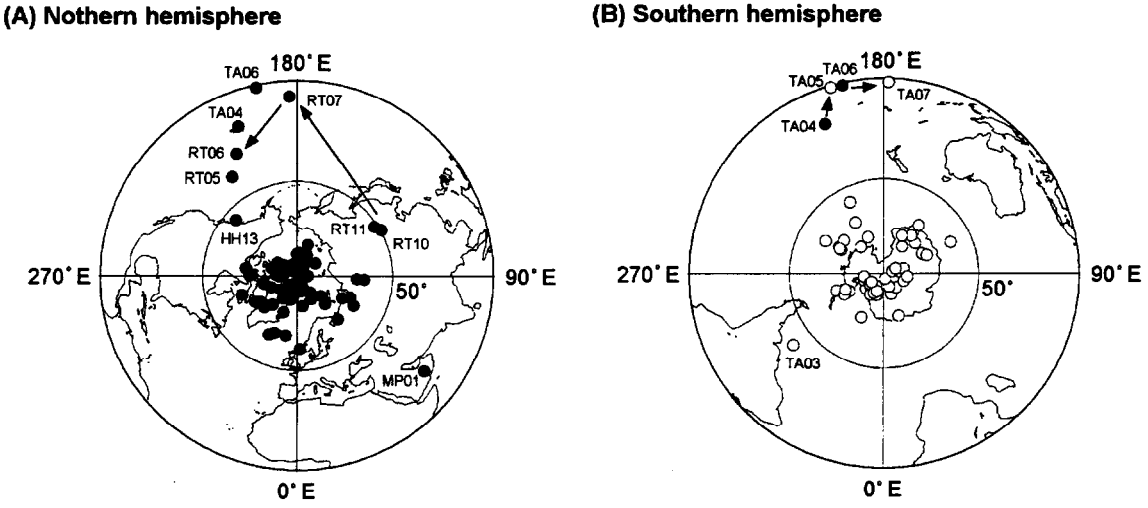

Figure 3.5: Equal area projections of the VGP positions.
(A) Nothern hemisphere and (B) the southern hemisphere. Arrows indicate the transitional VGP paths observed in the present results. Note that two VGPs of TA04 and TA06 in the southern hemisphere are plotted as a referrence.

If the absolute plate motion is not considered, the mean VGP positions are calculated as follows; Lat=85.8°, Long=342.5°, A_{95}=2.9° and ASD=14.4° for the normal polarity (N=83); Lat=−86.4°, Long=215.6°, A_{95}=4.1° and ASD=15.7° for the reverse (N=48); Lat=86.4°, Long=359.4°, A_{95}=2.3° and ASD=14.9° for the combined (N=131). Note that these ASDs are calculated around the mean VGP positions. Though the mean VGPs except the reversed data are slightly apart from the geographic pole, some part of the discrepancy may be attributed to the absolute plate motion. If we correct the sampling localities for the plate motion, the mean VGPs move to new positions; Lat=86.9°, Long=330.6°, A_{95}=2.8° and ASD=13.8° for the normal (N=82); Lat=−87.1°, Long=228.0°, A_{95}=4.1° and ASD=15.6° for the reverse (N=48); Lat=87.5°, Long=356.0°,

A_{95}=2.3° and ASD=14.6° for the combined (N=130). It is noted that one normal polarity (RT10) is changed to the intermediate after the correction. These VGP positions are about 1° closer to the pole and all the ASD values become smaller than the before. This indicates that the correction for the absolute plate motion works well in the present data set. Thus we will discuss the directional data after the correction later.

In the present study, 95 out of 140 directional results were obtained from the lava sequences (Tables 3.3 and 3.4). Since a number of eruptions might possibly have occurred during a very short time period, the serial correlation of the paleodirections is checked between the adjacent lava flows. If the mean paleodirections of the adjacent flows are statistically indistinguishable from each other at a 95% confidence level, both data are assumed to belong the same vector group. If not, each flow is regarded as an independent vector. After the treatment, 95 paleodirections can be grouped into 45 vectors (Table 3.3 and 3.4). Combining the data from the dikes and the single lavas (Table 3.2), 90 independent vectors are given to be 53 normal, 31 reversed and 6 intermediate ones.

One may, however, oppose the grouping by the serial correlation because such filtering would cause an artificial and systematic error. This may be crosschecked by the reversal test (McFadden and McElhinny, 1990). They proposed that quality of the positive reversal test is classified into three levels by a critical angle (γ_c) between normal and reversed mean vectors: classification *A* of $\gamma_c < 5°$, *B* of $5° < \gamma_c < 10°$ and *C* of $10° < \gamma_c < 20°$. We apply the reversal test to the grouped VGP vectors and also to the raw VGPs with defining the following statistical parameters: R_N, a length of vector sum of the normal VGPs; R_R, that of the reversed VGPs; γ_c, a critical angle at a 95% level of confidence; γ, an angle between the normal and reversed VGP vectors. For the grouped data set (N=84) the parameters are calculated as R_N=51.1, R_R=29.7, $\gamma_c = 6.37°$ and $\gamma = 3.15°$, while those for the raw VGPs as R_N=79.6, R_R=46.2, $\gamma_c = 4.73°$ and $\gamma = 3.80°$ (N=130). Both results pass the reversal tests because of $\gamma < \gamma_c$, but the quality classification is *B* for the grouped VGPs whilst *A* for the raw VGPs. It means that the raw data set is more averaging out the PSV than the grouped one. This may be supported by Love (1998). He showed that direction changes in a few degrees were occasionally accompanied with intensity changes in tens of microteslas and remarked that the grouping based on the directional similarity was quite risky. Therefore we take the raw VGP data set in the PSV analysis.

Since it is known that ASD is sometimes seriously dependent on a cut off angle (e.g. Chauvin *et al.*, 1990; Shibuya *et al.*, 1995), we check its dependence of the prersent data set (Figure 3.6). As seen in this figure, the ASD of our data set is almost insensitive to the VGP cut off angle around 50°. Therefore the ASD value for the combined VGPs (N=130) around the mean is calculated to be 14.6° (+1.3°, -1.2°), and it is reliable for the last 5 Ma PSV in the Society Islands. This ASD is slightly larger than the previous results of 13.8° (+2.1°, -1.6°) by Duncan (1975), 13.9° (+1.7°, -1.2°) by Chauvin et al. (1990) and the Model G for the past 5 Ma (McFadden et al., 1988, 1991), though they are statistically indistinguishable at a 95% confidence level. These are summarized in Table 3.5.

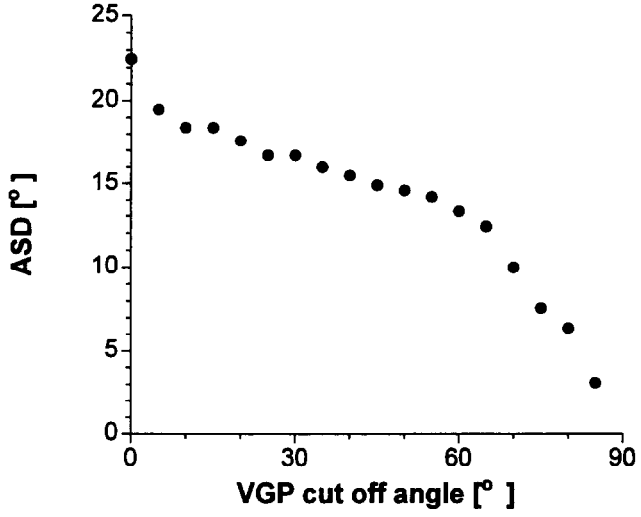

Figure 3.6: Cut off angle dependence of the ASD values for the combined data set.

	Age (Ma)	N	Lat	PLat	PLong	A_{95}	ASD
			this study				
Normal		82	−18.1°	86.9°	330.6°	2.8°	13.8° (+1.7°, -1.3°)
Reverse		48	−18.1°	−87.1°	228.0°	4.1°	15.6° (+2.6°, -1.9°)
Combined	0.5-4.6	130	−18.1°	87.5°	356.0°	2.3°	14.6° (+1.3°, -1.2°)
			previous studies				
Duncan (1975)	0.4-3.4	53	∼ −17°	87.7°	355.2°	3.9°	*13.8° (+2.1°, -1.6°)
Chauvin et al. (1990)	0.5-1.2	81	∼ −17.5°	88.9°	327.9°	2.7°	13.9° (+1.7°, -1.2°)

Table 3.5: Summary of mean VGP positions and angular standard deviations.
N, numbers of the data used for the calculation; Lat, mean site latitude for the data set; PLat, PLong, A_{95}, latitude and longitude of the mean VGP and its 95% confidence circle; ASD, angular standard deviation of the VGP with its 95% confidence limit.
(*) Note that ASD by Duncan (1975) is calculated around the geographic pole.

3.4.4 Time-averaged field

The inclination of the time-averaged field is calculated to be -34.7° (α_{95}=2.6) from the combined data set after the correction for the absolute plate motion. Since the inclination of the geocentric axial dipole (GAD) field is calculated to be -33.2° for the mean site latitude of 18.1°S, the time averaged field in the Society does not show a significant inclination anomaly at a 95% confidence limit. Although small amount of the offset is suggested from the mean VGP position, it seems insignificant. The situation is, however, changed if the plate motion is not taken into account. For example, the mean site latitude is calculated to be 16.9°S and its corresponding GAD inclination is -31.3°. As the mean inclination is preserved even if the plate motion was corrected, the inclination anomaly of -3.4° would be observed and statistically significant at a 95% confidence level.

This demonstrates the importance of the correction for the absolute plate motion. As the usual analysis concerning the inclination anomaly requires a resolution of 1°, the plate-motion correction cannot be ignored, especially for the mid-Pacific region. For the low latitudinal area of the Pacific Ocean, the GAD inclination is sensitive to the change in latitude. The Pacific plate evokes about 2° latitudinal change in sampling sites near the equator during 5 million years, resulting in about 4° inclination change in the GAD field. Johnson and Constable (1997) reported an inclination anomaly of -8.2° in the Hawaiian Islands for the past 5 Ma normal polarity data, but it may partly be ascribed to the plate motion.

3.5 Conclusions

The paleomagnetic and geochronological studies have been performed on the volcanic rocks from the Society Islands, French Polynesia. The K-Ar ages indicate that the collected samples range from 0.5 to 4.6 Ma. The absolute plate motion model of the Pacific plate is concordant with our dating results. For the paleodirections, 82 normal, 48 reversed and 10 intermediate directions were observed and their magnetostratigraphy agrees well with the geomagnetic polarity time scale by Cande and Kent (1995).

If we take into account the absolute plate motion, the mean VGP is located at Lat=87.5°, Long=356.0° and A_{95}=2.3° for the combined data set (N=130). They yield the ASD around the mean VGP of 14.6° (+1.3°, -1.2°). However, an alternative mean at Lat=86.4°, Long=359.4° and A_{95}=2.3° (N=131) would be obtained if the plate motion is not considered.

There is no significant inclination anomaly of the time-averaged field for the past 5 Ma in the Society Islands. However, an apparent anomaly of $-3.4°$ would be observed at a 95% confidence level (α_{95}=2.6) if the plate motion is not taken into account. This suggests that the correction for the absolute plate motion is required for the precise analysis of paleodirections, especially for a lower latitude region of the Pacific Ocean.

Chapter 4

Absolute paleointensities for the last 4 Ma in the Society Islands, French Polynesia

4.1 Introduction

The geomagnetic main field has its origin in the Earth's core. Since the dipole component is dominant in the field, restoration of the ancient dipole moment is essential to know the evolution of the Earth's deep interior. In the last decades, a number of the paleointensities have been accumulated, accompanied with the advance in the absolute paleointensity determination methods. Based on the volcanic data, McFadden and McElhinny (1982) estimated the time-averaged virtual dipole moment (VDM) as $8.67\pm3.63\times10^{22}\mathrm{Am}^2$ for the last 5 Ma. This is almost the same as the present dipole moment ($\sim8\times10^{22}\mathrm{Am}^2$), and this conclusion was not largely changed in the later analysis by Kono and Tanaka (1995). They analyzed the updated database (Tanaka and Kono, 1994) and obtained a mean VDM of $7.84\pm3.80\times10^{22}\mathrm{Am}^2$ for the last 10Ma.

However, this database involves a large number of the paleointensities restored by other than the Coe's version of the Thellier method (Coe, 1967). Since most paleomagnetists regard this method as the only reliable technique (e.g. Selkin and Tauxe, 2000), Juarez and Tauxe (2000) claimed the quality of the database. They carefully examined the Montpellier 1998 database (Perrin et al., 1998), which was updated from Tanaka and

Kono (1994), applying more stringent selection criteria and rejecting data other than those by the Coe's version of the Thellier method. Adding their new paleointensities from submarine basaltic glasses, they determined the time-averaged virtual axial dipole moment (VADM) for the last 0.3-5 Ma period to be $5.49\pm2.36\times10^{22}Am^2$. This is lower than the previous values (McFadden and McElhinny, 1982; Kono and Tanaka, 1995) and the present dipole moment.

The VADM estimated by Juarez and Tauxe (2000) is not far from the calibrated relative paleointensity records. The relative paleointensities are obtained by the normalization of natural remanent magnetization (NRM) to susceptibility, anhysteretic remanent magnetization (ARM), isothermal remanent magnetization (IRM) and so on, after demagnetizing to some level. Valet and Meynadier (1993) obtained an average VADM of $3.9\pm1.9\times10^{22}Am^2$ from the first continuous sedimentary records spanning the last 4 Ma. Gee et al. (1996) calibrated two Brunhes chron (0-0.78 Ma) sedimentary records from the equatorial Pacific (Valet and Meynadier, 1993) and the Sulu Sea (Schneider and Mello, 1996). The mean VADM resulted in $5.22\pm2.0\times10^{22}Am^2$ and $3.52\pm1.9\times10^{22}Am^2$, respectively. Guyodo and Valet (1999a) recently integrated 33 relative paleointensity records into a composite curve for the last 800 ka, named Sint-800, and fitted them to the volcanic data with the period of 0-40 ka. They concluded that the time-averaged field for the Brunhes chron was $6.0\pm1.5\times10^{22}Am^2$ in intensity. However, since NRM of the sediments are usually influenced by their rock magnetic properties (e.g. Tauxe, 1993), the sedimentary records of paleointensities are thought to have been somewhat suspicious. Long-term viscous remanent magnetization (VRM) also possibly contaminates the records (Kok and Tauxe, 1996).

On the contrary to its robustness of the Coe's version of the Thellier method, this method occasionally yields the erroneous absolute paleointensities from the typical basaltic samples (Chapter 2). In fact, the recent studies still gave high dipole moments. Laj et al. (2000) reported 89 Thellier results from 2.1-3.9 Ma lava in Oahu, Hawaii, and obtained VADMs ranging from $2.3\times10^{22}Am^2$ to $11.5\times10^{22}Am^2$ with an average of $7.0\pm2.3\times10^{22}Am^2$. Bogue (2001) gave an average VDM of $9.38\pm2.43\times10^{22}Am^2$ from 25 site mean paleointensities of 4 Ma lava flows from Kauai, Hawaii. Alva-Valdivia et al. (2001) reported the paleointensities from four lava flows erupted between 2.2 and 0.8 Ma in Mexico and their VDMs ranged from 6.4 to $9.1\times10^{22}Am^2$. It is therefore questioned that not a negligible

number of these paleointensities might possibly be originated from thermochemical remanent magnetization (TCRM). The paleointensity experiments of the Hawaiian 1960 lava showed that the ordinary Coe's version of the Thellier method seems to fail in detection of TCRM effect and tends to give higher intensities than the true one (Chapter 2).

In this chapter, we will retrieve the geomagnetic dipole moments over the last 4 Ma from the volcanic rocks of the Society Islands, French Polynesia. Although there are three previous paleointensity studies for the Society volcanic rocks (Senanayake et al., 1982; Roperch and Duncan, 1990; Chauvin et al., 1990), all of them did not pay attention to the long-term dipole variations. The applied method is not the Thellier method but the double heating technique of the Shaw method (Tsunakawa and Shaw, 1994) combined with the low temperature demagnetization (LTD-DHT Shaw method; Tsunakawa et al., 1997; Tsunakawa and Yamamoto, 1999). This is because the Society samples are typical hotspot basalts and the latter method is likely to screen inappropriate results from these samples efficiently (Chapter 2). We also perform typical rock magnetic measurements for the selected samples in order to verify the quality of the obtained paleointensities.

4.2 Samples and rock magnetic properties

Paleointensities were measured for the samples from 6 islands of the Society; Borabora, Tahaa, Raiatea, Huahine, Moorea and Tahiti. Their ages were determined or well estimated from the K-Ar geochronological study (Chapter 3). Paleodirections were also measured and described in the same chapter. Most of them have normal or reversed polarities. As for the rock magnetic properties, we have carried out the following measurements mainly for the samples yielding the successful paleointensity experiments (section 4.3).

4.2.1 Thermomagnetic property

Thermomagnetic analyses were done with the selected 48 samples by a vibrating sample magnetometer (MicroMag 3900 VSM, Princeton Measurement Corporation) in helium gas flow applying a 500mT DC field. The resultant curves can be classified into 6 different types; A, B, C, D, E and F (Figure 4.1) Most of them are interpreted as a product of the titanomagnetite with different Ti content, while one type as that with some degree of low temperature oxidation.

The type A was observed in 20 samples. They show a single phase of Ti-poor titanomagnetite with the good thermal stability, usually resulting in the Curie temperatures (T_c) higher than 500°C. The type B recognized in 11 samples resembles the type A, but a minor phase of Ti-rich titanomagnetite with T_c of 100 $\sim$ 400°C is superimposed. The type C was seen in one sample. There are two components of Ti-poor (T_c=200°C) and Ti-rich (T_c=560°C) titanomagnetites in the thermomagnetic curve. For the type D, 5 samples are characterized by a single phase of titanomagnetite with moderate Ti content, T_c of which ranges from 140°C to 260°C. They show a little increase in the saturation magnetization (M_s) in the cooling stage. Irreversible thermomagnetic curves were found in the type E of 7 samples. They show a relatively lower T_c component followed by a small bump of higher T_c in a heating curve. Since the higher T_c ranges from 530°C to 580°C, some amount of titanomaghemite were possibly produced by low temperature oxidation and they were transformed into the Ti-poor titanomagnetites during the laboratory heating. Finally, 4 samples yielded the type F curves. This type has the weakest magnetization and some paramagnetic behavior is recognized as a vertical offset in thermomagnetic curves.

All the measurements are summarized in Table 4.1 together with the identified T_c.

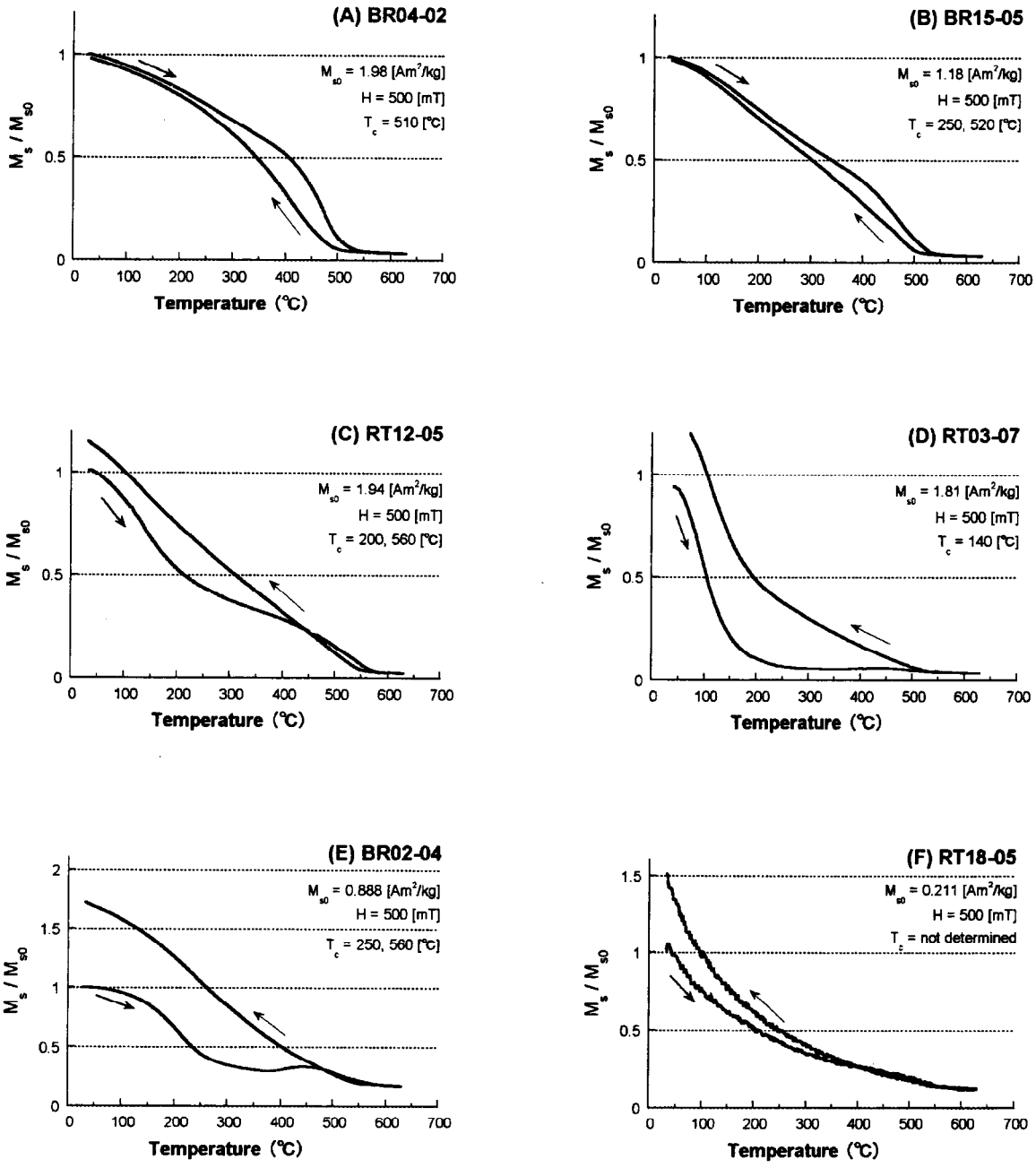

Figure 4.1: Six classification types of thermomagnetic curves.
All of the measurements were performed in helium gas flow under a DC field of 500mT.

4.2.2 Hysteresis property

Hysteresis parameters of saturation magnetization (M_s), remanent saturation magnetization (M_{rs}), coercivity (H_c) and remanent coercivity (H_{rc}) were measured for three or four small chips from each core used in the paleointensity experiments. The measurements were performed by a vibrating sample magnetometer at a room temperature. Total number of the measured chips is 656, and their hysteresis parameters are listed in Tables 4.2-4.8 with the paleointensity experimental results.

The Day plot (Day et al., 1977) for all the samples shows a linear trend mostly in the PSD region (Figure 4.2(A)). This trend is a common feature recognized in the samples of each island (Figures 4.2(B)-(F)) though the data from Huahine samples exhibit a little shift toward the SD region (Figure 4.2(E)). Some samples show relatively larger H_{rc}/H_c ratios, for instance, the Tahiti samples. It may be caused by superparamagnetic components. The plots also indicate that the samples consist of various grain sizes, probably an admixture of SD and MD judged from the microscopic observation in the next section. As the MD content is not so large, these samples are considered to be suited for the paleointensity measurements.

4.2.3 Reflected microscopy

42 samples from 39 sites were observed by an optical microscope with reflected light. The most typical feature is a multi-domain (MD) size grain with ilmenite lamellas due to high temperature oxidation of titanomagnetite. The representatives are exhibited in Figure 4.3. According to Wilson and Watkins (1967), high temperature oxidation indices of the samples are mostly identified to be low to moderate (I-IV) as in Table 4.1. The highest index of VI is recognized only in 2 samples from PU06 (Figure 4.3(F)). As suggested in the paleointensity study of the Hawaiian 1960 lava (Chapter 2), moderately oxidized samples tend to yield apparently higher intensities by the Thellier method because of the TCRM acquisition in their NRMs. Therefore an alternative method, the LTD-DHT Shaw method, is more appropriate for these samples. Oxidation state of TH02-04 and TH03-12 cannot be identified because their opaque minerals are too small to observe their textures by an optical microscope.

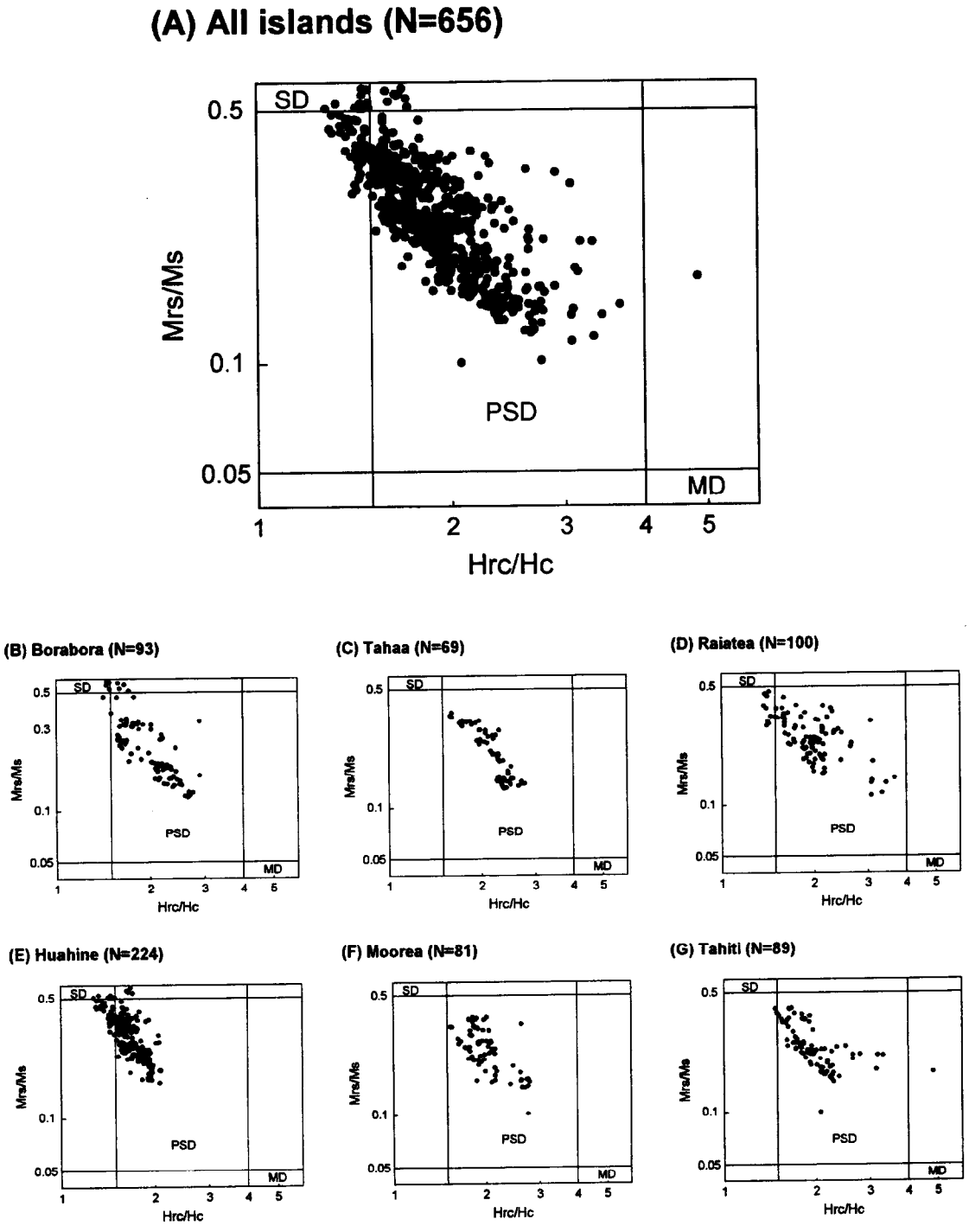

Figure 4.2: Day plots for the samples from (A) all islands and (B)-(G) each island.

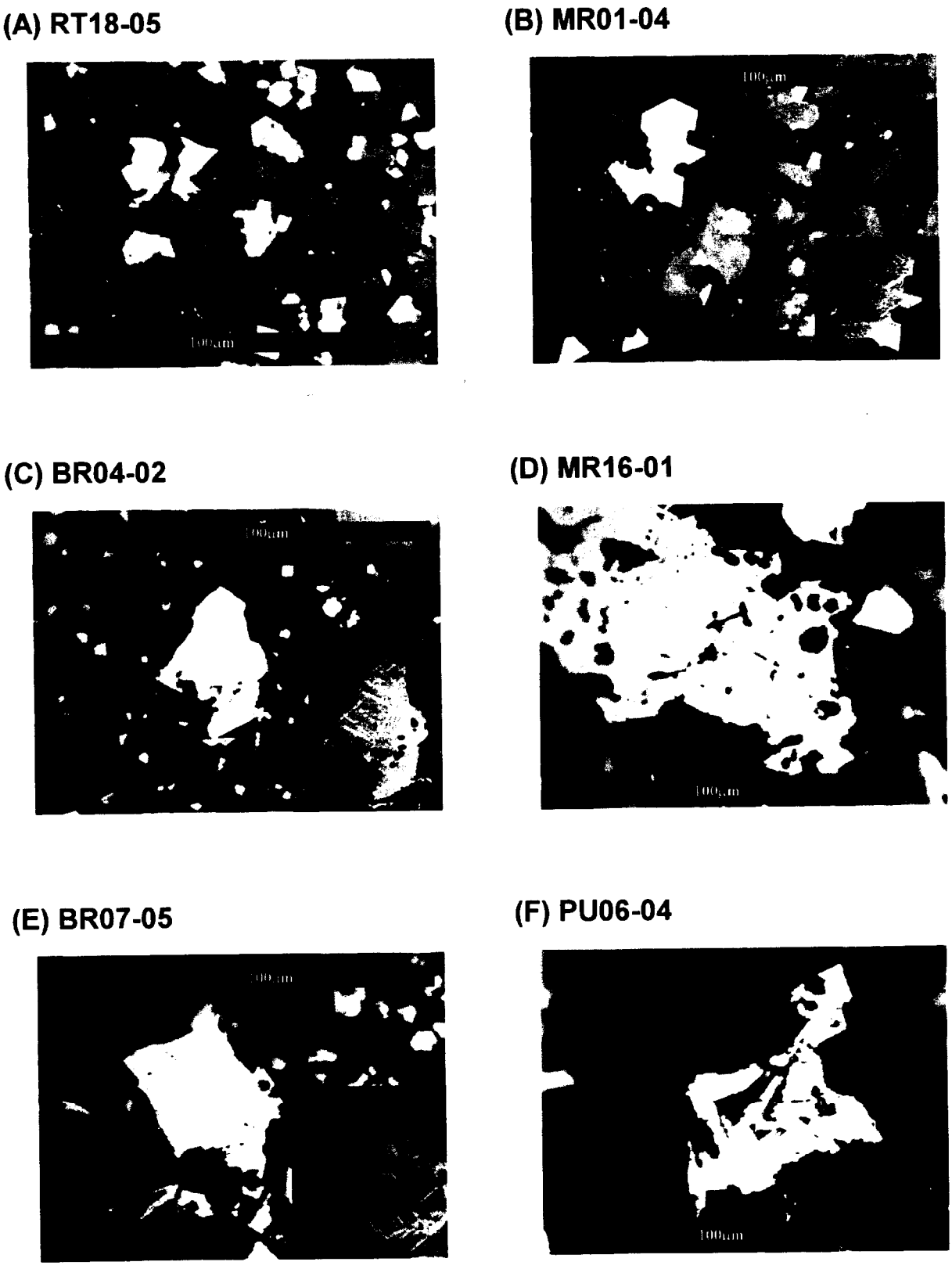

Figure 4.3: Representative examples of the reflected microscopy.
(A) Oxidation index of I, (B) II, (C) III, (D) IV, (E) V and (F) VI. These classifications are based on Wilson and Watkins (1967).

Site	Core ID	Ms-T	T_c (°C)	Oxidation
		Borabora		
BR02	BR02-04	E	250, 560	I-II
BR04	BR04-02	A	510	II-V
BR07	BR07-05	A	540	II-V
BR10	BR10-03	D	170	I
BR15	BR15-05	B	250, 520	I-III
BR16	BR16-03	F	N.d.	I
BR18	BR18-06	A	510	II-V
		Tahaa		
TA08	TA08-01	A	510	III-VI
TA11	TA11-05	B	120, 560	II-IV
TA13	TA13-10	A	540	-
TA15	TA15-06	A	520	III-VI
TA16	TA16-05	A	550	I-III
TA17	TA17-05	B	440, 560	I-III
		Raiatea		
RT03	RT03-07	D	140	I
RT05	RT05-06	A	550	-
RT10	RT10-03	B	210, 540	I-III
RT12	RT12-05	C	200, 560	I-II
RT18	RT18-05	F	N.d.	I
		Huahine		
HH01	HH01-05	-	-	II-IV
HH05	HH05-05	-	-	II-III
	HH05-07	E	290, 570	I-III
HH06	HH06-01	E	290, 530	I-II
HH08	HH08-01	E	450, 540	-
	HH08-04	-	-	I-II
HH09	HH09-06	A	540	I-III
	HH09-07	A	560	-
HH11	HH11-04	D	260	I-II
	HH11-07	D	250	I-II
HH12	HH12-04	E	320, 580	I-II
	HH12-07	E	310, 550	-
HH14	HH14-06	D	210	I
HH16	HH16-01	B	270, 530	I-II
	HH16-03	A	530	-
HH20	HH20-03	A	550	II-IV
		Moorea		
MR01	MR01-04	B	200, 560	II-III
MR06	MR06-06	A	550	III-IV
MR16	MR16-01	A	540	III-IV
	MR16-07	A	520	-
MR18	MR18-07	E	270, 550	-
MR23	MR23-02	B	200, 530	II-IV
MR30	MR30-07	B	150, 520	-
MR32	MR32-06	B	120, 560	I-III
		Tahiti		
PU01	PU01-04	A	550	I-II
PU04	PU04-02	F	570	I-II
PU05	PU05-02	F	580	I-II
PU06	PU06-04	A	580	V-VI
	TH01-01	A	580	IV-VI
TR02	TR02-03	B	110, 580	I-III
TH02	TH02-04	A	530	N/A
TH03	TH03-12	A	530	N/A
TH04	TH04-13	B	100, 560	I-III

Table 4.1: Results of the rock magnetic experiments.
Ms-T, classification of the thermomagnetic curve; T_c, identified Curie temperature; Oxidation, identified oxidation index after Wilson and Watkins (1967).

4.3 Paleointensity results

We applied the LTD-DHT Shaw method to 339 specimens. The AF demagnetization was carried out at 5 or 10mT intervals up to a peak field of 160mT. All the specimens were heated twice in vacuum at 610°C to give a TRM. The top temperature was kept in 20 and 30 minutes for the first (TRM1) and the second heating (TRM2), respectively, except a few specimens (see Tables 4.3, 4.5, 4.6 and 4.7). ARM was given in a 100μT DC field parallel to NRM or TRM, associated with an AC field of 160mT. All the remanence measurements and the AF demagnetizations were performed by an automatic spinner magnetometer (Natsuhara-Giken DSPIN-2; Kono et al., 1984; Kono et al., 1997) with a resolution better than $\pm 10^{-7}$Am^2. The detailed experimental procedures are referred to Chapter 2.

For the alteration due to the laboratory heating, we employed the ARM correction method (Rolph and Shaw, 1985) and checked its validity with the double heating test (Tsunakawa and Shaw, 1994). In the experiments, 40 out of 339 specimens were almost completely exploded during the first laboratory heating. The 299 experimental results were judged by the following selection criteria to obtain paleointensities.

1. Primary component of NRM is recognized in the orthogonal plot of AF demagnetization.

2. Linear portion in the NRM-TRM1* diagram, which should consist of the primary component of relatively higher coercivity, is not less than 15% of the original NRM ($f_N \geq 0.15$). The linear portion is defined by the correlation coefficient ($r_N \geq 0.995$) and the number of data points ($N \geq 5$). Note that the asterisk "*" denotes values after the ARM correction.

3. Linear portion in the TRM1-TRM2* diagram is determined in the same way as in the above ($r_T \geq 0.995$, $N \geq 5$). This fraction is not less than 15% of the original TRM1 ($f_T \geq 0.15$).

4. A slope of the linear portion in the TRM1-TRM2* diagram ranges in 1.00±0.05, because the representative experimental error is estimated to be ±5% in the present study.

The paleointensity results were discarded unless they satisfied the criteria. All of the obtained results are listed in Tables 4.2-4.8. Some of them were analyzed with the correction for changes in mass because small part of them was lost by a little explosion during the laboratory heating. These samples are indicated by the ID of "w" in the tables.

Judged from the criteria, we obtained 164 successful results with a success rate of 55%. The typical example is shown for each group of the thermomagnetic property (Figures 4.4(A)-(F)). They exhibit good linearity in both diagrams of NRM-TRM1* and TRM1-TRM2* (e.g. Figure 4.4(A)), and most of the linear segments are composed of more than 30% of NRM and 90% of TRM1 (Figure 4.6). These results do not show any correlations with the slopes of the ARM0-ARM1 diagrams (Figure 4.7(A)), indicating that the ARM corrections do not evoke systematic errors in the measured paleointensities. This is also supported from the evidence that there are no correlations between the paleointensities and the hysteresis parameters (Figures 4.7(B) and (C)). The 135 experimental results were rejected because (1) the slopes of the linear portion in the TRM1-TRM2* diagrams are out of 1.00±0.05 (e.g. Figure 4.5(A)) and (2) the linear portions are not detected in the NRM-TRM1* diagrams due to $r_N < 0.995$ (e.g. Figure 4.5(B)).

In the usual paleointensity experiments, the internal consistency is sometimes unsatisfying with a cooling unit, as stated in the Chapter 2. It is therefore needed to check it by the multi-specimen test. For the present study, there are 6 outliers in 5 cooling units, that is, BR16-04-1, RT12-01-1, RT12-02-1, RT18-07-2, HH11-07-1 and HH12-02-2. These are indicated by their sample ID with "m" in Tables 4.2, 4.4 and 4.6. For example, the average and standard deviation of 6 samples from RT12 is calculated to be 8.67±1.03μT if RT12-01-1 (14.1μT) and RT12-02-1 (17.8μT) are omitted (Table 4.4). Since hysteresis parameters of these exceptional samples are not so different from the others, the degree of TCRM affection may be critical for them as discussed for the Hawaiian 1960 lava (Chapter 2). The similar situation is recognized for HH11-07-1 and HH12-02-2. For another example, 9.86μT yielded from BR16-04-1 is clearly lower than the others from the site of BR16 (Table 4.2). If BR16-04-1 is excluded, the other four data give a mean paleointensity of 15.8μT with a standard deviation of 1.0μT. Therefore the paleointensity of BR16-04-1 is statistically discriminated at more than 4σ level. This exception, however, cannot be explained by TCRM affection because of its lower intensity. It may be related to its very low T_c phase and its heavily thermal alteration in the laboratory heating.

For the further multi-specimen test, we select site-mean paleointensities which satisfy that the mean is determined from more than 3 individual results and that the standard deviation is less than 20%. Four sites of BR07, BR10, RT10 and HH05 are omitted from this criterion because their standard deviation ranges from 22% to 53%. The reasons for these large inconsistencies may possibly be caused by TCRM, low temperature oxidation and local magnetic anomalies, though they will be clarified in the future studies. Consequently, we obtained 28 reliable mean paleointensities which are calculated more than three paleointensities within site and show a standard deviation less than 20%. All of them are non-transitional records of the geomagnetic field (Chapter 3), and they are listed in Table 4.9 together with the omitted data. Since the correction for the absolute plate motion is important for the precise analysis (Chapter 3), we will discuss VADM after the correction later.

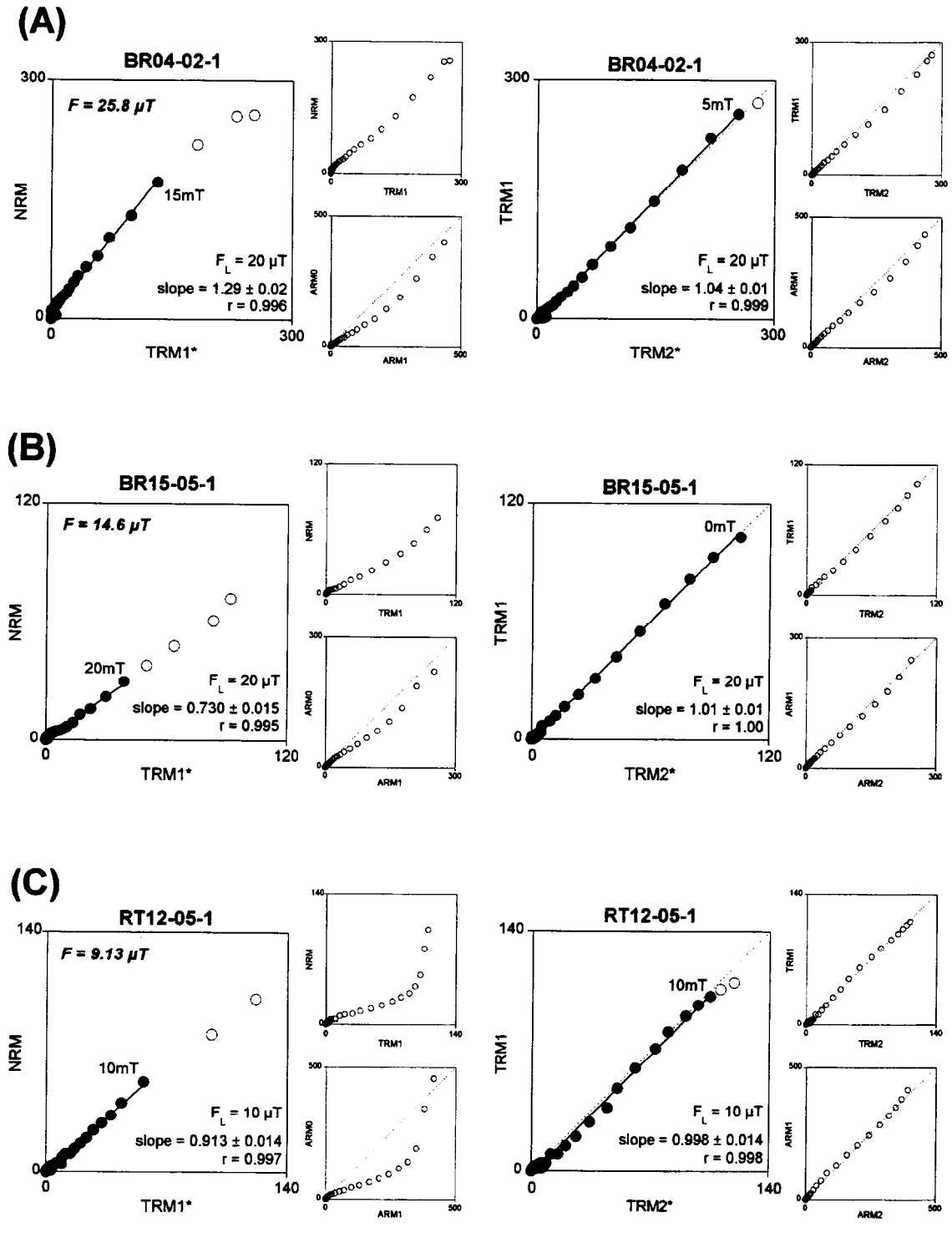

Figure 4.4: Representative successful results of the LTD-DHT Shaw method.

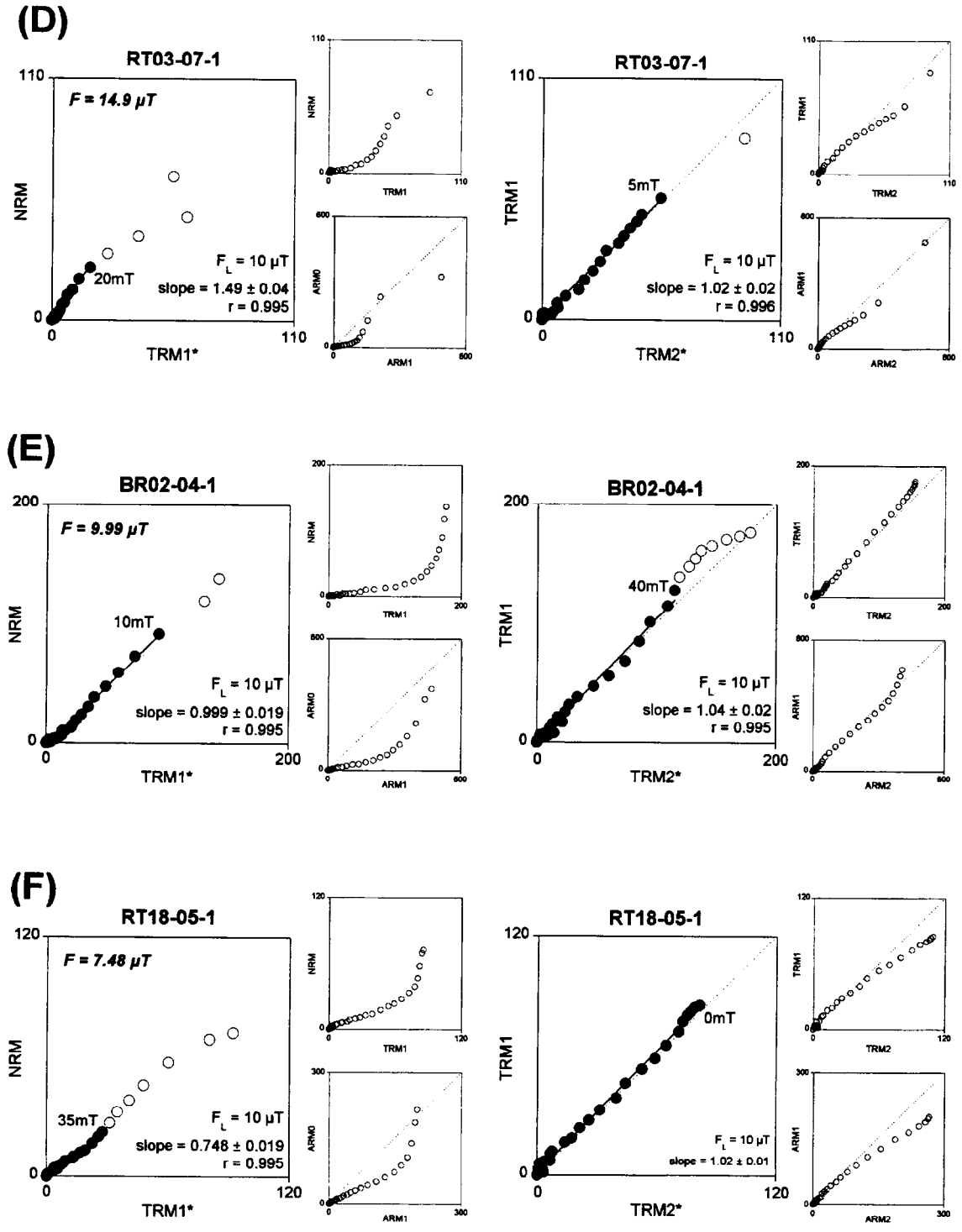

Figure 4.4: Representative successful results of the LTD-DHT Shaw method (continued).

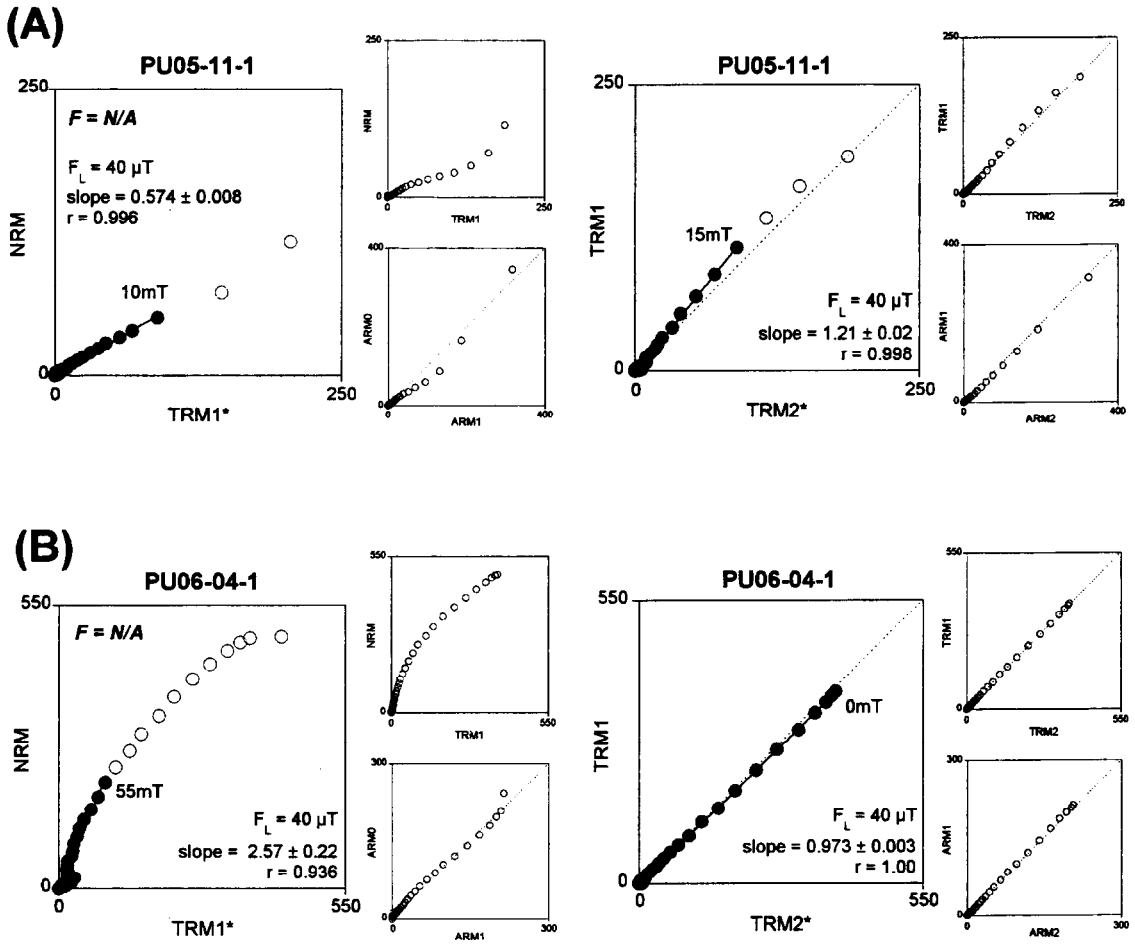

Figure 4.5: Representative rejected results of the LTD-DHT Shaw method.

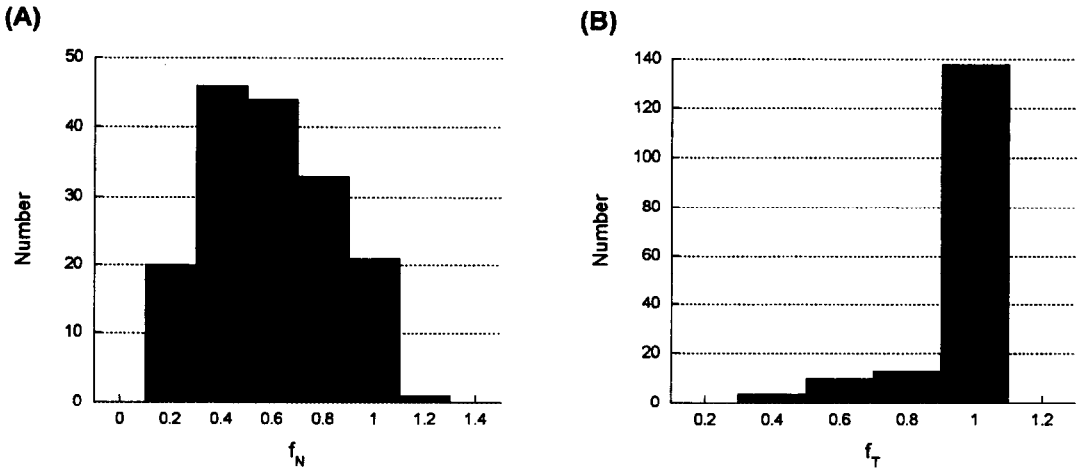

Figure 4.6: Distributions of (A) NRM fractions and (B) TRM fractions for the successful paleointensity results.

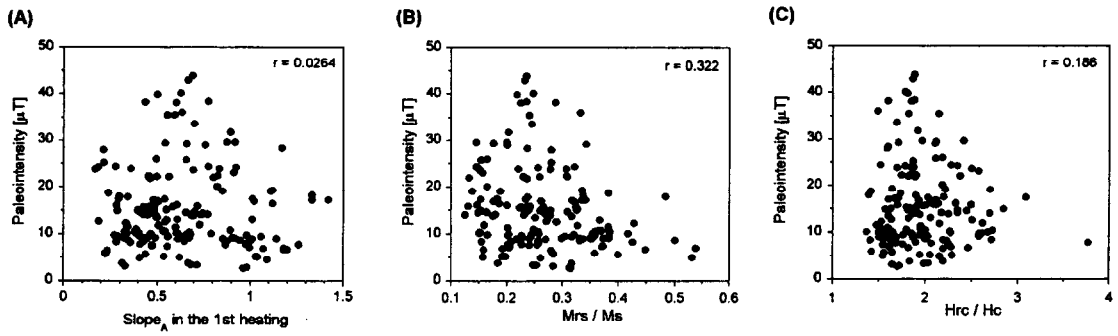

Figure 4.7: Relation of the obtained paleointensities with (A) the slopes in the ARM0-ARM1 diagram, (B) the ratios of remanent saturation magnetization to saturation magnetization (M_{rs}/M_s) and (C) the ratios of remanent coercivity to coercivity (H_{rc}/H_c).

Sample ID	NRM_0	H_{rc}/H_c	M_{rs}/M_s	1st heating					2nd heating					F_L	F
				H_L	$slope_A$	$slope_N$	f_N	r_N	H_L	$slope_A$	$slope_T$	f_T	r_T	(μT)	(μT)
BR02-04-1	139	1.647	0.2447	10	0.393	0.999	0.662	0.995	40	1.02	1.04	0.723	0.995	10.0	9.99
BR02-05-1	138	1.648	0.2579	10	0.404	0.506	0.655	0.998	40	0.934	1.05	0.703	0.997	20.0	10.1
BR02-06-1	133	1.630	0.2569	10	0.426	0.844	0.671	0.997	50	0.962	1.03	0.521	0.995	10.0	8.44
BR02-07-1	138	1.562	0.3050	10	0.406	0.958	0.998	0.750	45	1.04	1.05	0.620	0.995	10.0	9.58
BR04-01-2	283	2.109	0.2006	10	0.757	0.966	0.777	0.995	0	0.962	0.973	1.00	1.00	30.0	29.0
BR04-02-1	269	2.113	0.1536	15	0.658	1.29	0.671	0.996	5	0.913	1.04	0.949	0.999	20.0	25.8
BR04-03-2	294	1.905	0.3087	10	0.564	0.739	0.620	0.998	5	0.879	0.989	0.921	0.999	30.0	22.2
BR04-04-1w	246	-	-	10	0.524	0.966	0.539	0.999	5	0.848	0.922	0.952	0.997	20.0	-
BR04-06-2	337	-	-	15	0.573	1.29	0.640	0.997	0	0.939	1.16	1.00	0.999	20.0	-
BR04-07-1	384	1.713	0.3425	10	0.660	1.460	0.785	0.996	0	0.988	0.994	1.00	1.00	20.0	29.2
BR07-01-1	133	1.602	0.2481	5	0.388	0.549	0.664	0.995	35	0.936	0.959	0.498	0.997	20.0	11.0
BR07-02-1	219	-	-	10	0.200	1.89	0.220	0.982	0	0.942	0.767	1.00	0.990	10.0	-
BR07-05-1	156	2.501	0.1520	20	0.696	1.18	0.567	0.998	0	1.01	0.985	1.00	0.999	20.0	23.6
BR07-06-1	284	2.146	0.2407	15	0.553	3.55	0.678	0.997	5	0.974	0.979	0.962	0.998	10.0	35.5
BR08-01-2	467	-	-	15	0.191	2.44	0.805	0.995	10	1.08	0.888	1.00	0.999	20.0	-
BR08-02-2w	767	-	-	15	0.274	2.64	0.766	0.995	50	1.15	0.807	0.724	0.993	20.0	-
BR08-03-1	164	-	-	5	0.225	0.849	0.994	0.984	0	1.18	0.869	1.00	0.998	20.0	-
BR08-04-2	317	-	-	55	0.183	0.816	0.181	0.995	0	1.14	0.938	1.00	0.993	20.0	-
BR08-05-1	1100	-	-	15	0.446	3.72	0.757	0.998	30	1.09	1.06	0.961	0.999	20.0	-
BR08-06-1	985	-	-	15	0.510	3.59	0.723	0.998	0	1.00	1.10	1.00	0.998	20.0	-
BR08-07-1	623	-	-	20	0.222	9.39	0.693	0.992	0	1.01	0.996	1.00	0.998	10.0	-
BR09-03-1	148	-	-	5	0.885	0.352	0.687	0.975	10	0.842	1.00	0.861	0.998	40.0	-
BR10-01-1	65.0	1.551	0.5325	55	0.545	0.248	0.275	0.991	0	0.831	1.05	1.00	0.996	20.0	-
BR10-01-2	61.7	1.551	0.5325	65	0.621	0.500	0.232	0.996	0	0.826	1.04	1.00	0.997	10.0	5.00
BR10-02-2	129	-	-	40	1.25	1.97	0.486	0.995	0	0.834	0.913	1.00	0.995	5.00	-
BR10-03-1	83.3	1.825	0.4486	10	1.20	0.668	0.341	0.998	0	0.898	0.953	1.00	0.998	10.0	6.68
BR10-03-2	83.9	1.825	0.4486	55	1.33	0.761	0.403	0.992	0	0.852	0.912	1.00	0.995	10.0	-
BR10-04-1	149	1.548	0.5002	55	0.972	0.806	0.226	0.996	0	0.834	1.12	1.00	0.998	10.0	-
BR10-04-2	131	1.548	0.5002	65	0.944	0.867	0.196	0.995	0	0.851	1.03	1.00	0.999	10.0	8.67
BR10-05-2	114	-	-	50	0.911	1.49	0.365	0.995	0	0.816	0.908	1.00	0.997	5.00	-
BR10-07-2	78.1	1.615	0.5392	50	1.18	0.696	0.357	0.995	0	0.878	0.974	1.00	0.999	10.0	6.96
BR14-06-1	264	2.183	0.1652	15	0.821	0.503	0.591	0.999	0	0.922	0.980	1.00	1.00	40.0	20.1
BR15-01-2	65.1	2.496	0.1304	20	0.716	0.791	0.420	0.996	0	0.980	0.950	1.00	1.00	20.0	15.8
BR15-02-1	66.7	2.698	0.1250	20	0.737	0.699	0.467	0.995	0	0.925	0.984	1.00	0.999	20.0	14.0
BR15-03-1	70.7	2.620	0.1590	20	0.729	1.19	0.392	0.995	0	0.915	1.00	1.00	0.998	10.0	11.9
BR15-05-1	75.1	2.346	0.1645	20	0.700	0.730	0.419	0.995	0	0.973	1.01	1.00	1.00	20.0	14.6
BR15-06-2	69.9	2.448	0.1484	15	0.654	1.45	0.519	0.995	0	0.924	1.01	1.00	0.998	10.0	14.5
BR15-07-1	82.4	2.330	0.1464	20	0.607	1.61	0.414	0.995	0	0.947	1.02	1.00	0.999	10.0	16.1
BR16-01-2	230	1.669	0.3168	25	0.479	1.72	0.205	0.995	5	0.981	0.963	0.926	0.998	10.0	17.2
BR16-02-2	272	1.798	0.3268	25	0.446	0.765	0.214	0.995	0	0.980	1.03	1.00	0.999	20.0	15.3
BR16-03-1	269	1.882	0.2790	30	0.424	0.749	0.166	0.997	5	0.960	1.00	0.947	0.999	20.0	15.0
BR16-04-1m	110	2.274	0.3203	30	0.612	0.493	0.286	0.995	20	0.912	1.02	0.786	0.998	20.0	9.86
BR16-05-1	85.7	-	-	10	0.463	1.22	0.738	0.996	20	0.902	1.12	0.883	0.998	10.0	-
BR16-05-2	119	-	-	30	0.290	0.521	0.217	0.995	0	0.970	1.13	1.00	0.999	20.0	-
BR16-06-1	255	1.705	0.3235	25	0.462	1.57	0.195	0.995	20	0.965	1.01	0.731	0.999	10.0	15.7
BR16-07-2	248	-	-	5	0.863	1.04	0.919	0.995	25	1.00	1.07	0.738	0.999	20.0	-
BR18-01-1	271	-	-	15	1.07	0.867	0.611	0.998	0	1.03	0.944	1.00	1.00	20.0	-
BR18-02-1	242	2.199	0.1827	15	1.01	0.870	0.628	0.998	0	1.01	1.01	1.00	1.00	20.0	17.4
BR18-04-2	214	-	-	15	0.942	0.804	0.572	1.00	0	0.966	1.11	1.00	1.00	20.0	-
BR18-06-1	233	2.114	0.1764	15	1.02	0.843	0.593	0.999	0	0.992	1.03	1.00	1.00	20.0	16.9
BR18-07-1	250	2.076	0.1860	15	1.12	0.819	0.599	0.999	0	0.973	1.04	1.00	1.00	20.0	16.4
BR18-08-1	304	2.217	0.1886	15	1.11	1.90	0.647	0.997	0	1.00	0.984	1.00	1.00	10.0	19.0

Table 4.2: Experimental results for the Borabora samples.
NRM_0, initial NRM intensity after LTD in $10^{-5}Am^2/kg$; H_{rc}/H_c, M_{rs}/M_s, mean ratio of the hysteresis parametes; H_L, the lowest coercivity force taken for the linear segments; $slope_A$, slope of ARM spectra ($\geq H_L$) before and after laboratory heating; $slope_N$, $slope_T$, r_N, r_T, f_N, f_T, slope, correlation coefficients and NRM and TRM1 fractions of the linear segment in the NRM-TRM1* and TRM1-TRM2* diagrams; F_L, laboratory induced DC field for TRM1 and TRM2; F, calculated paleointensity.
Sample ID with "w" and "m" denotes that the paleointensity is calculated with the correction for the mass change and is excluded in the calculation for the flow average by the multi-specimen test, respectively.

Sample ID	NRM_0	H_{rc}/H_c	M_{rs}/M_s	1st heating					2nd heating					F_L	F
				H_L	$slope_A$	$slope_N$	f_N	r_N	H_L	$slope_A$	$slope_T$	f_T	r_T	(μT)	(μT)
TA01-05-1	57.9	-	-	-	-	-	-	-	15	1.03	1.21	0.590	0.999	40.0	-
TA01-07-1	47.4	-	-	-	-	-	-	-	25	0.868	1.29	0.439	0.998	40.0	-
TA02-08-1	79.5	-	-	-	-	-	-	-	25	0.833	0.954	0.705	0.998	40.0	-
TA03-02-1	301	-	-	20	0.330	0.291	0.046	0.966	15	0.941	1.04	0.908	0.999	10.0	-
TA03-06-1	360	-	-	20	0.249	0.352	0.032	0.978	15	1.02	1.02	0.955	0.997	10.0	-
TA04-01-1	84.2	-	-	10	0.445	0.159	0.269	0.969	15	0.991	0.969	0.863	0.996	20.0	-
TA04-08-1	61.5	-	-	20	0.337	0.657	0.543	0.972	0	1.03	0.975	1.00	0.997	10.0	-
TA07-07-1	35.0	-	-	15	1.09	0.223	0.392	0.996	0	1.01	0.973	1.00	0.999	20.0	4.46
TA08-01-1	79.7	2.416	0.1452	25	0.871	1.48	1.14	0.997	0	1.02	0.969	1.00	0.999	20.0	29.6
TA08-02-2*	149	2.379	0.1322	30	0.801	1.10	0.281	0.996	0	1.01	0.980	1.00	1.00	20.0	22.0
TA08-03-2	156	2.280	0.1447	35	0.776	1.22	0.227	0.995	0	1.00	0.979	1.00	1.00	20.0	24.4
TA08-04-1	211	-	-	15	0.991	1.03	0.548	0.987	0	1.00	0.990	1.00	0.999	20.0	-
TA08-05-1	301	2.346	0.1475	30	0.970	0.516	0.143	0.990	0	0.998	0.972	1.00	1.00	40.0	-
TA08-05-2	260	2.346	0.1475	35	0.921	1.21	0.170	0.995	0	1.01	0.999	1.00	1.00	20.0	24.2
TA08-06-1*	260	2.703	0.1379	25	0.849	0.949	0.189	0.995	0	0.985	1.03	1.00	1.00	20.0	19.0
TA08-07-2	289	2.428	0.1395	40	0.757	1.33	0.102	0.995	0	1.01	0.963	1.00	1.00	20.0	-
TA10-06-1	153	-	-	30	0.850	0.492	0.135	0.987	10	0.931	0.951	0.753	0.999	40.0	-
TA11-01-2	1500	1.846	0.3266	30	1.03	1.07	0.071	0.995	0	0.956	1.01	1.00	0.999	20.0	-
TA11-02-2	940	-	-	20	0.848	3.47	0.132	0.979	0	0.983	1.02	1.00	0.996	10.0	-
TA11-04-1	601	-	-	20	0.842	4.23	0.118	0.989	0	1.02	0.975	1.00	0.999	10.0	-
TA11-05-1	468	1.868	0.3072	20	0.822	1.12	0.279	0.998	5	0.987	0.981	0.981	0.999	20.0	22.4
TA11-06-2	264	2.581	0.1567	25	0.910	1.15	0.244	0.995	0	0.982	0.986	1.00	0.999	20.0	23.0
TA11-07-1	415	1.875	0.3062	20	0.832	2.39	0.303	0.996	0	1.02	0.966	1.00	0.999	10.0	23.9
TA13-01-1	111	-	-	20	0.558	0.179	0.0860	0.909	0	0.844	0.936	1.00	0.999	40.0	-
TA13-02-1	139	-	-	20	0.355	0.377	0.0680	0.957	20	0.945	1.05	0.669	0.996	10.0	-
TA13-03-1	110	-	-	20	0.385	0.461	0.0860	0.934	20	0.868	0.988	0.708	0.996	10.0	-
TA13-06-1	103	-	-	20	0.441	0.245	0.0990	0.936	10	0.790	0.952	0.810	0.999	20.0	-
TA13-07-1	139	-	-	20	0.366	0.559	0.0900	0.953	15	0.877	1.01	0.791	0.996	10.0	-
TA13-10-1	104	2.266	0.1503	15	0.605	1.02	0.351	0.996	0	1.00	0.990	1.00	0.999	10.0	10.2
TA13-11-1	101	-	-	20	0.451	0.478	0.120	0.970	0	0.895	0.976	1.00	0.998	10.0	-
TA15-01-1	81.7	2.247	0.2045	10	0.866	0.768	0.934	0.995	5	0.983	0.998	0.980	1.00	10.0	7.68
TA15-02-2	87.3	2.193	0.2081	20	0.699	0.897	0.825	0.988	0	1.02	1.06	1.00	1.00	10.0	-
TA15-02-3	91.0	2.193	0.2081	10	0.873	0.844	0.942	0.995	0	1.02	0.999	1.00	1.00	10.0	8.44
TA15-05-1	92.9	2.270	0.2043	20	0.778	0.445	0.634	0.984	0	1.03	1.01	1.00	1.00	20.0	-
TA15-05-2	93.7	2.270	0.2043	5	0.996	0.714	0.988	0.995	0	1.01	1.05	1.00	0.999	10.0	7.14
TA15-06-1	74.3	2.464	0.1589	5	1.18	0.669	0.991	0.998	0	1.04	1.00	1.00	1.00	10.0	6.69
TA15-07-1	85.0	2.279	0.1925	5	1.07	0.686	0.995	0.995	0	0.984	1.03	1.00	1.00	10.0	6.86
TA16-03-2	105	-	-	20	0.707	0.271	0.113	0.973	0	1.00	0.980	1.00	0.997	10.0	-
TA16-04-1	61.0	2.035	0.2468	20	0.683	0.339	0.173	0.995	0	1.00	1.00	1.00	0.999	10.0	3.39
TA16-05-1	59.1	1.987	0.2539	15	0.717	0.333	0.216	0.996	0	0.999	1.02	1.00	0.998	10.0	3.33
TA16-06-1	17.1	1.726	0.3126	20	0.983	0.275	0.802	0.995	0	1.02	1.02	1.00	0.999	10.0	2.75
TA16-07-1	21.6	1.707	0.3147	20	0.962	0.260	0.603	0.995	0	1.02	1.01	1.00	0.999	10.0	2.60
TA17-02-2w	28.0	-	-	20	0.290	0.387	0.647	0.989	0	1.04	0.953	1.00	0.996	10.0	-
TA17-04-1w	35.0	2.194	0.2801	30	0.233	0.650	0.532	0.995	0	1.10	0.972	1.00	0.998	10.0	6.50
TA17-05-1	42.5	2.154	0.2615	15	0.407	0.485	0.633	0.995	20	0.985	0.982	0.932	0.997	10.0	4.85
TA17-06-1w	34.1	-	-	20	0.168	0.267	0.274	0.895	0	0.985	0.989	1.00	0.997	10.0	-
TA17-07-1w	45.2	-	-	20	0.165	0.107	0.321	0.978	0	0.973	0.928	1.00	1.00	40.0	-
TA19-05-1	85.1	1.593	0.3529	15	0.611	0.224	0.683	0.999	25	0.794	1.05	0.697	0.999	40.0	8.96
TA20-01-1	95.6	-	-	15	0.945	0.236	0.716	0.999	0	0.990	0.915	1.00	1.00	40.0	-

Table 4.3: Experimental results for the Tahaa samples.
* TA08-02-2 and TA08-06-1 were heated at 610°C for 30 (TRM1) and 40 minutes (TRM2).

Sample ID	NRM_0	H_{rc}/H_c	M_{rs}/M_s	1st heating					2nd heating					F_L	F
				H_L	$slope_A$	$slope_N$	f_N	r_N	H_L	$slope_A$	$slope_T$	f_T	r_T	(μT)	(μT)
RT03-01-1	276	-	-	20	0.270	0.907	0.401	0.983	35	1.03	1.01	0.608	0.995	10.0	-
RT03-02-1	120	1.905	0.1924	20	0.143	0.484	0.429	0.970	15	0.948	1.10	0.967	0.999	20.0	-
RT03-03-2	94.8	-	-	15	0.382	0.976	0.602	0.995	15	0.808	1.22	0.533	0.998	20.0	-
RT03-04-2	49.8	-	-	15	0.317	0.649	0.542	0.994	5	0.733	1.08	0.701	0.991	20.0	-
RT03-05-1	113	-	-	-	-	-	-	-	5	0.864	1.00	0.888	0.998	20.0	-
RT03-06-2	90.8	3.091	0.1532	20	0.292	1.73	0.537	0.995	5	0.810	1.05	0.756	0.998	10.0	17.3
RT03-07-1	67.5	2.849	0.1539	20	0.287	1.49	0.363	0.995	5	0.770	1.02	0.673	0.996	10.0	14.9
RT05-06-1	43.2	2.056	0.1975	20	0.536	0.260	0.621	0.995	0	1.01	0.969	1.00	0.999	20.0	5.20
RT10-01-2w	73.7	1.837	0.3167	15	0.312	0.384	0.479	0.995	0	0.990	1.01	1.00	0.999	10.0	3.84
RT10-01-3	24.9	1.837	0.3167	20	0.261	0.324	0.737	0.962	0	0.990	1.03	1.00	0.998	10.0	-
RT10-02-1	32.7	-	-	20	0.261	0.332	0.488	0.964	0	1.01	1.05	1.00	0.999	10.0	-
RT10-03-1	104	1.648	0.2840	25	0.225	0.577	0.330	0.995	0	0.996	0.953	1.00	0.997	10.0	5.77
RT10-03-2	41.7	1.648	0.2840	15	0.327	0.308	0.661	0.995	0	0.993	1.02	1.00	0.997	10.0	3.08
RT12-01-1m	147	2.349	0.2723	10	0.426	0.707	0.536	0.995	0	0.990	1.04	1.00	0.998	20.0	14.1
RT12-02-1m	130	1.899	0.2372	15	0.342	1.78	0.502	0.996	0	1.02	1.01	1.00	0.999	10.0	17.8
RT12-03-2	113	2.234	0.2576	15	0.357	0.822	0.310	0.996	0	0.990	1.02	1.00	0.995	10.0	8.22
RT12-04-1	92.8	2.000	0.2567	10	0.347	0.857	0.469	0.995	0	1.02	1.00	1.00	0.997	10.0	8.57
RT12-04-2	92.2	2.000	0.2567	15	0.325	1.05	0.422	0.995	15	1.06	0.987	0.907	0.996	10.0	10.5
RT12-05-1	102	1.982	0.2405	10	0.446	0.913	0.523	0.997	10	1.00	0.998	0.927	0.998	10.0	9.13
RT12-06-2	110	1.903	0.2269	15	0.409	0.792	0.335	0.995	0	0.971	1.05	1.00	0.998	10.0	7.92
RT12-07-2	128	2.071	0.2405	30	0.473	0.768	0.217	0.997	10	0.982	1.05	0.930	0.999	10.0	7.68
RT18-02-2	137	1.500	0.3532	15	0.465	1.99	0.601	0.995	0	0.866	1.04	1.00	0.995	5.0	10.0
RT18-03-1	48.1	2.235	0.3721	20	0.681	0.331	0.506	0.990	0	0.835	0.912	1.00	0.999	20.0	-
RT18-05-1	74.6	1.760	0.3726	35	0.472	0.748	0.312	0.995	0	0.744	1.02	1.00	0.998	10.0	7.48
RT18-06-2	103	1.668	0.3494	10	0.442	0.924	0.764	0.996	25	0.940	1.01	0.788	0.999	10.0	9.24
RT18-07-1	79.1	1.942	0.3163	15	0.559	1.89	0.767	0.996	0	0.838	0.995	1.00	0.996	5.0	9.45
RT18-07-2m	218	1.942	0.3163	15	0.493	1.37	0.695	0.995	0	0.944	1.05	1.00	0.999	10.0	13.7
RA01-15-1	191	2.507	0.2892	20	0.542	0.629	0.563	0.995	0	1.06	1.04	1.00	0.999	20.0	12.6

Table 4.4: Experimental results for the Raiatea samples.

Sample ID	NRM_0	H_{rc}/H_c	M_{rs}/M_s	1st heating					2nd heating					F_L	F
				H_L	$slope_A$	$slope_N$	f_N	r_N	H_L	$slope_A$	$slope_T$	f_T	r_T	(μT)	(μT)
HH01-02-2w	227	1.884	0.2350	40	0.692	4.38	0.320	0.995	0	1.01	1.04	1.00	1.00	10.0	43.8
HH01-03-2	206	-	-	40	0.714	4.62	0.291	0.981	0	1.01	1.04	1.00	0.999	10.0	-
HH01-04-2w	209	1.865	0.2316	35	0.666	1.43	0.343	0.995	0	1.02	1.04	1.00	1.00	30.0	42.9
HH01-06-1	237	1.887	0.2351	55	0.825	1.31	0.237	0.991	25	0.967	1.62	0.603	0.999	40.0	-
HH01-06-2	247	1.887	0.2351	30	0.774	1.28	0.481	0.996	0	0.99	1.02	1.00	1.00	30.0	38.4
HH01-07-2w	253	-	-	35	0.745	2.06	0.366	0.990	0	0.990	1.05	1.00	0.999	20.0	-
HH04-05-1w	207	1.819	0.2989	20	1.05	0.655	0.640	0.991	0	1.02	1.03	1.00	1.00	40.0	-
HH05-01-2w	137	1.476	0.3821	10	0.340	0.575	0.885	0.995	55	1.24	1.01	0.665	0.997	20.0	11.5
HH05-02-2	108	1.528	0.4280	10	0.332	1.23	0.911	0.995	45	1.17	1.04	0.842	0.995	10.0	12.3
HH05-03-2w	166	1.413	0.3826	15	0.239	1.87	0.467	0.998	30	1.11	1.05	0.903	0.995	10.0	18.7
HH05-05-2w	228	1.616	0.5803	55	0.323	0.721	0.172	0.968	0	1.11	1.14	1.00	0.999	10.0	-
HH05-06-2	153	-	-	15	0.276	2.84	0.894	0.988	0	1.03	1.04	1.00	0.995	10.0	-
HH05-07-2	134	1.392	0.4832	15	0.296	0.893	0.769	0.997	0	1.06	1.02	1.00	0.998	20.0	17.9
HH06-01-2	108	1.556	0.3563	10	0.504	0.174	0.779	0.989	0	1.25	1.03	1.00	0.998	20.0	-
HH06-02-2	108	-	-	45	0.368	0.255	0.152	0.995	0	1.14	1.09	1.00	0.999	10.0	-
HH06-03-2	97.1	-	-	10	0.418	0.251	0.820	0.989	0	1.42	1.01	1.00	0.996	10.0	-
HH06-04-1	92.7	1.580	0.4146	0	0.475	0.101	1.00	0.989	0	1.04	1.46	1.00	0.998	40.0	-
HH06-04-2	94.7	1.580	0.4146	35	0.337	0.212	0.222	0.986	0	1.23	1.11	1.00	0.997	10.0	-
HH06-05-2	124	1.549	0.3709	15	0.555	0.744	0.693	0.995	0	1.04	1.05	1.00	0.999	10.0	7.44
HH06-06-2	94.1	-	-	15	0.429	0.522	0.667	0.991	0	1.07	1.01	1.00	0.999	10.0	-
HH06-06-3	97.4	-	-	15	0.446	0.517	0.645	0.987	0	1.06	1.02	1.00	0.998	10.0	-
HH06-07-2	118	1.559	0.3997	20	0.439	0.287	0.497	0.995	0	1.11	1.04	1.00	1.00	20.0	5.74
HH07-01-2	13.5	1.672	0.4140	-	-	-	-	-	0	1.04	0.978	1.00	0.998	40.0	-
HH07-07-1w	23.6	1.519	0.5551	20	0.094	0.128	0.615	0.978	45	1.06	1.74	0.755	0.999	40.0	-
HH08-01-2	105	1.696	0.2785	20	0.168	1.19	0.366	0.995	0	1.06	0.990	1.00	0.999	20.0	23.8
HH08-02-1	104	1.815	0.2770	15	0.560	0.517	0.570	0.998	35	0.818	3.38	0.396	0.986	40.0	-
HH08-02-2	128	1.815	0.2770	20	0.204	1.40	0.338	0.995	15	1.02	0.933	0.958	0.998	20.0	-
HH08-03-2	109	1.786	0.2557	25	0.182	1.21	0.323	0.995	0	1.02	1.01	1.00	0.999	20.0	24.2
HH08-04-1	162	1.592	0.2793	10	0.530	0.633	0.675	0.998	30	0.795	1.85	0.568	0.995	40.0	-
HH08-04-2	154	1.592	0.2793	20	0.212	1.40	0.350	0.995	10	1.00	0.951	0.978	0.999	20.0	28.0
HH08-04-2-1*	178	1.592	0.2793	20	0.268	0.703	0.404	0.991	30	1.13	0.784	0.933	1.00	40.0	-
HH08-05-1	122	1.872	0.2793	20	0.214	1.26	0.404	0.995	10	1.01	0.958	0.978	0.999	20.0	25.2
HH08-07-2	157	1.521	0.3216	15	0.277	1.22	0.455	0.996	0	0.987	1.00	1.00	0.999	20.0	24.4
HH09-01-2	363	-	-	10	1.12	0.976	0.892	0.998	0	1.08	1.06	1.00	1.00	20.0	-
HH09-03-2	422	1.647	0.3349	10	1.12	0.961	0.903	0.998	0	1.05	1.05	1.00	1.00	20.0	19.2
HH09-04-1	367	1.735	0.3368	5	1.33	0.912	0.980	0.997	0	1.10	1.01	1.00	0.999	20.0	18.2
HH09-05-1**	420	1.667	0.3413	0	1.31	0.367	1.00	0.998	0	1.09	1.10	1.00	1.00	50.0	-
HH09-05-2	394	1.667	0.3413	5	1.33	0.853	0.976	0.998	0	1.08	1.02	1.00	1.00	20.0	17.1
HH09-06-1**	391	1.714	0.3390	0	1.24	0.480	1.00	0.998	0	1.10	0.866	1.00	1.00	50.0	-
HH09-06-2	370	1.714	0.3390	0	1.42	0.853	1.00	0.998	0	1.08	1.05	1.00	1.00	20.0	17.1
HH09-06-2-1*	378	1.714	0.3390	0	1.43	0.424	1.00	0.998	0	1.05	1.10	1.00	0.999	40.0	-
HH09-07-2	366	1.706	0.3346	0	1.42	0.860	1.00	0.998	0	1.06	1.05	1.00	0.999	20.0	17.2
HH10-01-1	114	1.785	0.2229	10	0.270	0.401	0.504	0.996	20	0.974	1.63	0.919	0.998	40.0	-

Table 4.5: Experimental results for the Huahine samples (HH01~HH10).

* HH08-04-2-1 and HH09-06-2-1 were heated at 610°C for 7 (TRM1) and 15 minutes (TRM2).

** HH09-05-1 and HH09-06-1 were heated for 15 (TRM1) and 30 minutes (TRM2).

Sample ID	NRM_0	H_{rc}/H_c	M_{rs}/M_s	1st heating					2nd heating					F_L	F
				H_L	$slope_A$	$slope_N$	f_N	r_N	H_L	$slope_A$	$slope_T$	f_T	r_T	(μT)	(μT)
HH11-01-2	222	-	-	15	0.800	0.592	0.209	0.995	0	0.828	0.737	1.00	0.998	30.0	-
HH11-02-2	206	1.629	0.2391	15	0.394	0.751	0.216	0.995	20	0.814	1.02	0.703	0.995	20.0	15.0
HH11-03-2	192	1.608	0.2613	10	0.498	0.568	0.447	0.995	20	0.872	1.04	0.744	0.997	30.0	17.0
HH11-04-2	239	1.608	0.2506	15	0.496	0.668	0.263	0.995	25	0.893	1.02	0.694	0.997	20.0	13.4
HH11-04-2-2*	297	1.608	0.2506	15	0.649	0.310	0.273	0.984	35	0.782	1.24	0.523	0.996	40.0	-
HH11-05-2	228	1.574	0.2596	15	0.480	0.585	0.294	0.995	25	0.861	1.02	0.668	0.997	25.4	14.9
HH11-06-2	218	-	-	10	0.446	0.617	0.369	0.986	25	0.860	1.01	0.633	0.997	30.0	-
HH11-07-1m	206	1.600	0.2368	10	1.17	0.710	0.426	0.995	0	0.909	0.955	1.000	0.998	40.0	28.4
HH11-07-2	221	1.600	0.2368	15	0.667	0.538	0.294	0.995	20	0.610	0.859	0.622	0.996	30.0	-
HH12-01-2	118	1.371	0.4176	20	0.335	1.01	0.491	0.995	0	1.07	0.985	1.00	0.999	10.0	10.1
HH12-02-2m	93.9	1.426	0.3581	25	0.222	0.593	0.306	0.996	0	1.15	0.963	1.00	0.997	10.0	5.93
HH12-03-2	112	1.410	0.4260	25	0.282	0.834	0.552	0.996	0	1.08	1.03	1.00	0.998	10.0	8.3
HH12-04-1**	136	1.509	0.3851	10	0.468	0.177	0.584	0.998	25	0.999	1.19	0.912	0.999	50.0	-
HH12-04-2	139	1.509	0.3851	15	0.381	1.05	0.467	0.998	0	1.02	1.02	1.00	0.999	10.0	10.5
HH12-04-2-2*	153	1.509	0.3851	25	0.311	0.308	0.365	0.997	45	1.22	0.856	0.793	0.997	40.0	-
HH12-06-2	120	1.523	0.3584	20	0.273	0.966	0.391	0.997	0	1.14	0.991	1.00	0.999	10.0	9.66
HH12-07-1**	110	1.532	0.3832	20	0.325	0.182	0.405	0.998	0	1.00	1.02	1.00	0.999	50.0	9.10
HH12-07-2	102	1.532	0.3832	20	0.291	0.952	0.426	0.999	0	1.06	1.02	1.00	0.999	10.0	9.52
HH13-07-1	290	1.553	0.3622	35	0.604	0.167	0.136	0.985	35	0.632	1.91	0.427	0.993	50.0	-
HH14-06-1	127	1.557	0.3585	15	0.301	0.132	0.107	0.984	30	0.884	2.23	0.708	0.995	40.0	-
HH15-02-1	302	1.939	0.1746	20	0.410	0.140	0.140	0.991	15	0.920	2.00	0.899	0.999	40.0	-
HH15-03-1	341	1.878	0.1696	10	0.379	0.227	0.194	0.955	20	0.876	1.91	0.720	0.998	40.0	-
HH16-01-1	302	1.603	0.2871	20	0.561	7.05	0.503	0.996	15	0.978	0.205	0.665	0.997	40.0	-
HH16-01-2-2*	304	1.603	0.2871	20	0.436	0.956	0.540	0.998	0	1.06	1.01	1.00	0.999	40.0	38.2
HH16-02-2	405	1.493	0.3320	20	0.634	1.20	0.550	0.999	0	0.991	1.05	1.00	1.00	30.0	36.0
HH16-03-1	402	1.692	0.2443	15	0.700	1.12	0.636	0.998	30	1.08	1.05	0.494	0.996	30.0	33.6
HH16-04-1	355	1.669	0.2634	20	0.672	5.19	0.466	0.993	15	0.984	0.244	0.721	0.997	40.0	-
HH16-06-1	405	1.967	0.1992	10	0.917	0.988	0.824	0.998	30	1.08	1.04	0.446	0.998	30.0	29.6
HH16-07-2	381	1.921	0.2026	10	0.894	1.06	0.815	0.998	0	1.00	1.05	1.00	1.00	30.0	31.8
HH17-03-1	428	1.659	0.3589	15	0.602	1.03	0.652	0.999	30	0.993	1.71	0.996	0.639	40.0	-
HH17-07-1	476	1.801	0.2355	15	0.845	0.973	0.623	0.997	0	1.02	1.08	1.00	1.00	40.0	-
HH18-01-1	304	2.002	0.1789	15	0.802	0.785	0.313	0.999	0	0.949	1.16	1.00	0.999	40.0	-
HH19-03-1	399	1.882	0.2228	15	0.812	0.946	0.540	0.998	35	0.997	1.52	0.223	0.997	40.0	-
HH19-06-1	428	1.913	0.2078	15	0.867	0.951	0.578	0.997	20	0.974	1.20	0.580	0.999	40.0	-
HH20-01-1	460	1.851	0.2241	10	0.602	0.952	0.594	0.999	0	1.03	1.05	1.00	1.00	40.0	38.1
HH20-02-2	475	-	-	15	0.532	1.91	0.413	0.997	30	1.01	1.08	1.00	1.00	20.0	-
HH20-03-1w	490	1.784	0.2466	15	0.659	1.18	0.392	0.992	0	0.922	0.930	1.00	0.992	40.0	-
HH20-03-2	501	1.784	0.2466	10	0.625	1.58	0.570	0.999	25	1.05	1.05	0.566	0.999	25.4	40.1
HH20-03-2-1*	505	1.784	0.2466	20	0.306	1.36	0.304	0.989	45	1.62	0.638	0.230	0.993	40.0	-
HH20-04-1	474	-	-	15	0.510	3.99	0.409	0.998	0	1.01	1.08	1.00	0.999	10.0	-
HH20-05-1w	463	1.823	0.2400	15	0.592	0.887	0.393	0.999	0	0.974	1.05	1.00	1.00	40.0	35.5
HH20-05-2	455	1.823	0.2400	15	0.555	1.02	0.420	0.999	0	0.987	1.09	1.00	1.00	40.0	-
HH20-06-2	497	1.811	0.2177	15	0.497	3.98	0.394	0.997	20	1.05	1.04	0.756	0.997	10.0	39.8
HH20-07-2	497	-	-	10	0.638	1.90	0.541	1.00	0	1.01	1.09	1.00	1.00	20.0	-
HH21-01-1	358	1.746	0.3369	35	0.805	0.518	0.220	0.996	5	0.953	1.15	0.962	0.999	40.0	-

Table 4.6: Experimental results for the Huahine samples (HH11~HH21).
* HH11-04-2-2, HH12-04-2-2 and HH16-01-2-2 were heated at 610°C for 7 (TRM1) and 15 minutes (TRM2).
** HH12-04-1 and HH12-07-1 were heated for 15 (TRM1) and 30 minutes (TRM2).

Sample ID	NRM_0	H_{rc}/H_c	M_{rs}/M_s	1st heating					2nd heating					F_L	F
				H_L	$slope_A$	$slope_N$	f_N	r_N	H_L	$slope_A$	$slope_T$	f_T	r_T	(μT)	(μT)
MR01-01-2	100	2.253	0.1751	10	0.696	0.692	0.791	0.998	0	1.01	0.997	1.00	1.00	20.0	13.8
MR01-02-1*	97.6	2.174	0.1791	10	0.772	0.352	0.829	0.996	0	0.939	1.05	1.00	1.00	40.0	14.1
MR01-03-1	135	2.094	0.2359	10	0.465	0.790	0.592	0.998	5	0.931	1.05	0.963	0.999	20.0	15.8
MR01-04-1*	124	2.128	0.2418	10	0.482	0.396	0.634	0.999	0	0.956	1.01	1.00	0.999	40.0	15.8
MR01-06-2	108	1.981	0.2226	10	0.444	0.777	0.676	0.997	0	0.978	1.01	1.00	0.999	20.0	15.5
MR06-01-2	106	1.545	0.3310	0	1.00	0.859	1.00	0.996	0	1.03	1.02	1.00	0.996	10.0	8.59
MR06-02-1	68.9	1.764	0.2429	0	1.06	0.472	1.00	0.999	0	0.990	0.989	1.00	0.999	20.0	9.44
MR06-03-1*	101	-	-	0	1.01	0.181	1.00	0.983	5	1.01	1.02	0.982	1.00	40.0	-
MR06-04-2	71.6	1.870	0.2184	5	1.14	0.899	0.983	0.995	0	0.992	1.02	1.00	0.999	10.0	8.99
MR06-05-1	83.0	1.689	0.2552	15	1.26	0.386	0.839	0.997	0	0.991	1.01	1.00	0.999	20.0	7.72
MR06-06-1w*	101	1.687	0.2699	5	1.01	0.221	0.990	0.995	0	1.00	0.999	1.00	1.00	40.0	8.84
MR16-01-1*	44.6	2.730	0.1516	10	0.675	0.260	0.790	0.996	30	0.867	1.00	0.405	0.996	40.0	10.4
MR16-01-2	43.2	2.730	0.1516	10	0.620	0.554	0.771	0.998	5	0.921	0.942	0.935	0.999	15.7	-
MR16-02-1	42.3	2.718	0.1548	10	0.699	0.499	0.931	0.995	5	0.950	0.930	0.927	0.998	20.0	-
MR16-02-2	44.8	2.718	0.1548	10	0.648	0.533	0.773	0.996	5	0.947	0.981	0.929	0.997	15.7	8.37
MR16-03-2	46.8	2.613	0.1656	10	0.681	0.979	0.849	0.995	0	0.974	0.954	1.00	0.997	10.0	9.79
MR16-04-2	153	-	-	20	0.648	2.520	0.523	0.984	0	0.951	0.978	1.00	0.999	10.0	-
MR16-05-2	432	-	-	35	0.817	3.57	0.302	0.984	0	0.972	1.06	1.00	1.00	10.0	-
MR16-06-1	410	-	-	35	0.833	1.79	0.245	0.985	0	0.999	0.984	1.00	1.00	20.0	-
MR16-07-1*	279	2.754	0.1019	40	0.667	1.01	0.255	0.995	10	1.02	0.941	0.882	1.00	40.0	-
MR16-07-2	428	2.754	0.1019	30	0.741	3.65	0.344	0.991	0	1.01	0.987	1.00	1.00	10.0	-
MR22-07-1	82.0	-	-	15	1.01	0.327	0.583	0.999	0	0.992	1.01	1.00	0.999	40.0	13.1
MR23-01-2	79.4	-	-	15	0.522	1.250	0.661	0.998	0	1.04	0.921	1.00	0.997	10.0	-
MR23-02-1*	76.4	1.953	0.2008	10	0.600	0.285	0.726	0.998	0	1.02	0.994	1.00	0.999	40.0	11.4
MR23-03-1	81.6	1.859	0.2019	15	0.655	0.487	0.426	0.995	0	0.981	0.959	1.00	1.00	20.0	9.74
MR23-04-1	88.2	1.904	0.2686	10	0.743	0.714	0.931	0.999	0	0.985	1.02	1.00	0.999	20.0	14.3
MR23-05-1	79.8	1.877	0.2782	15	0.686	0.696	0.832	0.999	0	1.02	0.963	1.00	0.999	20.0	13.9
MR23-06-2	124	2.012	0.2650	20	0.585	1.57	0.749	0.996	0	1.02	0.979	1.00	0.999	10.0	15.7
MR23-07-2	95.0	2.058	0.2722	20	0.609	0.656	0.760	0.995	0	1.02	1.00	1.00	0.999	20.0	13.1
MR30-01-2	61.5	-	-	20	0.119	0.364	0.108	0.950	25	1.04	0.881	0.803	0.998	20.0	-
MR30-02-1*	66.3	-	-	10	0.194	0.198	0.275	0.985	0	1.03	0.870	1.00	0.998	40.0	-
MR30-03-2	43.6	-	-	20	0.160	0.256	0.203	0.964	15	1.02	0.847	0.917	0.995	20.0	-
MR30-06-2	36.2	-	-	10	0.208	0.281	0.384	0.984	25	1.08	0.866	0.813	0.998	20.0	-
MR30-07-1*	45.6	2.096	0.1554	10	0.231	0.126	0.335	0.984	25	1.04	0.938	0.829	0.999	40.0	-
MR32-01-1*	104	1.798	0.3584	10	0.542	0.266	0.781	0.999	0	1.03	0.979	1.00	0.998	40.0	10.6
MR32-02-1	103	1.951	0.3693	10	0.529	0.537	0.771	0.997	10	1.02	0.980	0.978	0.999	20.0	10.7
MR32-03-1	111	1.824	0.3673	10	0.540	0.575	0.815	0.998	0	1.04	0.930	1.00	0.997	20.0	-
MR32-03-2	69.0	1.824	0.3673	15	0.551	1.30	0.827	0.996	0	1.03	1.04	1.00	0.996	10.0	13.0
MR32-04-2	159	1.828	0.3252	15	0.548	1.51	0.761	0.996	0	1.01	1.01	1.00	0.999	10.0	15.1
MR32-05-2	172	1.928	0.3215	15	0.502	1.68	0.734	0.999	0	0.994	1.02	1.00	0.998	10.0	16.8
MR32-06-1*	121	2.154	0.3271	10	0.506	0.296	0.907	0.996	5	1.01	1.05	0.995	0.999	40.0	11.8
MR32-07-2	138	1.812	0.3084	20	0.407	1.47	0.493	0.996	0	1.00	1.00	1.00	0.999	10.0	14.7

Table 4.7: Experimental results for the Moorea samples.
* MR01-02-1, MR01-04-1, MR06-03-1, MR06-06-1w, MR16-01-1, MR16-07-1, MR23-02-1, MR30-02-1, MR30-07-1, MR32-02-1 and MR32-06-1 were heated at 610°C for 25 (TRM1) and 35 minutes (TRM2).

Sample ID	NRM_0	H_{rc}/H_c	M_{rs}/M_s	1st heating					2nd heating					F_L	F
				H_L	$slope_A$	$slope_N$	f_N	r_N	H_L	$slope_A$	$slope_T$	f_T	r_T	(μT)	(μT)
PU01-01-2	132	1.617	0.3363	20	0.852	0.903	0.881	0.996	0	1.04	1.01	1.00	0.997	10.0	9.03
PU01-02-1	122	-	-	20	0.735	0.389	0.865	0.953	0	1.03	0.993	1.00	0.998	20.0	-
PU01-03-2	157	1.523	0.3647	30	0.894	1.08	0.844	0.995	0	1.07	1.03	1.00	0.996	10.0	10.8
PU01-04-1	117	1.686	0.2986	15	0.673	0.454	0.895	0.996	0	1.05	0.971	1.00	0.996	20.0	9.08
PU01-06-1	149	1.504	0.3736	15	0.916	0.455	0.982	0.997	0	1.03	1.05	1.00	0.999	20.0	9.10
PU01-07-1	62.8	-	-	30	0.311	0.385	0.727	0.978	0	1.00	0.990	1.00	0.994	20.0	-
PU04-01-2	155	1.892	0.2365	10	0.459	1.09	0.575	0.997	5	0.898	0.998	0.947	0.999	20.0	21.8
PU04-02-1	195	1.845	0.2200	15	0.359	0.597	0.400	0.997	5	0.946	0.972	0.955	0.999	40.0	23.9
PU04-03-2	165	1.747	0.2586	10	0.495	1.11	0.598	0.995	5	0.911	1.02	0.938	0.999	20.0	22.2
PU04-06-1	162	1.848	0.2291	10	0.453	0.557	0.587	0.996	5	0.891	1.02	0.952	0.999	40.0	22.3
PU04-11-1	388	-	-	50	1.47	2.48	0.257	0.991	0	0.925	1.39	1.00	0.999	40.0	-
PU04-12-1	175	1.821	0.2331	10	0.460	1.10	0.573	0.997	5	0.922	0.977	0.944	0.998	20.0	22.0
PU05-01-2	135	1.639	0.2708	15	0.187	0.634	0.342	0.997	0	0.985	1.03	1.00	0.999	20.0	12.7
PU05-02-1	116	1.904	0.2305	10	0.451	0.349	0.416	0.995	5	0.859	1.04	0.915	0.999	40.0	14.0
PU05-03-2	142	2.031	0.2334	10	0.538	0.865	0.411	0.998	20	0.827	1.02	0.697	0.998	20.0	17.3
PU05-04-1	130	1.913	0.2260	10	0.425	0.389	0.410	0.995	5	0.852	1.00	0.908	0.999	40.0	15.6
PU05-05-2	190	-	-	15	0.152	1.22	0.199	0.995	0	0.969	1.11	1.00	0.995	10.0	-
PU05-11-1	172	-	-	10	0.663	0.574	0.435	0.996	15	0.913	1.21	0.572	0.998	40.0	-
PU05-12-1	144	2.141	0.2006	10	0.282	0.799	0.292	0.995	5	0.859	0.985	0.897	0.996	20.0	16.0
PU06-01-2	655	-	-	50	1.36	4.32	0.316	0.979	0	1.00	1.01	1.00	1.00	20.0	-
PU06-04-1	536	1.860	0.3397	55	1.09	2.57	0.429	0.936	0	1.03	0.973	1.00	1.00	40.0	-
PU06-05-1	794	-	-	55	1.08	1.88	0.226	0.978	0	1.03	1.02	1.00	1.00	40.0	-
PU06-11-1	857	-	-	50	1.18	5.27	0.317	0.988	0	1.04	1.00	1.00	1.00	20.0	-
PU08-01-2	1310	-	-	25	1.07	3.83	0.879	0.991	0	1.02	1.05	1.00	0.999	20.0	-
PU08-03-2	1450	-	-	25	1.04	4.04	0.870	0.994	0	1.04	0.987	1.00	1.00	20.0	-
PU08-11-2	1440	1.659	0.3973	40	0.959	2.22	0.682	0.972	0	1.02	1.02	1.00	1.00	40.0	-
TR02-01-2	76.4	-	-	10	0.828	0.432	0.996	0.979	5	0.942	1.08	0.883	0.999	20.0	-
TR02-02-1	103	2.676	0.2039	10	0.793	0.502	0.832	0.997	0	1.01	1.00	1.00	0.999	20.0	10.0
TR02-03-2	60.9	3.773	0.2018	15	0.976	0.790	0.967	0.995	0	0.951	1.02	1.00	0.998	10.0	7.90
TR02-04-1	100	2.586	0.2270	15	0.979	0.483	0.823	0.995	5	0.947	1.05	0.894	0.999	20.0	9.66
TR02-06-1	98.1	2.586	0.2270	15	0.904	0.461	0.731	0.996	5	0.946	0.984	0.884	0.998	20.0	9.22
TH02-03-2	326	2.184	0.1648	15	0.494	1.30	0.688	0.998	10	0.908	1.04	0.943	0.999	20.0	26.0
TH02-04-1	356	2.115	0.1759	15	0.541	0.736	0.722	0.997	10	1.00	0.958	0.946	1.00	40.0	29.4
TH02-13-1	217	-	-	25	0.545	0.531	0.396	0.995	10	0.942	1.07	0.951	1.00	20.0	-
TH03-03-2	36.3	2.192	0.1844	10	0.668	0.191	0.961	0.995	5	1.01	1.04	0.989	0.998	20.0	3.82
TH03-09-1	32.9	1.946	0.1918	20	1.03	0.261	0.647	0.995	0	0.985	1.01	1.00	1.00	20.0	5.22
TH03-12-1	12.9	2.063	0.1881	5	0.772	0.054	2.10	0.943	0	1.03	0.986	1.00	0.999	40.0	-
TH03-16-2	28.8	2.291	0.1578	20	1.04	0.254	0.745	0.995	0	1.01	0.978	1.00	1.00	20.0	5.08
TH04-03-1	230	-	-	10	0.330	0.481	0.489	0.981	30	0.974	1.030	0.610	0.998	20.0	-
TH04-04-1	229	-	-	10	0.370	0.543	0.575	0.019	30	0.986	1.05	0.655	0.998	20.0	-
TH04-13-1	194	2.030	0.3313	10	0.488	0.231	0.798	0.995	20	1.00	0.983	0.954	0.998	40.0	9.24

Table 4.8: Experimental results for the Tahiti samples.

Site	K-Ar Age (Ma)	n	N	F (±s.d.) (μT)	VDM (±s.d.) (10^{22}Am^2)	VADM' (±s.d.) (10^{22}Am^2)	VADM (±s.d.) (10^{22}Am^2)
BR02	3.21±0.09	4	4	9.53±0.76	2.20±0.18	2.22±0.18	2.18±0.17
BR04	3.75±0.05	4	6	26.5±3.3	6.22±0.77	6.18±0.77	6.07±0.75
(BR07)	3.67±0.05	3	4	(23.4±12.3)	(5.65±2.97)	(5.44±2.85)	(5.34±2.80)
(BR10)	4.01±0.31	4	9	(6.83±1.50)	(1.74±0.38)	(1.59±0.35)	(1.56±0.34)
(BR14)	-	1	1	(20.1)	-	-	-
BR15	3.43±0.06	6	6	14.5±1.5	3.06±0.32	3.37±0.35	3.31±0.34
BR16m	3.30±0.06	4	8	15.8±1.0	3.44±0.21	3.68±0.23	3.61±0.22
BR18	3.51±0.05	4	6	17.4±1.1	3.54±0.23	4.05±0.27	3.98±0.26
(TA07)	3.24±0.05	1	1	(4.46)	-	-	-
TA08	3.14±0.06	5	8	23.8±3.9	5.96±0.97	5.54±0.90	5.46±0.89
TA11	2.57±0.13	3	6	23.1±0.8	5.65±0.18	5.37±0.18	5.29±0.17
(TA13)	3.11±0.04	1	7	(10.2)	-	-	-
TA15	2.90±0.05	5	7	7.4±0.7	1.44±0.14	1.71±0.17	1.69±0.16
TA16	2.97±0.04	4	5	3.02±0.40	0.512±0.068	0.701±0.093	0.691±0.092
(TA17)	2.99±0.04	2	5	(5.68±1.17)	-	-	-
(TA19)	-	1	1	(8.96)	-	-	-
(RT03)	2.65±0.03	2	7	(16.1±1.7)	-	-	-
(RT05)	-	1	1	(5.20)	-	-	-
(RT10)	2.77±0.04	3	5	(4.23±1.39)	(1.00±0.33)	(0.981±0.322)	(0.968±0.317)
RT12m	2.61±0.03	6	8	8.67±1.03	1.88±0.22	2.01±0.24	1.99±0.24
RT18m	2.67±0.03	4	6	9.03±1.08	2.18±0.26	2.09±0.25	2.07±0.25
(RA01)	2.45±0.05	1	1	(12.6)	-	-	-
HH01	2.72±0.03	3	6	41.7±2.9	10.2±0.7	9.67±0.67	9.54±0.66
(HH05)	2.68±0.04	4	6	(15.1±3.7)	(3.50±0.86)	(3.50±0.86)	(3.45±0.85)
(HH06)	2.58±0.05	2	9	(6.59±1.20)	-	-	-
HH08	3.19±0.13	5	9	25.1±1.7	6.01±0.40	5.83±0.39	5.75±0.39
HH09	(4.01±0.05)	5	9	17.8±1.0	4.12±0.22	4.12±0.22	4.06±0.22
HH11m	3.09±0.04	4	9	15.1±1.5	3.60±0.36	3.50±0.35	3.45±0.35
HH12m	2.52±0.04	6	9	9.54±0.76	2.42±0.19	2.21±0.18	2.18±0.17
HH16	-	5	7	33.9±3.4	7.65±0.76	7.86±0.79	7.75±0.78
HH20	2.83±0.09	4	10	38.4±2.1	8.21±0.46	8.91±0.49	8.78±0.49
MR01	1.58±0.04	5	5	15.0±1.0	3.49±0.23	3.45±0.22	3.43±0.22
MR06	1.62±0.08	5	6	8.72±0.64	2.03±0.15	2.00±0.15	1.99±0.15
MR16	1.51±0.04	3	9	9.52±1.03	2.18±0.24	2.19±0.24	2.17±0.24
(MR22)	-	1	1	(13.1)	-	-	-
MR23	1.55±0.06	6	7	13.0±2.1	2.20±0.36	3.00±0.49	2.97±0.49
MR32	1.50±0.04	7	8	13.3±2.4	2.05±0.36	3.05±0.54	3.03±0.54
PU01	1.12±0.02	4	6	9.50±0.87	2.17±0.20	2.18±0.20	2.17±0.20
PU04	0.92±0.03	5	6	22.4±0.8	3.74±0.14	5.15±0.19	5.13±0.19
PU05	1.03±0.02	5	7	15.1±1.8	3.44±0.41	3.47±0.41	3.45±0.41
TR02	-	4	5	9.21±0.93	2.24±0.23	2.11±0.21	2.10±0.21
(TH02)	0.72±0.11	2	4	(27.7±2.4)	-	-	-
TH03	-	3	4	4.71±0.77	1.18±0.19	1.08±0.18	1.08±0.18
(TH04)	0.51±0.10	1	3	(9.24)	-	-	-

Table 4.9: Statistical results of the paleointensities.
Site, Site ID; n, N, number of the specimens used for the calculation and measurement; F, VDM, VADM, mean paleointensity, virtual dipole moment and virtual axial dipole moment at the latitude with the correction for the absolute plate motion. VADM' indicates the VADM calculated without the correction.
Note that the parenthetic values are reference ones and not used in the discussion.

4.4 Discussion on the last 4 Ma geomagnetic dipole moment

From 28 reliable site-mean paleointensities (Table 4.9), we obtained a mean VDM of $3.68\pm2.32\times10^{22}Am^2$ and a mean VADM of $3.76\pm2.24\times10^{22}Am^2$ for the last 4 Ma. This is nearly half of the present dipole moment, and is considerably lower than the last 10 Ma mean VDM of $7.84\pm3.80\times10^{22}Am^2$ from the volcanic rocks (Kono and Tanaka, 1995). One of the major reasons for this discordance is the quality of the previous database as described in the section 4.1.

Our result is also 32% lower than the mean VADM of $5.49\pm2.36\times10^{22}Am^2$ for the last 0.3-5 Ma from the carefully selected Thellier results with volcanic rocks and submarine basaltic glasses (Juarez and Tauxe, 2000). To examine this discrepancy more carefully, we re-analyze the previous Thellier data with the same conditions as in our selection criteria of site-mean paleointensities;

1. Each mean paleointensity is calculated from more than 3 individual results.

2. Its standard deviation is less than 20%.

A number of the Thellier results from volcanics are available from the Montpellier 98 database (Perrin et al., 1998). Although high quality data are very scarce (Juarez and Tauxe, 2000), 41 data for 0.3-4 Ma satisfy the above conditions (Table 4.10). The data for 0-0.3 Ma are not adopted in the present analysis because the recent field seems to have been unusually high (Juarez and Tauxe, 2000). Adding 33 data from several recently published studies (Table 4.11; Goguitchaichvili et al, 1999, 2001; Laj et al., 2000; Alva-Valdivia et al., 2001), 74 selected Thellier data give a mean VADM of $5.99\pm2.16\times10^{22}Am^2$. This is still 59% higher than our result. Although nearly half of these Thellier data are distributed around 0.3-0.6 Ma (Figure 4.8(A)), the average is not changed ($5.94\pm2.45\times10^{22}Am^2$, N=37) if they are excluded from the calculation.

What is the reason for such discordance between our result and the Thellier data? One of the possible reasons is that some of the data are the misleading of the ancient geomagnetic field, which may be related to the methodological problem. As stated in the Chapter 2, some volcanic rocks possibly suffer from the thermochemical remanences, yielding the anomalous paleointensities as high as about 50% in the Thellier experiments.

Since most of the selected Thellier data are restored from the basaltic samples similar to the Hawaiian 1960 lava, this possibility cannot be ignored. For example, the selected Thellier data contain 10 results from 2.1-3.9 Ma lavas in Oahu, Hawaii (Laj et al., 2000; Table 4.11). In their results, one Thellier diagram (KO26-146B; Fig 5, Laj et al., 2000) appears to resemble the two-slope behavior observed in our results from the Hawaiian 1960 lava (e.g. Figure 2.8, Chapter 2). This suggests that their samples are possibly affected by TCRM more or less and that some of them might occasionally give high paleointensities. Other selected Thellier data also seem to have the same problems. Hence we can conclude that our paleointensities are more reliable and the time-averaged geomagnetic dipole moment for the last 4 Ma is nearly half of the present dipole moment. This implies that the present-day geomagnetic field is very intensive.

By the way, as seen in Figure 4.8(A), time-sequential changes in VADMs of our results happen to be consistent with those of the equatorial Pacific sedimentary record (Valet and Meynadier, 1993). In fact, their mean VADM of $3.9\pm1.9\times10^{22}\mathrm{Am}^2$ for the last 4 Ma is similar to our mean value and is almost unchangeable if their relative paleointensities are re-calibrated with our results. It is known that the volcanic data are spot-readings of the geomagnetic field while the sedimentary record may average out very short period variations. However, the concordance between our results and the sedimentary record is preserved in the averaged intensity variations for some period, that is to say, 0.5 Ma intervals for the last 4 Ma (Figure 4.8(B)). On the other hand, the selected Thellier data seem to be systematically higher than the sedimentary record both in the time-sequential change (Figure 4.8(A)) and the 0.5 Ma averages (Figure 4.8(B)).

The calibration of this equatorial Pacific sedimentary record is complicated. In details, this record was calibrated for the past 140 ka with the synthetic sedimentary record of Meynadier at al. (1992). It was also calibrated by the Mediterranean sedimentary record spanning the last 80 ka (Tric et al., 1992), which was further fitted to the past 40 ka Thellier results consisting of the volcanic and the archeomagnetic data. Namely, only the period of 40 ka, which is 1% of the whole period of the record, was adopted for the calibration. Therefore the ambiguity of the calibration seems to be so large that the direct comparison with our data may possibly lead us to some misunderstanding. Further, there are also some possibilities of the erroneous intensities for these Thellier results except the archeomagnetic data. In order to calibrate the relative paleointensities more accurately,

we have to obtain a vast number of the reliable absolute paleointensities by the LTD-DHT Shaw method, which are evenly spaced for the time.

Site	Age (Ma)	N	F (±s.d.) (μT)	VDM (±s.d.) (10^{22}Am^2)	VADM (±s.d.) (10^{22}Am^2)
Otake et al. (1993)					
Zao 02	1.00±0.00	5	32.4±4.9	7.22±1.09	5.74±0.87
Tanaka et al. (1995)					
RK01	2.58±0.20	3	99.2±18.6	16.5±3.1	13.9±2.6
RK23	2.58±0.20	5	38.1±7.4	5.01±0.97	5.33±1.03
RK24	2.58±0.20	4	32.1±3.8	4.31±0.51	4.49±0.53
Schnepp and Hradetzky (1994)					
AK	0.40±0.40	5	22.1±1.7	3.08±0.24	3.44±0.27
AV3	0.40±0.40	6	52.2±3.4	7.59±0.49	8.14±0.53
DLO	0.40±0.40	7	53.5±7.8	7.87±1.15	8.35±1.22
DO	0.40±0.40	5	49.7±4.3	10.8±0.9	7.75±0.67
EM1	0.40±0.40	5	40.8±2.6	5.93±0.38	6.36±0.41
EMU	0.40±0.40	7	39.5±2.9	6.35±0.47	6.16±0.45
FLSO	0.40±0.40	5	26.4±1.0	4.47±0.17	4.11±0.16
FLY	0.40±0.40	6	62.0±2.7	10.1±0.4	9.67±0.42
FW	0.40±0.40	6	15.5±1.7	2.80±0.31	2.42±0.27
GI	0.40±0.40	5	23.6±3.9	4.00±0.66	3.67±0.61
GO	0.40±0.40	5	11.1±0.7	1.86±0.12	1.73±0.11
GOS	0.40±0.40	5	29.1±2.1	4.68±0.34	4.53±0.33
HA	0.40±0.40	5	28.4±3.7	4.69±0.61	4.43±0.58
KB	0.40±0.40	6	33.6±2.0	4.78±0.28	5.24±0.31
MO	0.40±0.40	11	44.1±3.9	7.00±0.62	6.88±0.61
MOW	0.40±0.40	6	55.6±5.3	8.49±0.81	8.67±0.83
RB	0.40±0.40	11	48.7±5.3	7.53±0.82	7.60±0.83
ST	0.40±0.40	11	49.6±4.3	8.08±0.70	7.72±0.67
WA	0.40±0.40	11	47.1±6.0	7.67±0.98	7.35±0.94
WO	0.40±0.40	5	54.4±2.9	8.52±0.45	8.47±0.45
SR	0.48±0.03	5	26.9±3.0	3.78±0.42	4.19±0.47
U	0.51±0.03	6	30.4±2.6	4.76±0.41	4.74±0.41
RI	0.55±0.03	5	43.6±3.1	7.87±0.56	6.80±0.48
RO	0.55±0.40	5	33.6±1.4	4.59±0.19	5.23±0.22
SK	0.55±0.40	5	41.3±2.7	5.87±0.38	6.43±0.42
SM	0.55±0.40	6	34.5±3.5	5.55±0.56	5.38±0.55
SMA	0.55±0.40	7	49.3±7.9	8.79±1.41	7.69±1.23
FI	0.59±0.05	6	31.8±6.1	4.62±0.89	4.96±0.95
Schnepp (1995)					
EK	0.40±0.40	9	29.1±2.5	4.50±0.39	4.53±0.39
KP	0.40±0.40	5	31.0±3.2	4.79±0.50	4.82±0.50
Schnepp (1996)					
HS,TH1	0.35±0.05	6	51.1±1.8	8.30±0.29	7.95±0.28
FK	0.37±0.04	6	29.4±1.3	4.64±0.21	4.57±0.20
ET,MY1,MY2,MY3	0.40±0.40	15	45.3±4.4	6.56±0.64	7.05±0.69
SI	0.41±0.03	7	32.6±3.8	5.10±0.59	5.08±0.59
MK	0.42±0.03	7	43.4±3.2	6.86±0.51	6.75±0.50
HL	0.47±0.05	3	50.5±4.9	8.10±0.79	7.85±0.76
HB	0.49±0.08	6	41.6±4.1	6.95±0.69	6.47±0.64

Table 4.10: Selected Thellier data from the Montpellier 98 database (Perrin et al., 1998). Site, Site ID; N, number of the specimens yielding the paleointensity; F, VDM, VADM, mean paleointensity, virtual dipole moment and virtual axial dipole moment for each site.

Site	Age (Ma)	N	F (±s.d.) (μT)	VDM (±s.d.) (10^{22}Am^2)	VADM (±s.d.) (10^{22}Am^2)
Laj et al. (2000)					
KO08	2.07	3	31.0±3.2	7.04±0.73	6.80±0.70
KO10	2.08	3	26.5±1.5	5.87±0.33	5.80±0.30
KO13	2.10	3	40.3±2.0	8.85±0.44	8.90±0.40
HN11	3.12	3	52.4±4.7	13.0±1.2	11.5±1.0
HN15	3.12	3	48.2±7.2	12.3±1.8	10.5±1.6
KP01	3.22	3	16.8±1.1	4.35±0.28	3.70±0.20
PPA06	3.30	3	28.1±4.5	6.11±0.98	6.10±1.30
OKP04	3.89	4	28.3±5.2	4.49±0.83	6.20±1.10
OKP03	3.90	5	29.5±3.6	4.81±0.59	6.40±0.80
OKP02	3.92	5	23.9±3.4	4.53±0.64	5.20±0.70
Goguitchaichvili et al. (1999)					
KY'12A	~2.00±0.10	3	45.4±5.2	6.87±0.79	6.36±0.73
KY7	2.05±0.02	4	25.6±1.3	3.37±0.17	3.59±0.18
FL'1/FL'2	2.05±0.02	7	22.7±1.9	3.45±0.29	3.18±0.27
HU20	2.05±0.02	3	40.1±5.6	6.08±0.85	5.62±0.78
FL*7	~2.10±0.10	3	48.3±1.5	6.49±0.20	6.77±0.21
HU8	~2.10±0.10	4	46.7±2.7	6.73±0.39	6.54±0.38
HU5	~2.10±0.10	6	30.9±6.1	4.46±0.88	4.33±0.85
HU4B	~2.10±0.10	5	32.6±5.6	4.66±0.80	4.57±0.78
HU4A	~2.10±0.10	4	24.7±3.5	3.75±0.53	3.46±0.49
HU'3/4A	~2.10±0.10	7	31.2±1.7	4.92±0.27	4.37±0.24
PV2	~2.10±0.10	3	53.4±1.6	7.70±0.23	7.48±0.22
PV1	~2.10±0.10	5	28.5±4.4	3.96±0.61	3.99±0.62
Goguitchaichvili et al. (2001)					
DG3-12W	3.60±0.10	3	27.8±4.8	6.37±1.10	4.74±0.82
DG3-13W	3.60±0.10	3	18.6±1.2	4.17±0.27	3.17±0.20
DG3-3Y	3.60±0.10	3	18.6±3.3	4.37±0.78	3.17±0.56
DG4-9Y	3.60±0.10	4	25.2±4.5	4.38±0.78	4.30±0.77
DG4-12Y	3.60±0.10	3	25.0±0.5	4.20±0.08	4.26±0.09
DG4-15Y	3.60±0.10	4	19.5±2.4	3.33±0.41	3.32±0.41
DG4-16Y	3.60±0.10	4	25.5±2.6	4.38±0.45	4.35±0.44
Alva-Valdivia et al. (2001)					
TS	0.80±0.10	7	36.5±5.2	9.12±1.30	8.30±1.18
TP	0.80±0.10	7	38.1±7.2	8.43±1.59	8.66±1.64
SRG3	2.20±0.30	4	34.7±7.3	8.15±1.71	7.90±1.66
SRG8	1.00±0.10	3	30.6±4.3	6.43±0.90	6.97±0.98

Table 4.11: Selected Thellier data from the recent studies.

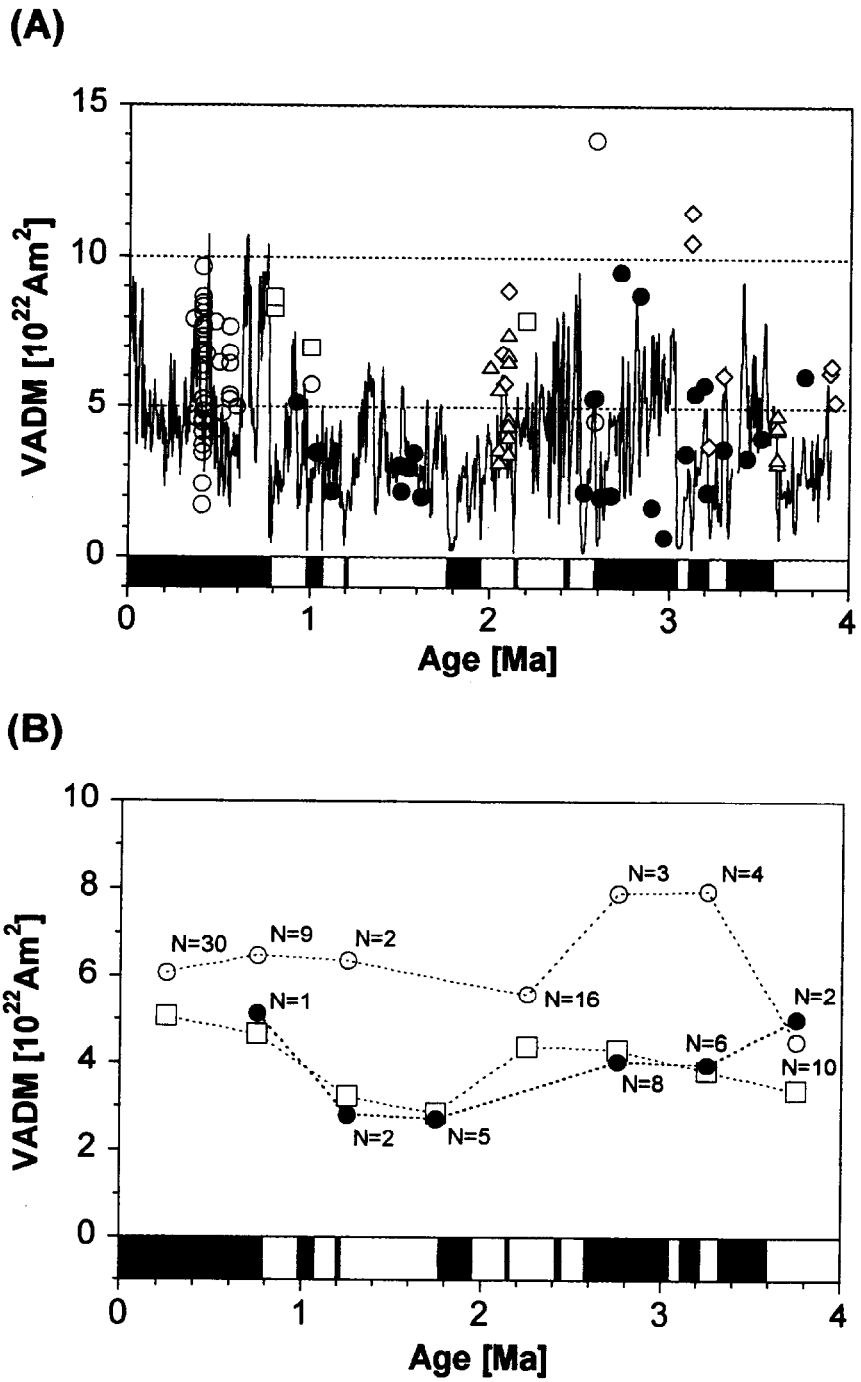

Figure 4.8: (A) Last 4 Ma VADM variation in our data (solid circles), the selected Thellier data (open circles, Perrin et al., 1998; open squares, Alva-valdivia et al., 2001; open triangles, Goguitchaichvili et al., 1999, 2000; open diamonds, Laj et al., 2000) and the equatorial Pacific sedimentary record (solid lines; Valet and Meynadier, 1993).
(B) The data are averaged at 0.5 Ma intervals; the present results (solid circles), the selected Thellier data (open circles) and the equatorial Pacific sedimentary record (open squares). N indicates the number of the data calculated for the corresponding average.

4.5 Conclusions

We measured 164 absolute paleointensities from the last 4 Ma basaltic lavas in the Society Islands, applying the LTD-DHT Shaw method. After the multi-specimen test, 28 reliable site-mean paleointensities gave the mean VDM of $3.68\pm2.32\times10^{22}Am^2$ and the mean VADM of $3.76\pm2.24\times10^{22}Am^2$ for the last 4 Ma. They are about 30-50% lower than the previous estimations and the carefully re-evaluated moment from the previous volcanic data. The major reason for these discordances is thought to be a systematic bias in the previously reported paleointensities obtained by the Coe's version of the Thellier method. Although our result happens to be consistent with the equatorial Pacific sedimentary record ($3.9\pm1.9\times10^{22}Am^2$), its calibration seems to be insufficient because only 1% period of the record was adopted for the indirect calibration.

The newly determined paleointensities indicate that the present dipole moment is about two times of the last 4 Ma average and that the characteristics of the present field may not be representative of the geomagnetic field. We have to be careful with extending the characteristics in the present-day field to the ancient.

Chapter 5

Conclusions

In order to restore the reliable geomagnetic dipole moments for the last 4 Ma, we first examined the reliability of absolute paleointensity determinations on the volcanic rocks. According to our comprehensive investigation of the paleointensity measurements and various rock magnetic analyses on the Hawaiian 1960 lava, we conclude that, if natural remanent magnetizations (NRMs) of volcanic samples are affected by thermochemical remanent magnetization (TCRM), the Coe's version of the Thellier method tends to give considerably higher intensities, especially for samples with medium high temperature oxidation. On the other hand, the double heating technique of the Shaw method combined with low temperature demagnetization (LTD-DHT Shaw method) efficiently screens inappropriate results and thus give a good mean paleointensity. This is because of the validity of the double heating test, the anhysteretic remanent magnetization (ARM) correction and the LTD treatment.

Secondly, the paleodirections and K-Ar ages have been measured for the volcanic rocks from the Society Islands, French Polynesia. The K-Ar ages indicate that the collected samples range from 0.5 to 4.6 Ma, and they are concordant with the absolute motion model of the Pacific plate. For the paleodirections, 82 normal, 48 reversed and 10 intermediate directions were observed. Their magnetostratigraphy agrees well with the geomagnetic polarity time scale. The mean VGP is located at Lat=87.5°, Long=356.0° and A_{95}=2.3° for the combined data set (N=130). This mean position is close to the geographic north pole and there is no significant inclination anomaly of the time-averaged field. Hence it is concluded that these data average out the paleosecular variation well.

Finally, the paleointensity measurements have been performed on the Society samples. As these samples are from typical hotspot basalts showing medium degree of high temperature oxidation, we applied the LTD-DHT Shaw method. After the careful data analyses, we obtained 164 successful paleointensities for the last 4 Ma. 28 reliable site-mean paleointensities were further selected from them, resulting in a mean VDM of $3.68\pm2.32\times10^{22}Am^2$ and a mean VADM of $3.76\pm2.24\times10^{22}Am^2$. They are about 30-50% lower than the previous estimations. This inconsistency is suggested to be caused by some bias in the previously reported paleointensities obtained by the Thellier method. Since the newly determined average of the last 4 Ma VDM is nearly half of the present dipole moment, it is implied that the present-day field is very intensive and may not be representative of the geomagnetic field. We have to be careful with extending the characteristics in the present-day field to the ancient.

References

Alva-Valdivia, L.M., Goguitchaichvili, A., Urrutia-Fucugauchi, J., 2001. Further constraints for the Plio-Pleistocene geomagnetic field strength: New results from the Los Tuxtlas volcanic field (Mexico). Earth Planets Space, 53: 873-881.

Baag, C., Helsley, C.E., Xu, S., and Lienert, B.R., 1995. Deflection of paleomagnetic directions due to magnetization of the underlying terrain. J. Geophys. Res., 100: 10013-10027.

Blais, S., Guille, G., Maury, R.C., Guillou, H., Miau, D., and Cotten, J., 1997. Geology and petrology of Raiatea Island (Society Islands, French Polynesia). C. R. Acad. Sci. Paris, série IIa, 324: 435-442.

Blais, S., Guille, G., Guillou, H., Chauvel, C., Maury, R.C., and Caroff, M., 2000. Geology, geochemistry and geochronology of Borabora island (Society Islands, French Polynesia). C. R. Acad. Sci. Paris, Earth Planet. Sci., 331: 579-585.

Bogue, S. W., 2001. Geomagnetic field behaviour before and after the Kauai reverse-normal polarity transition. J. Geophys. Res., 106: 447-461.

Cande, S.C., and Kent, D.V., 1995. Revised calibration of the geomagnetic polarity timescale for the Late Cretaceous and Cenozoic. J. Geophys. Res., 100: 6093-6095.

Chauvin, A., Roperch, P., and Duncan, R.A., 1990. Records of geomagnetic reversals from volcanic islands of French Polynesia 2. Paleomagnetic study of flow sequence (1.2-0.6Ma) from the Island of Tahiti and discussion of reversal models. J. Geophys. Res., 95: 2727-2752.

Coe, R.S., 1967. Paleointensities of the Earth's magnetic field determined from Tertiary and Quaternary rocks. J. Geophys. Res., 72 : 3247-3262.

Coe, R.S., Gromme, S., and Mankinen, E.A., 1978. Geomagnetic paleointensities from radiocarbon-dated lava flows on Hawaii and the question of the pacific nondipole low. J. Geophys. Res., 83: 1740-1756.

Cox, A., 1970. Latitude dependence of the angular dispersion of the geomagnetic field. Geophys. J. R. Astr. Soc., 20: 253-269.

Day, R., Fuller, M., and Schmidt, V.A., 1977. Hysteresis properties of titanomagnetites: grain-size and compositional dependence. Phys. Earth Planet. Int., 13: 260-267.

Duncan, R.A., 1975. Paleosecular variation at the Society Islands, French Polynesia. Geophys. J. R. Astr. Soc., 41: 245-254.

Duncan, R.A., and McDougall, I., 1976. Linear volcanism in French Polynesia. J. Volcanol. Geotherm. Res., 1: 197-227.

Dunlop, D.J., and Özdemir, Ö, 1997. Rock Magnetism: Fundamentals and frontiers. Cambridge Univ. Press: 573p.

Gee, J., Schneider, D.A., and Kent, D.V., 1996. Marine magnetic anomalies as recorders of geomagnetic intensity variations. Earth Planet. Sci. Let., 144: 327-335.

Goguitchaichvili, A., Prevot M., and Camps, P., 1999. No evidence for strong fields during the R3-N3 Icelandic geomagnetic reversal. Earth. Planet. Sci. Let., 167: 15-34.

Goguitchaichvili, A., Camps, P., and Urrutia-Fucugauchi, J., 2001. On the features of the geodynamo following reversals or excursions: by absolute geomagnetic paleointensity data. Phys. Earth Planet. Int., 124: 81-93.

Gripp, A.E., and Gordon, R.G., 1990. Current plate velocities relative to the hotspots incorporating the NUVEL-1 global plate motion model. Geophys. Res. Let., 17: 1109-1112.

Gubbins, D., and Kelly, P., 1993. Persistent patterns in the geomagnetic field over the last 2.5 Myr. Nature, 365: 829-832.

Guillou, H., Blais, S., Guille, G., Maury, R.C., Le Dez, A., and Cotten, J., 1998. Age (K-Ar) and duration of the subaerial build-up of Moorea, Raiatea and Maupiti (Society Islands, French Polynesia). Géologie de la France, 3: 29-36.

Guyodo, Y., and Valet, J.P., 1999a. Global changes in intensity of the Earth's magnetic field during the past 800 kyr. Nature, 36: 234-238.

Guyodo, Y., and Valet, J.P., 1999b. Integration of volcanic and sedimentary records of paleointensity: Constraints imposed by irregular eruption rates. Geophys. Res. Let., 23: 3393-3396.

Heider, F., Dunlop, D.J., and Soffel, H.C., 1992. Low-temperature and alternating field demagnetization of saturation remanence and thermoremanence in magnetite grains (0.037μm to 5mm). J. Geophys. Res., 97: 9371-9381.

Hildenbrand, T.G., Rosenbaum, J.G., and Kauahikaua, J.P., 1993. Aeromagnetic study of the island of Hawaii. J. Geophys. Res., 98: 4099-4119.

Hill M.J., and Shaw, J., 2000. Magnetic field intensity study of the 1960 Kilauea lava flow, Hawaii, using the microwave paleointensity technique. Geophys. J. Int., 142: 487-504.

Johnson, C., and Constable, C.G., 1995. The time averaged field as recorded by lava flows over the past 5 Myr. Geophys. J. Int., 122: 489-519.

Johnson, C., and Constable, C.G., 1996. Paleosecular variation recorded by lava flows over the past five million years. Phil. Trans. R. Soc. Lond. A., 354: 89-141.

Johnson, C., and Constable, C.G., 1997. The time averaged geomagnetic field: global and regional biases for 0-5 Ma. Geophys. J. Int., 131: 643-666.

Juarez, M.T., and Tauxe, L., 2000. The intensity of the time-averaged geomagnetic field: the last 5 Myr. Earth Planet. Sci. Let., 175: 169-180.

Kellogg, K., Larson, E.E., and Watson, D.E., 1970. Thermochemical Remanent Magnetization and Thermal Remanent Magnetization: Comparison in a Basalt. Science, 170: 628-630.

Kelly, P., and Gubbins, D., 1997. The geomagnetic field over the past 5 million years. Geophys. J. Int., 128: 315-330.

Kirschvink J.L., 1980. The least-squares line and plane and the analysis of paleomagnetic data. Geophys. J. R. astr. Soc., 62: 699-718.

Kok, Y.S., and Tauxe L., 1999. A relative geomagnetic paleointensity stack from Ontong-Java Plateau sediments for the Matuyama. J. Geophys. Res., 104: 25401-25413.

Kono, M., 1978. Reliability of paleointensity methods using alternating field demagnetization and anhysteretic remanence. Geophys. J. R. astr. Soc., 54: 241-261.

Kono, M., 1987. Changes in TRM and ARM in a basalt due to laboratory heating. Phys. Earth Planet. Int., 46: 1-8.

Kono, M., and Tanaka, H., 1995. Intensity of the geomagnetic field in geological time: A statistical study. The Earth's Central Part: Its Structure and Dynamics (T. Yukutake, ed.), Terrapub, Tokyo: 75-94.

Kono, M., Kitagawa, H., and Tanaka, H., 1997. Use of automatic spinner magnetometer-AF demagnetizer system for magnetostratigraphy and paleosecular variation studies (abstract). 8th Scientifiic Assembly IAGA, Uppsala.

Kono M., Tanaka, H., and Tsunakawa, H., 2000. Spherical harmonic analysis of paleomagnetic data: The case of linear mapping. J. Geophys. Res., 105: 5817-5833.

Kono, M., Hamano, Y., Nishitani T., and Tosha, T., 1984. A new spinner magnetometer: principles and techniques. Geophys. J. R. astr. Soc., 67: 217-227.

Kosterov, A.A., and Prévot, M., 1998. Possible mechanisms causing failure of Thellier paleointensity experiments in some basalts. Geophys. J. Int., 134: 554-572.

Laj, C., Mazaud, A., Weeks, R., Fuller, M., and Herrero-Bervera, E., 1991. Geomagnetic reversal paths. Nature, 351: 447.

Laj, C., Mazaud, A., Weeks, R., Fuller, M., and Herrero-Bervera, E., 1992. Geomagnetic reversal paths. Nature, 359: 111-112.

Laj, C., Szeremeta, N., Kissel, C., and Guillou, H., 2000. Geomagnetic paleointensities at Hawaii between 3.9 and 2.1 Ma: preliminary results. Earth Planet. Sci. Let., 179: 191-204.

Levi S., 1977. The effect of magnetite particle size on paleointensity determinations of the geomagnetic field. Phys. Earth Planet. Int., 13: 245-259.

Love J.J., 1998. Paleomagnetic volcanic data and geometric regularity of reversals and excursions. J. Geophys. Res., 103: 12435-12452

Mankinen, E.A., and Champion, D.E., 1993. Broad Trends in Geomagnetic Paleointensity on Hawaii During Holocene Time. J. Geophys. Res., 98: 7959-7976.

Matsumoto, A., 1989. Improvement for determination of potassium in K-Ar dating. Bull. Geol. Surv. Japan, 40(2): 65-70.

Matsumoto, A., Uto, K., and Shibata, K., 1989b. K-Ar dating by peak comparison method - New technique applicable to rocks younger than 0.5 Ma -. Bull. Geol. Surv. Japan, 40(10): 565-579.

McClelland, E., 1996. Theory of CRM acquired by grain growth, and its implications for TRM discrimination and paleointensity determination in igneous rocks. Geophys. J. Int., 126: 271-280.

McClelland, E., and Briden, J.C., 1996. An improved methodology for Thellier-type paleointensity determination in igneous rocks and its usefulness for verifying primary tnermoremanence. J. Geophys. Res., 101: 21995-22013.

McElhinny M.W., McFadden P.L., and Merrill R.T., 1996. The time-averaged paleomagnetic field 0-5 Ma. J. Geophys. Res., 101: 25007-25027.

McFadden, P.L., and McElhinny, M.W., 1982. Variations in the geomagnetic dipole. 2. Statistical analysis of VDM's for the past 5 million years. J. Geomag. Geoelectr., 34: 163-189.

McFadden P. L., and McElhinny M. W., 1990. Classification of the reversal test in palaeomagnetism. Geophys. J. Int., 103: 725-729.

McFadden, P.L., Merrill, R.T., and McElhinny, M.W., 1988. Dipole/quadrupole family modeling of paleosecular variation. J. Geophys. Res., 93: 11583-11588.

McFadden P.L., Merrill R.T., McElhinny M.W., and Lee S., 1991. Reversals of the Earth's magnetic field and temporal variations of the dynamo families. J. Geophys. Res., 96: 3923-3933.

Meynadier, L., Valet, J.P., Weeks, R., Shackleton, N.J., Hagee, V. L., 1992. Relative geomagnetic intensity of the field during the last 140 ka. Earth and Planetary Science Letters, 114: 39-57.

Miki, D., 1999. Estimate of the ages of lava flows at Sakurajima Volcano, Kyushu, Japan; Inferred from paleomagnetic directions and paleointensities. Bull. Volc. Soc. Japan, 44: 111-122.

Otake, H., Tanaka, H., Kono, M., and Saito, K., 1993. Paleomagnetic study of Pleistocene lavas and dykes of the Zao volcano group, Japan. J. Geomag. Geoelectr., 45: 595-612.

Ozima, M., Ozima, M., and Akimoto, S., 1964. Low temperature characteristics of remanent magnetization of magnetite - Self-reversal and recovery phenomena of remanent magnetization -. J. Geomag. Geoelectr., 16: 165-177.

Perrin, M., Schnepp, E., and Shcherbakov, V., 1998. Update of the paleointensity database. EOS, Trans. Amer. Geophys. Union, 79: 198.

Rolph, T.C., and Shaw, J., 1985. A new method of paleofield magnitude correction for thermally altered samples and its application to Lower Carboniferous lavas. Geophys. J. Int., 80: 773-781.

Roperch P., and Duncan R.A., 1990. Records of geomagnetic reversals from volcanic islands of French Polynesia 1. Paleomagnetic study of a polarity transition in a lava sequence from the island of Huahine. J. Geophys. Res., 95: 2713-2726.

Schneider, D.A., and Mello G.A., 1996. A high-resolution marine sedimentary record of geomagnetic paleointensity variation. Earth Planet. Sci. Let., 144: 297-314.

Schnepp, E., 1995. Paleointensity study of Quaternary East Eifel phonolitic rocks (Germany). Geophys. J. Int., 121: 627-633.

Schnepp, E., 1996. Geomagnetic paleointensities derived from volcanic rocks of the Quaternary East Eifel volcanic fiewkld, Germany. Phys. Earth Planet. Int., 94: 23-41.

Schnepp, E., and Hradetzky, H., 1994. Combined paleointensity and 40Ar/39Ar age spectrumdata from volcanic rocks of the West Eifel field (Germany): evidence for an early Brunhes geomagnetic excursion. J. Geophys. Res., 99: 9061-9076.

Selkin, P.A., and Tauxe, L., 2000. Long-term variations in paleointensity. Phil. Trans. R. Soc. Lond. A, 358: 1065-1088.

Senanayake, W.E., McElhinny, M.W., McFadden, P.L., 1982. Comparison between the Thelliers' and Shaw's paleointensity methods using basalts less than 5 million years old. J. Geomag. Geoelectr., 34: 141-161.

Shaw, J., 1974. A new method of determining the magnitude of the paleomagnetic field. Application to five historic lavas and five archaeological samples. Geophys. J. R. astr. Soc., 76: 637-651.

Shibata, K., 1968. K-Ar age determinations on granitic and metamorphic rocks in Japan. Geol. Surv. Japan Report, 227: 1-73.

Shibuya, H., Cassidy, J., Smith, I.E.M., Itaya, T., 1995. Paleomagnetism of young New Zealand basalts and longitudinal distribution of paleosecular variation. J. Geomag. Geoelectr., 47: 1011-1022.

Singer B.S., Hoffman K.A., Chauvin A., Coe R.S., and Pringle M.S., 1999. Dating transitionally magnetized lavas of the late Matuyama Chron: Toward a new 40Ar/39Ar timescale of reversals and events. J. Geophys. Res., 104: 679-693

Tanaka H., 1999. Theoretical background of ARM correction in the Shaw paleointensity method. Geophys. J. Int., 137: 261-265.

Tanaka, H., and Kono, M., 1991. Preliminary Results and Reliability of Paleointensity Studies on Historical and ^{14}C Dated Hawaiian Lavas. J. Geomag. Geoelectr., 43: 375-388.

Tanaka, H., and Kono, M., 1994. Paleointensity database provides new resource. EOS, Trans. Amer. Geophys. Union, 75: 498.

Tanaka, H., Kono, M., and Kaneko, S., 1995. Paleosecular variation of direction and intensity from two Pliocene-Pleistocene lava sections in southwestern Iceland. J. Geomag. Geoelectr., 47: 89-102.

Tanaka H., Kawamura, K., Nagao, K., and Houghton, B.F., 1997. K-Ar ages and paleosecular variation of direction and intensity from Quaternary lava sequence in the Ruapehu volcano, New Zealand. J. Geomag. Geoelectr., 49: 587-599.

Tarduno, J.A., Cottrell, R.D., and Smirnov, A.V., 2001. High geomagnetic intensity during the Mid-Cretaceous from Thellier analyses of single plagioclase crystals. Science, 291: 1779-1783.

Tauxe, L., 1993. Sedimentary records of relative paleointensity of the geomagnetic field: Theory and practice. Rev. Geophys., 31: 319-354.

Thellier, E., and Thellier, O., 1959. Sur l'intensite du champ magnetique terrestre dans le passe historique et geologique. Ann. Geophys., 15: 285-376.

Tric, E., Valet, J.P., Tucholka, P., Paterne, M., Labeyrie, L., Guichard, F., Tauxe, L., and Fontugne, M., 1992. Paleointensity of the geomagnetic field during the last 80,000 years. J. Geophys. Res., 97: 9337-9351.

Tsunakawa, H., and Shaw, J., 1994. The Shaw method of paleointensity determinations and its application to recent volcanic rocks. Geophys. J. Int., 118: 781-787.

Tsunakawa, H., and Yamamoto, Y., 1999. Paleointensity measurement of the Hawaiian 1960 lava and its implications for the reliability of paleointensity determinations (abstract). Eos(Trans.Am.Geophys.Un.), 80, Fall Meeting suppl.: F300-301.

Tsunakawa, H., Shimura, K., and Yamamoto, Y., 1997. Application of double heating technique of the Shaw method to the Brunhes epoch volcanic rocks (abstract). 8th Scientific Assembly IAGA, Uppsala.

Uto, K., Conrey, R.M., Hirata, T., and Uchiumi, S., 1995. Improvements of the K-Ar dating system at Geological Survey of Japan. -Introduction of computer-controlled mass-spectrometry and pipette spike reservoir-. Bull. Geol. Surv. Japan, 46(5): 239-249.

Valet, J.P., and Meynadier, L., 1993. Geomagnetic field intensity and reversals during the past four million years. Nature, 36: 234-238.

Valet, J.P., and Herrero-Bervera, E., 2000. Paleointensity experiments using alternating field demagnetization. Earth Planet. Sci. Let., 177: 43-58.

Valet, J.P., Brassart, J., Meur, I. Le, Soler, V., Quidelleur, X., Tric, E. and Gillot, P.Y., 1996. Absolute paleointensity and magnetomineralogical changes. J. Geophys. Res., 101: 25029-25044.

Vlag P., Alva-Valdivia, L., de Boer, C.B., Gonzalez, S., and Urrutia-Fucugauchi, J., 2000. A rock- and paleomagnetic study of a Holocene lava flow in Central Mexico. Phys. Earth Planet. Int., 118: 259-272.

Watkins, N.D., and Haggerty, S.E., 1967. Primary oxidation variation and petrogenesis in a single lava. Contr. Mineral. and Petrol., 15: 251-271.

Wilson, R.L., and Watkins, N.D., 1967. Correlation of petrology and natural magnetic polarity in Columbia Plateau basalts. Geophys. J. Roy. Astron. Soc., 12: 405-424.

Xu, S., and Dunlop, D.J., 1995. Thellier paleointensity determination using PSD and MD grains (abstract). Eos(Trans.Am.Geophys.Un.), 76, Fall Meeting suppl.: F170.

Acknowledgements

I am very grateful to Professor Hideo Tsunakawa for his extensive support, discussion and encouragement throughout the study. I also express my gratitude to Dr. Hidetoshi Shibuya, Kumamoto University, for his courtesy of providing the Hawaiian samples and critical reading of the manuscript.

Dr. Kozo Uto, Geological Survey of Japan, is specially thanked for his high quality geochronological data. I appreciate Mr. Koichiro Shimura for his vast amounts of the preliminary paleodirectional results from the Society samples. I wish to thank Dr. M. Sudo and Dr. T. Sumii for their support in a series of the experiments for the K-Ar dating.

I would like to thank Dr. T. Kogiso, Dr. H.G. Barsczus, Dr. H. Oda, Dr. T. Yamazaki and Dr. E. Kikawa for collecting and preparing the Society samples. I am also grateful to Dr. H. Tanaka for the courtesy of preparing the geographical maps for the sampling of the Hawaiian lava.

Dr. N. Kobayashi, Dr. M. Matsushima and Dr. T. Okamoto are thanked for their kind support concerning the computer environment. I also appreciate Mr. N. Mochizuki and the member of Tsunakawa laboratory for discussions and supports throughout the study.

Finally, I wish to thank Dr. A. Yoshihara and Dr. T. Hatakeyama for their kindness of giving LaTeX style format for this thesis.

This study is supported from the 'Super Plume' project by the Science and Technology Agency of Japan.

List of Tables

List of Figures

Appendix

In this appendix, the detailed volcanostratigraphies are shown for the sampling sites of the seven islands in the Society.

[Maupiti]

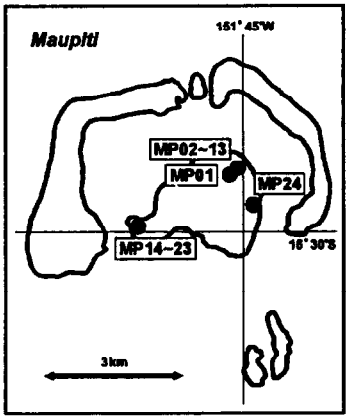

Dikes

Site ID	Outcrop	Age [Ma]	Polarity	α_{95}
MP01	Dike		△	4.35
MP24	Dike		●	9.18

★MP02~13

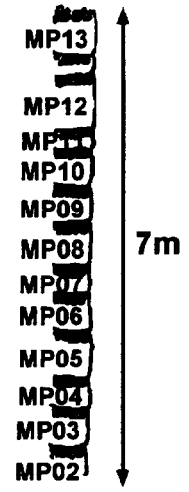

Lava sequence at the road side

Site ID	Outcrop	Age [Ma]	Polarity	α_{95}
MP13	Lava	4.61+/-0.05	●	5.29
MP12	Lava	4.55+/-0.05	●	5.76
MP11	Lava		●	3.57
MP10	Lava		●	7.88
MP09	Lava		●	2.92
MP08	Lava		●	3.82
MP07	Lava		●	7.67
MP06	Lava		●	6.47
MP05	Lava		●	2.28
MP04	Lava		●	2.53
MP03	Lava		●	2.44
MP02	Lava	4.52+/-0.05	●	3.65

★MP14~23

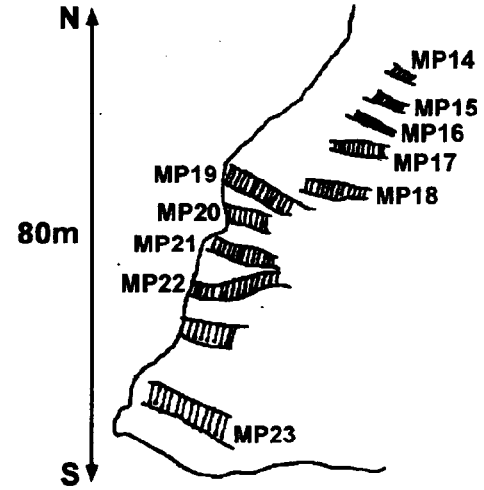

Dikes along the seaside

Site ID	Outcrop	Age [Ma]	Polarity	α_{95}
MP14	Dike		●	5.77
MP15	Dike		●	4.65
MP16	Dike		●	7.61
MP17	Dike		N.d.	20.21
MP18	Dike		●	7.02
MP19	Dike	4.52 +/- 0.05	●	3.19
MP20	Dike		●	6.31
MP21	Dike		●	4.21
MP22	Dike		N.d.	
MP23	Dike		●	4.03

[Borabora]

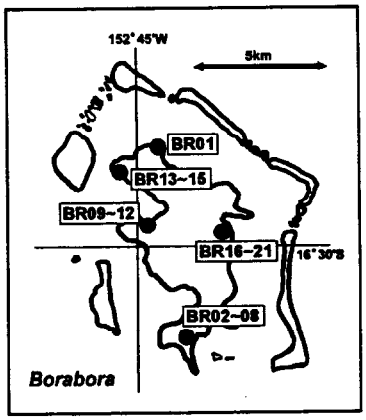

intrusion or massive flow

Site ID	Outcrop	Age [Ma]	Polarity	α_{95}
BR01	Dike		○	12.51

★BR02~08

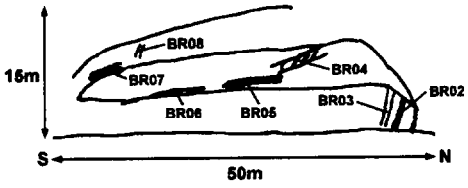

Outcrop near the under-construction hotel

Site ID	Outcrop	Age [Ma]	Polarity	α_{95}
BR02	Dike	3.21+/-0.09	●	3.21
BR03	Dike		●	5.28
BR08	Dike	3.37+/-0.05	●	2.38
BR07	Lava	3.67+/-0.05	○	4.17
BR04	Lava	3.75+/-0.05	○	4.17
BR05	Lava		○	2.41
BR06	Lava		○	3.02

★BR09~12

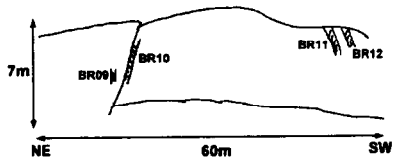

Dikes at the power plant

Site ID	Outcrop	Age [Ma]	Polarity	α_{95}
BR09	Dike		●	5.72
BR10	Dike	4.01+/-0.31	●	3.02
BR11	Dike		●	8.96
BR12	Dike		●	5.98

★BR13~15

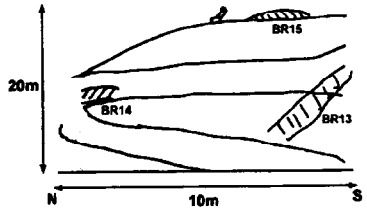

Outcrop near the canon spot

Site ID	Outcrop	Age [Ma]	Polarity	α_{95}
BR13	Dike?		○	5.12
BR15	Lava	3.43+/-0.06	○	2.83
BR14	Lava		○	3.09

★BR16~21

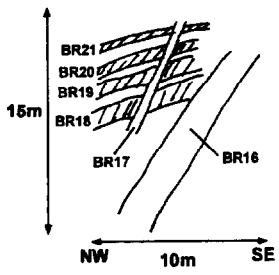

Outcrop along the road

Site ID	Outcrop	Age [Ma]	Polarity	α_{95}
BR16	Dike	3.30+/-0.06	●	4.94
BR17	Dike		●	14.40
BR21	Lava		●	6.47
BR20	Lava		●	5.39
BR19	Lava		●	5.27
BR18	Lava	3.51+/-0.05	●	3.18

[Tahaa]

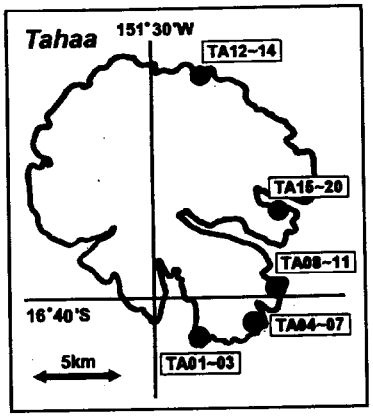

Several lava

Site ID	Outcrop	Age [Ma]	Polarity	α_{95}
TA12	Lava		○	4.53
TA13	Lava	3.11 +/- 0.04	○	6.34
TA14	Lava		N.d.	68.69

★TA01~03

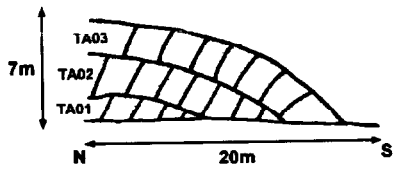

Lava sequence near the hotel

Site ID	Outcrop	Age [Ma]	Polarity	α_{95}
TA03	Lava	2.85+/-0.06	△	13.54
TA02	Lava		N.d.	61.55
TA01	Lava	3.14+/-0.06	N.d.	16.39

★TA04~07

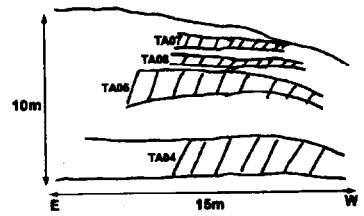

Lava sequence

Site ID	Outcrop	Age [Ma]	Polarity	α_{95}
TA07	Lava	3.24+/-0.05	△	5.27
TA06	Lava		▲	11.00
TA05	Lava		△	4.16
TA04	Lava	3.04+/-0.04	▲	11.80

★TA08~11

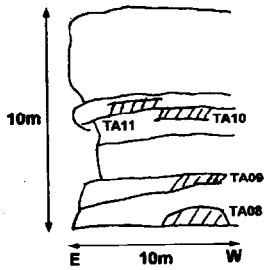

Lava sequence

Site ID	Outcrop	Age [Ma]	Polarity	α_{95}
TA11	Lava	2.57+/-0.13	○	12.39
TA10	Lava		○	6.90
TA09	Lava		○	3.30
TA08	Lava	3.14+/-0.06	○	7.50

★TA15~20

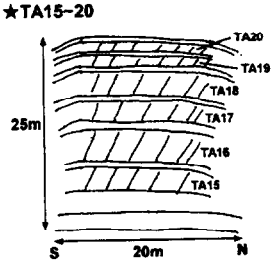

Lava sequence

Site ID	Outcrop	Age [Ma]	Polarity	α_{95}
TA20	Lava		●	5.44
TA19	Lava		●	9.22
TA18	Lava		●	3.70
TA17	Lava	2.99+/-0.04	●	5.95
TA16	Lava	2.97+/-0.04	●	7.65
TA15	Lava	2.90+/-0.05	●	1.96

[Raiatea]

Site ID	Outcrop	Age [Ma]	Polarity	α_{95}
RA01	Lava	2.45+/-0.05	●	3.24
RA04	Dike	2.55+/-0.03	N.d.	
RA05	Lava	2.60+/-0.07	●	14.72
RA02a	Lava	2.62+/-0.04	N.d.	
RA02b	Dike?	2.67+/-0.04	N.d.	
RA03	Lava	2.72+/-0.05	N.d.	

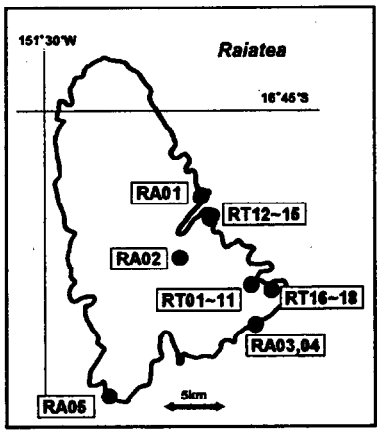

★RT01~11

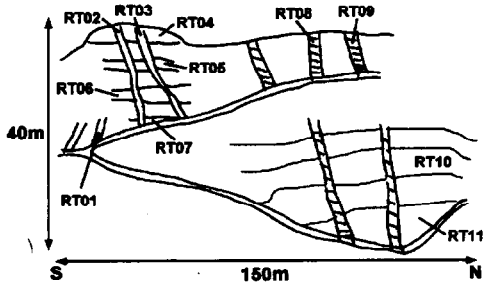

Outcrop at the big quarry

Site ID	Outcrop	Age [Ma]	Polarity	α_{95}
RT01	Dike		●	3.20
RT02	Dike		●	4.89
RT03	Dike	2.65 +/- 0.03	●	4.62
RT08	Dike		●	6.28
RT09	Dike		●	2.66
RT04	Lava		N.d.	42.27
RT05	Lava		▲	2.96
RT06	Lava		▲	4.80
RT07	Lava		▲	2.78
RT10	Lava	2.77 +/- 0.03	▲	9.34
RT11	Lava		●	8.79

★RT12~15

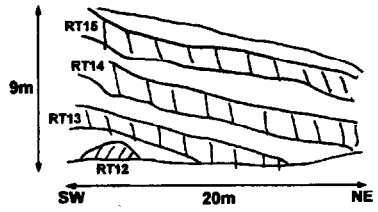

Outcrop along the road

Site ID	Outcrop	Age [Ma]	Polarity	α_{95}
RT15	Lava		●	2.92
RT14	Lava		●	2.41
RT13	Lava		●	4.16
RT12	Lava	2.61 +/- 0.03	●	1.98

★RT16~18

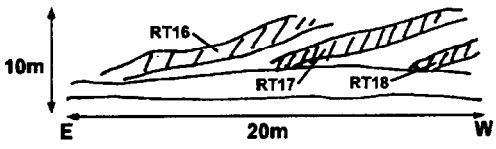

Outcrop along the road

Site ID	Outcrop	Age [Ma]	Polarity	α_{95}
RT16	Lava		●	8.50
RT17	Lava		●	13.30
RT18	Lava	2.67 +/- 0.03	●	4.86

[Huahine]

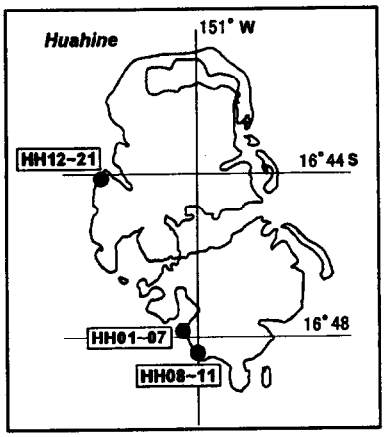

★HH01~07

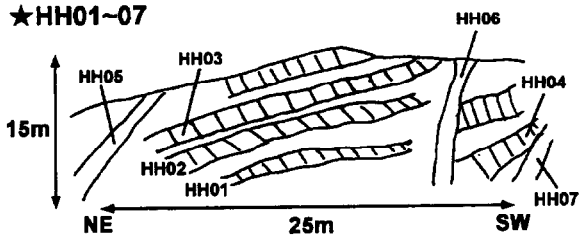

Lava sequence and dikes

Site ID	Outcrop	Age [Ma]	Polarity	α_{95}
HH06	Dike	2.58+/-0.05	●	2.55
HH07	Dike		●	5.04
HH05	Dike	2.68+/-0.04	●	4.39
HH03	Lava		●	2.69
HH02	Lava		●	1.77
HH01	Lava	2.72+/-0.03	●	1.77
HH04	Lava		●	2.00

★HH08~11

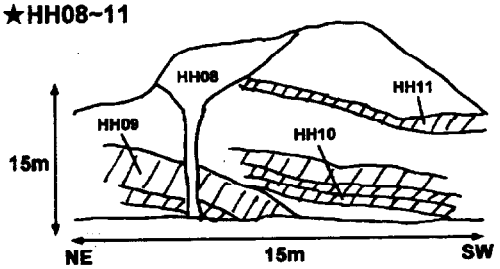

Outcrop along the road

Site ID	Outcrop	Age [Ma]	Polarity	α_{95}
HH08	Dike	3.19+/-0.13	●	2.40
HH11	Lava	3.09+/-0.04	●	4.42
HH10	Lava		●	4.70
HH09	Lava	4.01+/-0.05	●	3.42

★HH12~21

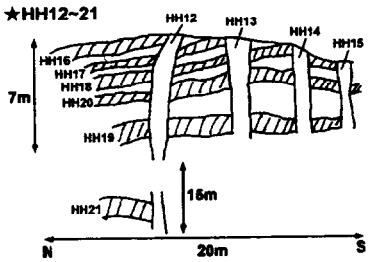

Outcrop along the road

Site ID	Outcrop	Age [Ma]	Polarity	α_{95}
HH12	Dike	2.52+/-0.04	●	5.10
HH13	Dike		●	6.60
HH14	Dike		●	10.61
HH15	Dike		N.d.	30.62
HH16	Lava		●	2.08
HH17	Lava		●	2.88
HH18	Lava		●	4.40
HH20	Lava	2.83+/-0.09	●	1.73
HH19	Lava		●	2.30
HH21	Lava		●	1.94

[Moorea]

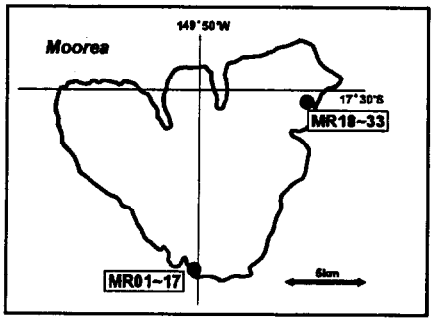

★MR01~17

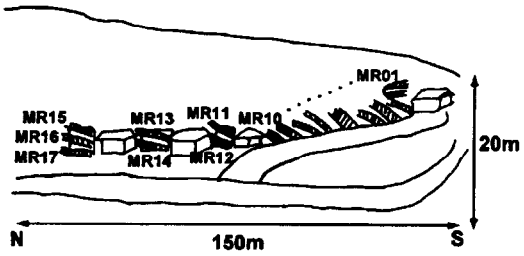

★MR18~28

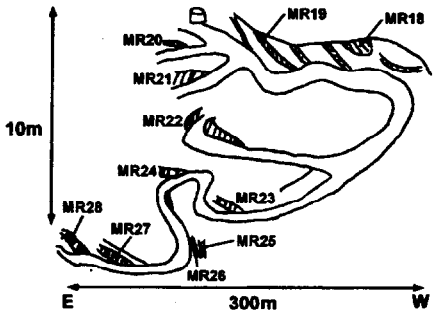

★MR29~33

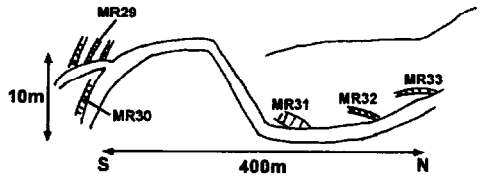

Lava sequence along the slope

Site ID	Outcrop	Age [Ma]	Polarity	α_{95}
MR01	Lava	1.58+/-0.04	○	2.45
MR02	Lava		○	3.85
MR03	Lava		○	2.36
MR04	Lava		○	0.86
MR05	Lava		○	2.40
MR06	Lava	1.62+/-0.08	○	4.78
MR07	Lava		○	3.19
MR08	Lava		○	4.85
MR09	Lava		○	4.60
MR10	Lava		○	3.58
MR11	Lava		○	2.07
MR12	Lava		○	3.26
MR13	Lava		○	3.92
MR14	Lava		○	4.75
MR15	Lava		○	5.75
MR16	Lava	1.51+/-0.04	○	3.03
MR17	Lava		○	7.81

Outcrop along the road

Site ID	Outcrop	Age [Ma]	Polarity	α_{95}
MR18	Lava		N.d.	
MR19	Lava		○	5.66
MR20	Lava		○	6.62
MR21	Lava		○	1.78
MR22	Lava		○	4.44
MR23	Lava	1.55+/-0.06	○	5.99
MR24	Lava		○	4.47
MR25	Lava		○	3.32
MR26	Lava		○	3.43
MR27	Lava		○	4.17
MR28	Lava		○	3.90
MR29	Lava		○	3.82
MR30	Lava	1.53+/-0.02	N.d.	
MR31	Lava		○	3.38
MR32	Lava	1.50+/-0.04	○	3.58
MR33	Lava		○	5.23

[Tahiti]

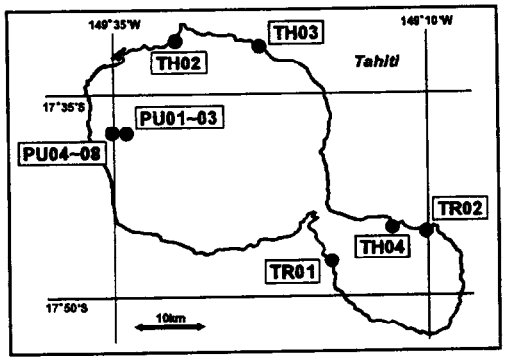

★PU01~03

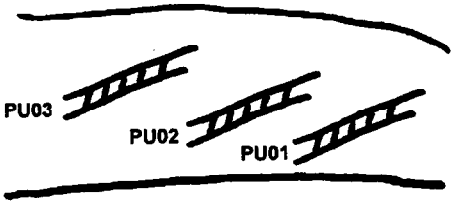

Lava sequence in Punaruu Valley

Site ID	Outcrop	Age [Ma]	Polarity	α_{95}
PU03	Lava		○	8.14
PU02	Lava		N.d.	
PU01	Lava	1.12 +/- 0.02	○	4.62

★PU04~08

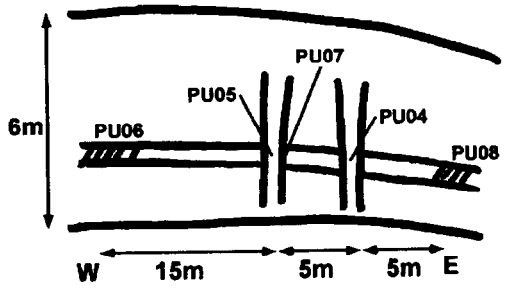

Lava and dikes in Punaruu Valley

Site ID	Outcrop	Age [Ma]	Polarity	α_{95}
PU05	Dike	1.03+/-0.02	●	6.14
PU04	Dike	0.92+/-0.03	●	4.12
PU06,08	Lava	0.99+/-0.08	○	5.06

Outcrops in Tahiti Iti

Site ID	Outcrop	Age [Ma]	Polarity	α_{95}
TR01	Lava?		●	10.97
TR02	Lava?		●	5.11

Site ID	Outcrop	Age [Ma]	Polarity	α_{95}
TH04	Lava	0.51+/-0.10	●	3.71
TH02	Lava	0.72+/-0.11	●	4.68
TH03	Lava		●	7.69